NASA Technical Memorandum 100195

The Effect of Microgravity on Flame Spread Over a Thin Fuel

Sandra L. Olson
Lewis Research Center
Cleveland, Ohio

December 1987

NASA

NASA Technical Memorandum 100195

The Effect of Microgravity on Flame Spread Over a Thin Fuel

Sandra L. Olson

December 1987

National Aeronautics and
Space Administration

Lewis Research Center
Cleveland, Ohio 44135

Contents

	Page
1.0 Summary	1
2.0 Introduction	1
2.1 Problem Definition	1
2.2 Review of Previous Work	2
2.2.1 Flame spread theories	2
2.2.2 Normal-gravity research	3
2.2.3 Microgravity research	4
2.3 Important Parameters in Flame Spread	4
3.0 Symbols	5
4.0 Experimental Apparatus and Procedures	6
4.1 Fuel Samples	6
4.2 Ignition System	7
4.3 Sample Holder	7
4.4 Atmosphere	7
4.5 Photography	7
4.6 Sequence of Events During a Test	8
4.7 Data Requirements Technique	9
4.8 Limitations of the Data	9
5.0 Results and Discussion	10
5.1 Effect of Ambient Oxygen Concentration	10
5.1.1 Discussion of microgravity results for a single thickness of fuel	10
5.1.2 Discussion of normal-gravity results for a single thickness of fuel	13
5.1.3 Discussion of microgravity results for a double thickness of fuel	13
5.1.4 Discussion of normal-gravity results for a double thickness of fuel	14
5.2 Effect of Gravity	14
5.2.1 Comparison of normal-gravity and microgravity results for a single thickness of fuel	14
5.2.2 Comparison of normal-gravity and microgravity results for a double thickness of fuel	16
5.3 Effect of Fuel-Bed Thickness	16
5.3.1 Comparison of microgravity results for single and double thicknesses of fuel	16
5.3.2 Comparison of normal-gravity results for single and double thicknesses of fuel	17
5.4 Discussion of Extinction Mechanism	18
6.0 Comparison of Data With Other Data and Theories	19
6.1 Experimental Correlations	19
6.1.1 Power-law relation between spread rate and percent oxygen	19
6.1.2 Correlation of normal-gravity and microgravity data with elevated-gravity data	19
6.1.3 Comparison of extinction limits	20

6.2 Comparison With Theoretical Predictions 21
6.2.1 Comparison with de Ris theory 21
6.2.2 Appropriateness of characteristic length 22
6.2.3 Effect of Damkohler number on flame spread rate 23

7.0 Conclusions and Recommendations for Further Research 24
7.1 Conclusions 24
7.2 Recommendations for Further Research 25

Acknowledgments 25

Appendixes

A—Data Sheets 26

B—Error Analysis 28
B.1 Experimental Errors 28
B.1.1 Error in measurement of sample length 28
B.1.2 Error in sample width 28
B.1.3 Error in measurement of sample area density 28
B.1.4 Error in oxygen concentration of chamber environment 28
B.1.5 Error in initial temperature of the experiment 28
B.1.6 Error in determination of extinction limits 28
B.2 Calculation Errors 29
B.2.1 Repeatability of point measurement 29
B.2.2 Error in determination of time 29
B.2.3 Error in estimate of flame spread rate 29
B.2.4 Error in estimate of flame dimensions 29

C—Experimental Facilities 31
C.1 Rationale For Use of Two Facilities 31
C.2 Experiment Package for 2.2-sec Drop Tower 31
C.3 Operations of 2.2-sec Drop Tower 31
C.4 Experiment in 5.18-sec Zero Gravity Facility 31
C.5 Operations of 5.18-sec Zero Gravity Facility 31

D—Supporting Computer Software 34
D.1 Film Analysis Program 34
D.2 Plotting and Least-Squares-Fit Program 38

References 44

1.0 Summary

A flame spreading over a thermally thin cellulose fuel was studied in a quiescent microgravity environment obtained through the use of the NASA Lewis Research Center microgravity facilities. Flame spread over two different fuel thicknesses was studied in ambient oxygen-nitrogen environments from the limiting oxygen concentration to 100 percent oxygen at 1 atm pressure. Comparative normal-gravity tests were also conducted.

Gravity was found to play an important role in the mechanism of flame spread. In lower oxygen environments, the buoyant flow induced in normal gravity was found to accelerate the flame spread rate as compared to the microgravity flame spread rates. It was also found to stabilize the flame in oxidizer environments, where microgravity flames in a quiescent environment extinguish. In oxygen-rich environments, however, it was determined that gravity does not play an important role in the flame spread mechanism.

Fuel thickness influences the flame spread rate in both normal gravity and in microgravity. The flame spread rate varies inversely with fuel thickness in both normal gravity and in an oxygen-rich microgravity environment. In lower oxygen microgravity environments, however, the inverse relation breaks down because finite-rate kinetics and heat losses become important. Two different extinction limits were found in microgravity for the two thicknesses of fuel. This is in contrast to the normal-gravity extinction limit, which was found to be independent of fuel thickness.

The extinction mechanism in microgravity was determined to be different from that in normal gravity. In microgravity the flame is quenched because of excessive thermal losses, whereas in normal gravity the flame is extinguished by blowoff. An extinction boundary for flame spread over a thin fuel is presented and suggests that there is a fundamental low oxygen flammability limit at a forced-flow velocity lower than the normal-gravity buoyant velocity at extinction.

2.0 Introduction

2.1 Problem Definition

Many processes contribute to the propagation of a flame over a solid fuel. Conduction, convection, and radiation of heat from the flame to the solid fuel and to the environment all play important roles in the balance of heat produced within the flame to heat lost to the environment and heat used in vaporizing fuel. Surface pyrolysis of the fuel and gas-phase chemical reactions are both vital processes involved in the production of heat needed to sustain the flame. Species diffusion and convection must also occur so that the appropriate mixture of fuel and oxidizer are present within the reaction zone to allow the reaction to proceed. Additionally, the products of reaction must be removed so that they do not extinguish the flame. With all of these interacting processes involved in flame spread, it can be difficult to determine which is dominating the spread process.

Figure 1(a) shows a schematic of a flame spreading over a solid fuel in a quiescent environment. The figure is drawn in flame-fixed coordinates, so the fuel actually feeds into the flame at the flame spread rate V_f. The fuel is assumed to be thermally thin, which means that there is no temperature gradient across the thickness of the fuel. The fuel is initially at ambient temperatures, but as it enters the preheat zone it is heated and begins to pyrolyze. The fuel continues to pyrolyze until all of the fuel is consumed or until the surface temperature drops to a level which does not sustain the reaction.

In the gas phase, the flow environment of the flame depends on whether gravity is present or not. Figure 1(b) shows the upstream velocity profiles of the flame in microgravity. A flame spreading over a solid fuel in a quiescent environment in microgravity induces no natural convection either to oppose or to assist the flame spread. Thus the flame has only a uniform opposed flow, which is the flame spread rate V_f.

A flame spreading over a solid fuel in normal gravity is greatly influenced by its orientation with respect to the gravity vector. A flame spreading in a direction opposed to the gravity vector, or "up" a sample, is observed to spread faster than a flame spreading in the same direction as the gravity vector, or "down" the sample. This is because, in the case of the upward propagating flame, the natural convection enhances the heat transfer from the flame to the unburned fuel and allows the flame to spread more rapidly than it could if the convective heat transfer did not occur. In the case of the downward propagating flame, the natural convective flow of hot product gases transfers the heat away from the unburned fuel. This work will compare the downward propagating flame with a flame spreading in microgravity.

In the case of the downward-burning flame in normal gravity, the natural-convection velocity profile of the flame has been experimentally measured by Hirano (ref. 1), and is shown in figure 1(c). It is composed of a boundary layer flow

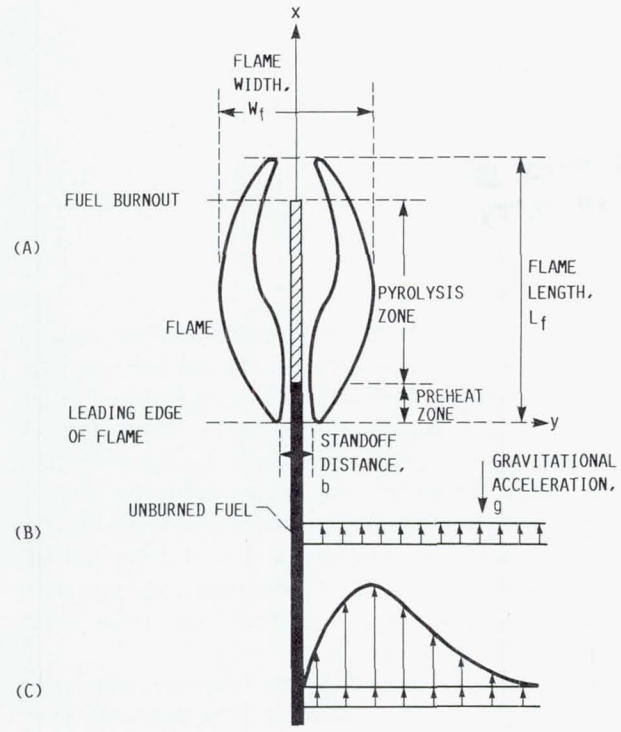

(a) Schematic.
(b) Microgravity velocity profile.
(c) Natural-convection velocity profile.

Figure 1.—Schematic of flame spread over a thin fuel, with microgravity and natural-convection velocity profiles in flame-fixed coordinates.

beginning with no slip at the fuel surface (at velocity V_f), reaching a minimum in front of the flame zone, and tapering off at increasing y values to the ambient oxidizer flow velocity V_f.

Because of the order of magnitude difference in the characteristic velocities in normal gravity and in microgravity, V_b and V_f, one would expect the heat and mass transfer to be substantially different in the two cases. In normal gravity, the natural convective flow assists the flame by drawing in fresh oxidizer and sweeping away the products of combustion, but it also removes heat with these products. If the heat removed becomes excessive, either because of a very high convective velocity or because of a very low reaction rate, the flame will be extinguished.

In microgravity, the characteristic velocity is much smaller, so the heat removed by way of convection will also be much smaller. In this case, it is reasonable to envision conditions under which a normal-gravity flame would extinguish, while the comparable microgravity flame would still be steady. In microgravity the flame obtains fresh oxidizer only by diffusion or by moving into new regions of oxidizer and leaving behind hot combustion products. If the flame spread rate is very slow, it is conceivable that the flame would extinguish unless diffusion could provide sufficient mass transfer.

2.2 Review of Previous Work

Flame spread over a solid fuel is a fundamental combustion problem. The area has seen a considerable amount of experimental and theoretical work; a wide variety of fuels in many different geometries have been used to study effects of environmental parameters on flame spread and extinction. This section is divided into three subsections: (1) a discussion of the various theories developed to describe flame spread over thermally thin solid fuels, (2) a review of normal-gravity downward spread experimental results, and (3) a summary of experiments that have been done in microgravity.

2.2.1 Flame spread theories.—The first significant treatment of flame spread over thermally thin fuels was the thermal model of flame spread developed by de Ris (ref. 2), who solved the energy and species conservation equation for an explicit expression of the flame spread rate. Although the model does account for gas-phase conduction, convection, and radiation, it assumes infinite-rate chemistry, constant velocity flow, and constant properties, including a constant vaporization temperature. His expression for the flame spread rate is

$$V_f = \sqrt{2}\,\frac{\lambda(T_f - T_{\text{vap}})}{\rho_s C_p \tau (T_{\text{vap}} - T_\infty)} \tag{2.2.1}$$

The importance of this model is that it predicted the surprising result that, for a thermally thin fuel, the flame spread rate should be independent of the magnitude of the opposing flow velocity.

The next significant theory to describe flame spread was published by Frey and T'ien (ref. 3). They were concerned that the thermal theory of de Ris could not be applied near extinction, where finite-rate kinetics become important, so they developed a numerical model in which they accounted for gas-phase chemistry by using a one-step, second-order Arrhenius expression and a one-step, first-order Arrhenius expression for the solid fuel pyrolysis. By assuming constant velocity flow and constant properties (except for not specifying an a priori vaporization temperature) and by neglecting radiation, they were able to solve numerically the steady gas-phase and unsteady solid-phase energy and species equations alternately until neither phase solution changed. The results of the computations indicated that the flame spread rate increased with decreasing opposed flow or with increasing ambient oxidizer concentration. The Frey and T'ien model is thus more extensive than the thermal theory of de Ris, which assumes infinite-rate chemistry. Frey and T'ien were also the first group to correlate the flame spread rate (dimensional) with a Damkohler number, which is the ratio of flow time to chemical time.

Vedha-Nayagam and Altenkirch (ref. 4) developed a model which calculates the flame spread over thin fuels. By assuming an experimentally observed surface temperature profile, they decoupled the gas and solid phases. The solid phase was solved

for an approximate spread rate based on the solid-phase energy balance. The gas phase, including buoyant flows, was solved by using the boundary layer equations through a similarity solution and asymptotic matching with the upstream flow field. For a thermally thin fuel the computed temperatures compared well with experimental data, but computed gas-phase velocities were somewhat high compared to measured velocities. Since the gas-phase solution was not used to calculate the approximate spread rate, no conclusions can be drawn about the effect of gas-phase flow on the spread rate.

The most recently developed model of a steady flame stabilized over thermally thin fuels in microgravity is by Chen (ref. 5). This model solves the steady two-dimensional Navier-Stokes equations, and energy and species equations by using finite-rate kinetics for both gas and solid phases, and radiative heat loss from the fuel surface. The model was modified to describe a spreading flame (C.H. Chen, Flame Propagation: Effect of Solid-Phase Heat Conduction, 1986 Technical Meeting of the Eastern States Section of the Combustion Institute, 1986). Chen found that, as the Damkohler number increased (opposed flow velocity decreased), the flame spread rate increased. This agrees with the simpler Frey and T'ien model. Chen identifies a quench limit in very-low-speed flow which is caused by radiative heat loss from the fuel surface.

2.2.2 Normal-Gravity Research.—In 1968, Friedman (ref. 6) published a review paper summarizing the state-of-the-art of flame spread research, emphasizing the uncertainty as to which variables were dominating the combustion process. Conduction, convection, radiation, aerodynamic effects, surface chemistry, gas-phase chemistry, and species diffusion were all implicated as possible controlling mechanisms. In his concluding remarks, Friedman urged that a more basic understanding of the propagation mechanism was needed.

Spurred by this, McAlevy, Magee, and Lastrina (refs. 7 to 9) performed many experiments on downward propagating flames over thermally thin cellulosic materials and determined that the fuel surface pyrolysis temperature is independent of pressure and oxygen concentration. They also correlated the flame spread rate as a power-law function of oxygen mass fraction and pressure. They determined that, for thin cellulosic samples with downward propagating flame, the flame spread rate was nearly independent of pressure but increased almost linearly with increasing oxygen mass fraction.

Campbell (refs. 10 and 11) published papers on the downward burning characteristics of filter paper. He concluded from his experiments with different types of paper that the shape of the flame was independent of paper properties. Parker (ref. 12) measured surface temperatures of cellulosic materials with a downward propagating flame. He reported that the leading edge of the flame extended slightly over the pyrolysis front in air at ambient pressures. This confirmed his visual observations that the pyrolysis region of the flame was contained within the flame. The leading edge of the flame then acted as the source of heat to preheat the fuel directly beneath it. Figure 1 shows this in terms of a preheat zone and a pyrolysis zone.

Frey and T'ien experimentally studied the near-limit flame spread over thermally thin solid fuels (ref. 13) and found that the McAlevy and Magee flame-spread power-law correlations do not hold when the flame is near extinction. The departure from the power-law relationship was believed to be due to the spread rate mechanism near extinction being controlled by either finite-rate kinetics or an increased heat loss to the sample holder. From this they called for further work to improve the chemical kinetics mechanism used in modeling in order to better describe the mechanisms controlling the flame spread.

The effect of buoyancy on flame spread down thermally thin fuels was studied by Altenkirch et al. (ref. 14). The buoyant level was increased by using a 15-m-diameter centrifuge and obtaining gravitational accelerations of up to 4.25 times that of normal earth gravity. They found that an increase in the buoyant level, brought on by an increase in the gravity level, caused the spread rate to decrease until blowoff was observed. They also correlated the flame spread data (nondimensionalized by using a characteristic buoyant velocity) with a Damkohler number. However, the correlation does not approach unity nondimensional spread rate at infinite Damkohler number as one would expect if the nondimensionalization were correct.

Three groups of experimentalists in the mid-1970's generated the bulk of the experimental data for downward flame spread over thermally thin fuels with opposed flow. Hirano et al. (refs. 1 and 15) obtained velocity measurements and temperature profiles of the spreading flame by using particle tracing techniques and fine wire thermocouples. They found that heat transfer ahead of the flame occurred mainly in the gas phase. Their measured preheat zone size agreed with that measured by Parker (ref. 12). The observed flame spread rate was also shown through analysis of temperature and velocity measurements to be closely related to the gas-phase velocity gradient just in front of the leading edge of the flame. The previously discussed models all assumed a uniform opposed flow, and thus do not predict a velocity gradient effect.

A second group of researchers, lead by Sibulkin (ref. 16), studied the effects of forced-flow velocity on the flame spread rate and found that the spread rate is constant for downward burning, thermally thin fuel for a range of forced-flow velocities from zero to some upper limit. Although they did not agree with his interpretation, they referenced a comment made by Glassman concerning flame spread rate as a function of forced-flow velocity. Glassman interpreted their experimental data showing a constant flame spread rate over a range of flow velocities as an indication that, in the region of low forced-flow velocities, the natural convection velocities induced by the flame dominate the flame spread. Sibulkin et al. believed that, although the buoyant velocities may have contributed to the observed results, they are not sufficient to explain them.

The last group of experimentalists to study flame spread with opposed flow was led by Fernandez-Pello (refs. 17 and 18).

This group published experimental results which demonstrated that for thin fuels the flame spread rate always decreases as the opposed velocity increases, but that for a range of very-low-velocity forced flows, the flame spread is again found to be independent of the forced-flow velocity. The authors concluded that this supported Glassman's interpretation of Sibulkin's results for forced-flow velocities smaller than the natural convection velocities induced by the flame; the flame spread rate was independent of forced-flow velocity because the dominating velocity was that induced within the flame.

Despite repeated attempts in normal gravity to resolve the fundamental issue of the role of gravity on flame spread, no consensus has been reached. Questions remain as to the influence of the induced buoyant flow versus an opposed forced flow on the flame spread process. Additionally, when both types of flow are present, there is yet an uncertainty as to which flow dominates over what range of these flows. The only way to determine conclusively the effect of gravity on flame spread is to conduct a series of experiments in low gravity on flame spread in opposed flow (velocities below that induced by buoyancy). The intent of this work is to provide a baseline with zero velocity forced flow which will provide insight into the controlling mechanism(s) of flame spread in low gravity.

2.2.3 Microgravity research.—In this section the microgravity experiments which have been conducted to study flame spread over thermally thin solid fuels are summarized. In general, the experiments are simple in that the only data obtained from them is photographic in nature.

The earliest microgravity experiments were conducted by Kimzey et al. (ref. 19) in a KC 135 aircraft flying Keplerian trajectories. Materials tested included paper, but no spread rate data from that test were published. They found that ignition in microgravity is very similar to that in normal gravity, but concluded that combustion is suppressed in microgravity. Because of the g-jitter on the aircraft, a steady-state burning was not achieved.

Another series of aircraft tests was conducted by Neustein et al. (ref. 20) with inconclusive results. The single successful microgravity experiment burning cotton cloth in an opposed flow of 25 cm/sec of 100 percent oxygen at 3.5 psia indicated that the flame spread rate in low gravity was identical to the spread rate in normal gravity with no forced flow. However, the normal-gravity test with the same flow environment as the microgravity test had a spread rate that was 1.3 times faster. Also, microgravity experiments with no flow gave spread rates that were much lower (8 to 18 percent of 1 g) than those measured in normal gravity.

Combustion experiments were also performed on Skylab with solid fuel and analyzed by Kimzey (ref. 21). Although the dim blue flame did not register on the experiment recorder, the astronaut narration of the test described a blue flame propagating across a paper sample.

Andracchio and coworkers (refs. 22 to 24) conducted a series of microgravity experiments studying square pieces of thin fuels burning in a quiescent environment. They found that very thin fuels burned just slightly slower than their normal-gravity counterparts. The thicker the fuel the greater the discrepancy in the spread rates.

The most recent experiment in flame spread in microgravity is being prepared for a space shuttle flight now anticipated for 1989. In this experiment Altenkirch, the principal investigator, will vary oxygen concentration and pressure for flames spreading over ashless filter paper in a quiescent environment. Preliminary ground-based microgravity experiments were conducted to test the apparatus, but because of the very slow spread rates of the material a steady-state flame was not achieved in the 5 sec of test time. To date no comparisons of normal-gravity spread rates to microgravity spread rates have been made from these tests. Altenkirch did, however, attempt to correlate the spread rate data obtained by Andracchio and Cochran (ref. 24) in his Science Requirements Document (ref. 25). Altenkirch's conclusion was that it is difficult to interpret the limited data because property data for cellulose acetate are unknown, the measured spread rates were time dependent, and the normal-gravity data used for comparison were primarily horizontal spread rather than vertical spread. He did note, however, that the trend of the correlation was the same as in normal gravity.

The available low-gravity experimental data are sketchy at best. Results from one experiment seem to contradict the results of others. It is the intention of this work to resolve some of these contradictions and shed some light on the fundamental mechanism of flame spread in the absence of gravity.

2.3 Important Parameters in Flame Spread

A great deal of work has been conducted in the past on normal-gravity flame spread, as discussed in the preceding section. In this section the significance of the various correlations of the experimental data used in the literature will be discussed.

The earliest flame spread correlation (other than de Ris' theory (ref. 2)) was published by McAlevy and Magee (refs. 7 and 8). Expressing mathematically their assumption that flame spread is a continuous, diffusive gas-phase ignition process, McAlevy and Magee wrote that the flame spread rate is equal to l^*/t, where l^* is the characteristic preheat length and t is the time it takes for the flame to reach a location after the first effects of the flame are felt. From an analysis of the gas-phase energy equation, assuming a power-law dependence upon time for the fuel vaporization rate, they determined that t is a power-law function of pressure and ambient oxidizer concentration. The experimentally measured values of l^* were similarly described by a power-law relationship so that the final result of the analysis is that V_f is proportional to $(PY_{ox}^m)^o$. The experimental data were used to evaluate m and o. For a thin

fuel burning vertically downward it was found that $mo = 0.96$ and $o = 0.12$. This indicates that flame spread varies almost linearly with oxygen concentration but is only a weak function of pressure. A problem with this correlation is that it is based on a major assumption that the fuel vaporization rate has a power-law dependence upon time. This assumption drives the form of the correlation so that the correlation is somewhat artificial.

The second, more fundamental correlation was introduced by Frey and T'ien (ref. 3). On the basis of their theory of flame spread, discussed in section 2.2.1, they correlated flame spread rate (dimensional) with the Damkohler number. They were able to qualitatively predict the near-limit behavior observed experimentally (ref. 3), and they were able to predict flame extinction at low Damkohler numbers (high opposed-flow velocities). Additionally, comparisons with Altenkirch's centrifuge data (ref. 14) gave strong experimental support to the correlation.

Altenkirch (ref. 14) modified this theoretical correlation by nondimensionalizing the flame spread rate with a buoyant velocity, which is a function of the gravity level. Additionally, he multiplied this ratio by a ratio of the solid- to gas-phase densities and a ratio of the fuel half-thickness to a buoyant length, also a function of the gravity level. The total expression for nondimensional spread rate is independent of gravity. Altenkirch then normalized this by its limiting value (zero chemical time, infinite Damkohler number), which was obtained by using the de Ris expression for the spread rate for infinite-rate kinetics. The Damkohler number used becomes a function of pressure and gravity level so that data at different pressures and gravity levels fall on the same curve. Different curves, however, are generated for each oxygen concentration. From the fit of the data, Altenkirch concluded that for low Damkohler numbers, where finite-rate kinetics (high opposed-flow velocity) become important, the power-law correlation was not appropriate.

Altenkirch, however, noted limitations of the correlation for two reasons. First, in the limit of infinite Damkohler number the dimensionless expression for flame spread rate should approach unity but does not. Second, the effect of varied oxygen concentration, a fundamental variable in flame spread, is not properly represented in the correlation. In an attempt to resolve these perceived concerns with the correlation, he redefined the Damkohler number along the lines of Liñan's reduced Damkohler number (ref. 26). Replotted, the data for different oxygen concentrations do fall along the same line and approach unity at large Damkohler numbers.

Fernandez-Pello et al. (refs. 17 and 18) correlate their data with slightly different definitions of nondimensional spread rate and Damkohler number. Rather than using a characteristic buoyant velocity and length as intermediate nondimensionalization quantities, they simply nondimensionalized the spread rate with the limiting spread rate as predicted by equation (2.2.1). Also, they base their Damkohler number on the full expression of a second-order Arrhenius reaction rate rather than just the preexponential factor. The correlation of their data gives one curve for a wide variety of oxygen concentrations. The nondimensional spread rate does not approach unity as the Damkohler number becomes large, however, which it should if the nondimensionalization is appropriate.

Wichman and Williams (ref. 27) explain the offset in the curve by pointing out that in order to solve explicitly for the flame spread rate, de Ris had to use an approximate kernel which could have been incorrect by as much as a factor of 2. Using a constant to correct the de Ris equation (eq. (2.2.1)), they choose a value such that in the limit of infinite Damkohler number, the nondimensional spread rate approaches unity. Wichman and Williams conclude that although the de Ris theory is physically correct, for an accurate calculation of the flame spread rate, the preferred equation should be

$$V_f = 0.8\frac{\lambda(T_f - T_{\text{vap}})}{\rho_s C_p \tau (T_{\text{vap}} - T_\infty)} \tag{2.3}$$

In this work both the power-law and the nondimensional correlations will be used with the data and the results discussed.

3.0 Symbols

A_s	preexponential factor for pyrolysis rate law, 1/sec
b	standoff distance, cm (fig. 1)
C_p	gas-phase heat capacity, cal/g K
Da	Damkohler number
E_s	activation energy for pyrolysis rate law, cal/gmol
g	gravitational acceleration, cm/sec^2
ΔH_c	heat of combustion, cal/g
i	oxygen-to-fuel mass ratio
L_f	flame length, cm (fig. 1)
l^*	characteristic length, cm
m	constant, empirically determined
$m_{\text{ox},\infty}$	ambient oxidizer mass fraction
o	constant, empirically determined
P	pressure, atm
R	universal gas constant
T_∞	ambient temperature, K
T_f	flame temperature, K
T_{vap}	pyrolysis or vaporization temperature, K
$\overline{V}$	characteristic velocity, $V_b + V_f$, cm/sec

V_b	characteristic buoyant velocity, cm/sec
V_f	flame spread rate, cm/sec
$\overline{V_f}$	nondimensional flame spread velocity, V_f divided by equation (2.2.1)
$V_{f,\text{corrected}}$	corrected flame spread rate for comparison with other data
W_f	flame width, cm (fig. 1)
$\dot{w}_p$	rate of pyrolysis, g/cm sec
Y_{ox}	oxygen mass fraction
α	thermal diffusivity, cm^2/sec
λ	gas-phase thermal conductivity, cal/sec cm K
ν	gas-phase kinematic viscosity, cm/sec
ρ_s	fuel-bed density, g/cm^3
τ	fuel-bed half-thickness, cm

4.0 Experimental Apparatus and Procedures

To address the issue of whether the flame spread rate over a thermally thin fuel is a function of the ambient oxidizer flow environment, a microgravity research program was initiated to study flames spreading over a thin fuel in a quiescent microgravity environment. These microgravity tests were to be conducted in parallel with normal-gravity flame spread tests so that the spread rates in normal gravity and microgravity could be compared directly. In addition to varying the oxygen concentration of the environment, two different thicknesses of fuel were studied.

In this section, the experimental and data analysis techniques are described. Further information concerning error analyses, experiment packages, microgravity facilities, and supporting software is contained in appendixes A to D.

4.1 Fuel Samples

Because of the limited time available in the ground-based microgravity facilities (see appendix C for a description of the two facilities used during this work), it was very important to select a fuel which had a good chance of quickly establishing a steady-state flame spread in low gravity at low oxygen concentrations. Because of this, the most important criterion for fuel selection was a rapid flame spread velocity.

It was also important to be able to compare results with other works studying flame spread over thermally thin fuels. Thus, the primary composition of the fuel had to be cellulose (previously used fuels included index cards, paper tape, and onionskin).

Finally, the fuel must burn cleanly with a minimum residual ash, which could interfere with the flame spread process. This criterion proved to be a problem in the normal-gravity comparison tests, where many materials exhibited a tendency to form an ash or char behind the flame front which would then fold over and cause nonsymmetric flame propagation.

A number of different fuels were tested in normal gravity. Spread rates were measured in air. The material selected was a 76-μm-thick paper towel (National Stock No. 7920-00-543-6492, spec. UU-T-595, tradename Kimwipes), which burned 15 cm in approximately 10 sec. This was the fastest spread rate obtained in the materials screening tests. Fortuitously, this same material was also one of the materials exhibiting minimal ash formation. The area density of this material is 1.998×10^{-3} g/cm^2 ± 5.5 percent based on the total thickness of the material. The composition of this material as reported by the manufacturer is 99 percent cellulose wood fiber, 1 percent polyamide wet strength resin, and <0.1 percent dyes or colorants.

The samples used in these tests were 3 ± 0.2 cm wide by 15 ± 0.3 cm long. The width was selected on the basis of quenching distance work conducted by Sibulkin (ref. 16). In this work it was determined that widths less than 2 cm allowed significant heat losses to the sides of the holder, and thus the flame was not two dimensional. A width of 3 cm was selected for these tests to ensure that losses to the sides of the holder would not be significant. The maximum length which could be fitted into the experiment chamber for the 2.2-sec Drop Tower was 15 cm (see appendix C for a description of the experiment packages used). This length was sufficient for these tests because no flames were observed to be longer than 8.9 cm.

The paper sample was attached to the metal holder with double-sided tape. The sample was stretched tight across the holder to ensure a uniform fuel plane. The tape did not burn because the flame was quenched at the edge of the holder. The free ends of the sample did tend to bow slightly; however, this did not appear to influence the flame spread for the single thickness of fuel.

Some experiments were conducted with a double thickness of the fuel. No adhesive was used to hold the materials together in the exposed region of the fuel. This was done so that there would be no influence on the flame spread caused by another material. The double thickness was obtained by folding one larger sheet in half so that the two sides shared a common edge. This ensured that the two sides were of the same size and helped keep the two sheets together. The two sides of the sample were then attached to the two sides of the holder with tape and the holder halves fastened together with more tape. This system worked very well except near the ends of the sheets, where, because the ends were free, the two halves sometimes separated. This caused some distortion of the spread rate near the ends of the sample, which was taken into account in the analysis of the data.

Samples were dried in the experiment chamber for a minimum of 4 hr (frequently overnight) to remove moisture. This minimum time was conservatively based upon some tests conducted by Altenkirch (ref. 28), in which he determined that approximately 3 hr was required to dry samples much thicker than those used in this study.

4.2 Ignition System

The sample was ignited in microgravity by a 0.0254-cm-diameter Nichrome V wire woven in a sawtooth pattern over the top free end of the sample. Nichrome V was chosen on the basis of its past use as an igniter for low-gravity experiments. This wire was used because it heats very quickly and yet still withstands the amperage required to ignite the sample. In addition, it cools more rapidly than thicker, stronger wires. This characteristic is important for the low spread rate test, where the flames do not move far from the igniter and thus are still influenced by the presence of the wire.

The igniter was formed by using a pattern of nails to bend the wire into five sawteeth approximately 1 cm in length. It was necessary to precondition the wire by running current through it for a few seconds (approximately 3 A) to anneal it. This treatment made the wire more malleable. The five teeth of the igniter were woven alternately on the two sides of the sample so that approximately 2.5 of the 3 cm exposed to ignition was covered by igniter wire (figure 2). To ignite the sample, the wire (typically 3-Ω resistance) was exposed to 28 Vdc for between 0.3 and 0.5 sec. This was sufficient to cause ignition and yet minimized the heat input to the system.

In some tests the igniter wire was observed to break apart. This did not affect the flame spread unless the hot wire bent such that it touched unburned fuel. In those few cases it was necessary to redo the test.

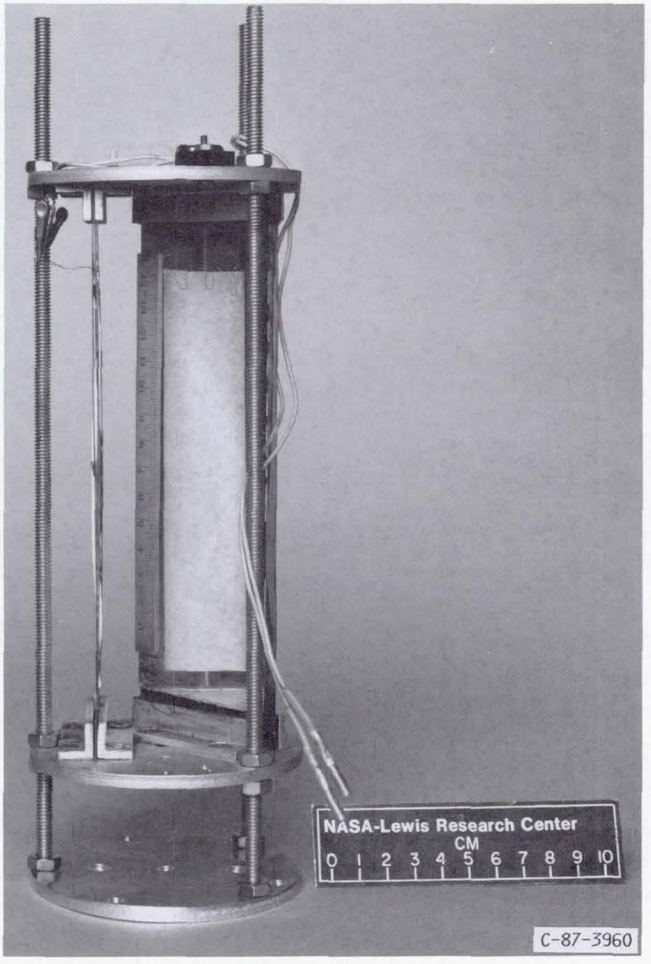

Figure 2.—Sample holder with sample and igniter wire mounted.

4.3 Sample Holder

The sample with the igniter wire woven across the top was mounted in a holder, shown in figure 2. This holder consisted of two spring metal plates held within a larger cylindrical framework. Each plate was 0.036 cm thick and had a 3- by 18-cm rectangular cutout within which the paper was mounted. A mirror was mounted at 45° to the plates so that two views of the sample were visible on the film of each test. The igniter wire ends were clipped to Teflon-coated wire attached to the holder. These wires were shielded from exposure to the flame by the holder and the mirror. When the holder was mounted in the experiment chamber and bolted down, the ignition system was connected to electrical leads inside the experiment chamber to complete the ignition circuit.

This design of the holder was driven primarily by the constraints of the 2.2-sec experiment chamber, shown in figure 3. Minor modifications to the holder were made for testing in the 5.18-sec Zero Gravity Facility package, shown figure 4. These changes involved a slightly modified igniter wiring system and a small lamp mounted on the holder rather than within the chamber as it was in the 2.2-sec tests. Functionally, there was no change in the experiment.

4.4 Atmosphere

The experiment chamber was sealed and evacuated for a minimum of 4 hr to dry the sample and then was filled to 1-atm pressure with oxygen and nitrogen. Pressure was not varied in this work because its effect on flame spread was relatively small in comparison to oxygen concentration, gravity level, and fuel-bed thickness. The concentration of oxygen and nitrogen was determined by partial pressures. The accuracy of mixing was 0.001 atm in both facilities. The uncertainty in the oxygen concentration was 1 percent, however, because of the limitations of the evacuation system used in the 2.2-sec facility.

4.5 Photography

The tests were recorded on high-speed motion picture film, which served as the only source of data for analysis. Camera framing rates were measured by using calibration marks left on the edge of the film by a timing light generator. The maximum error involved in time determination was ±0.08 sec.

The main difficulty in these tests was determining the proper camera settings and film development instructions so that the

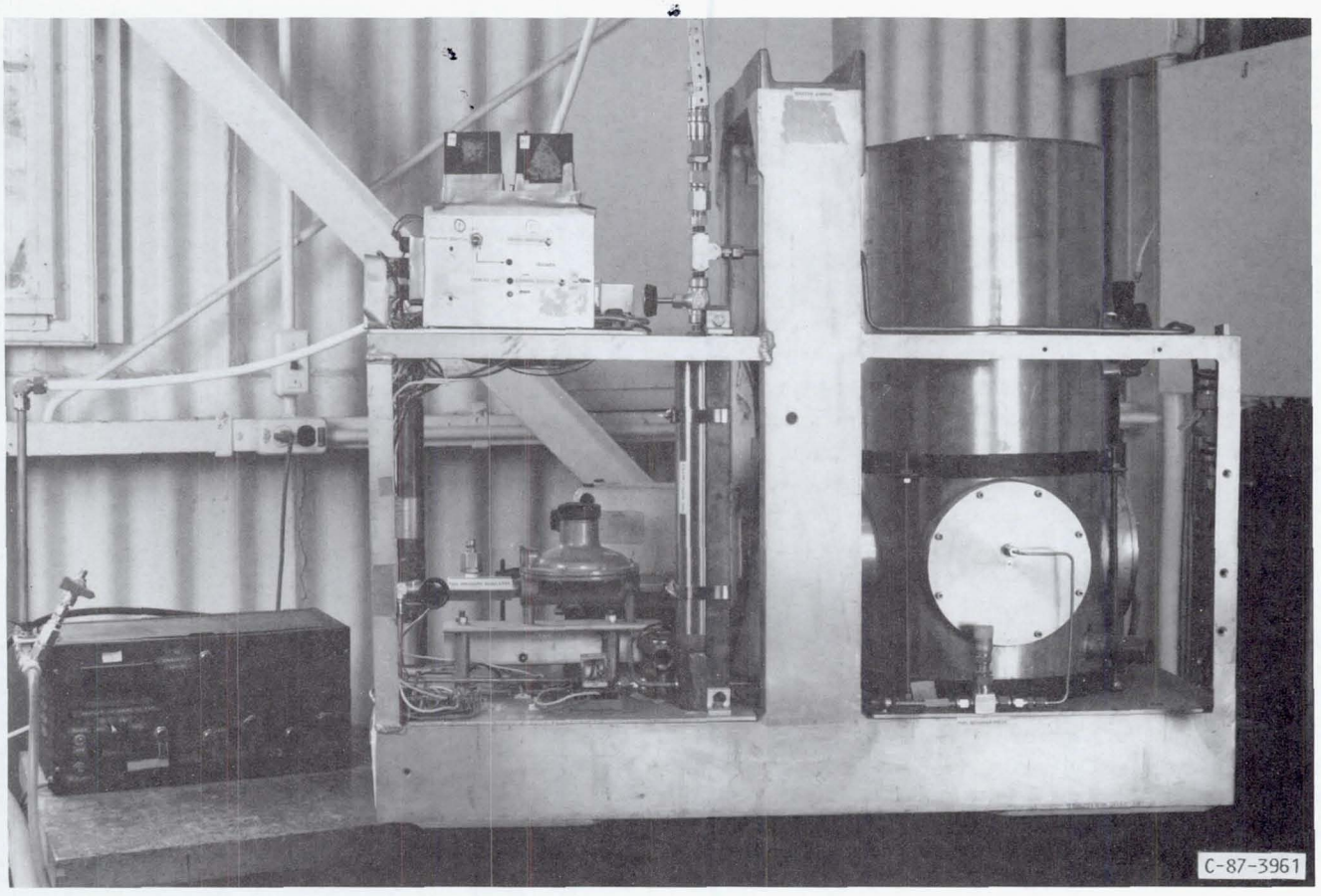

Figure 3.—Experiment package and gas-mixing system for 2.2-sec Drop Tower.

flames would be bright enough to see and yet not so bright that they appeared washed out. An added complication was that the intensity of the flames varied enormously from 100 percent oxygen to the extinction limit, which made estimating the appropriate setting almost impossible.

The most important region of the flame to observe is the leading edge of the flame. This region, however, is by far the most difficult to see because it is usually blue. Blue does not show up well on film, so in order to see the blue well it was necessary to force process the film. This invariably washed out most of the detail of the yellow soot regions of the flame.

In the 2.2-sec facility, the film used was high-speed tungsten Eastman Ektachrome video new film with an ASA rating of 400 for tungsten. The camera framing rate was 100 frames/sec. The camera *f*-stop was always set at 1.6, or full open. If the film required more light amplification, it was possible to have it force processed up to two *f*-stops more. This proved to be necessary for oxygen concentrations less than 30 percent in low gravity. In normal gravity, only at 21 percent and lower was force processing two stops necessary. Additionally, the framing rate was reduced to 50 frames/sec for some of the lower oxygen concentration tests to further enhance the light from the flame.

In the 5.18-sec Zero Gravity Facility, the film used was high-speed, Estar-based Kodak Ektachrome video new film. This film was used rather than the same film used in the 2.2-sec Drop Tower because the latter film offgasses in the vacuum of the large facility. It was necessary to slow the camera framing rate down dramatically to be able to see the very dim blue flames near extinction in microgravity. The camera framing rate was varied from 100 to 12 frames/sec. At the very low framing rate some distortion of the flame length occurred, the magnitude of which depended on the flame spread rate.

4.6 Sequence of Events During a Test

The camera was started approximately 3 sec before the test began so that it could reach normal operating speed prior to the drop. The internal chamber lights served to ease analysis of the films: the initial configuration of the experiment was confirmed, the location of the top and bottom of the paper as well as the left and right sides were noted, and the indication of the drop start was when the light went out. The time for experiment shutoff was varied depending on the facility and whether the test was in normal gravity or in microgravity.

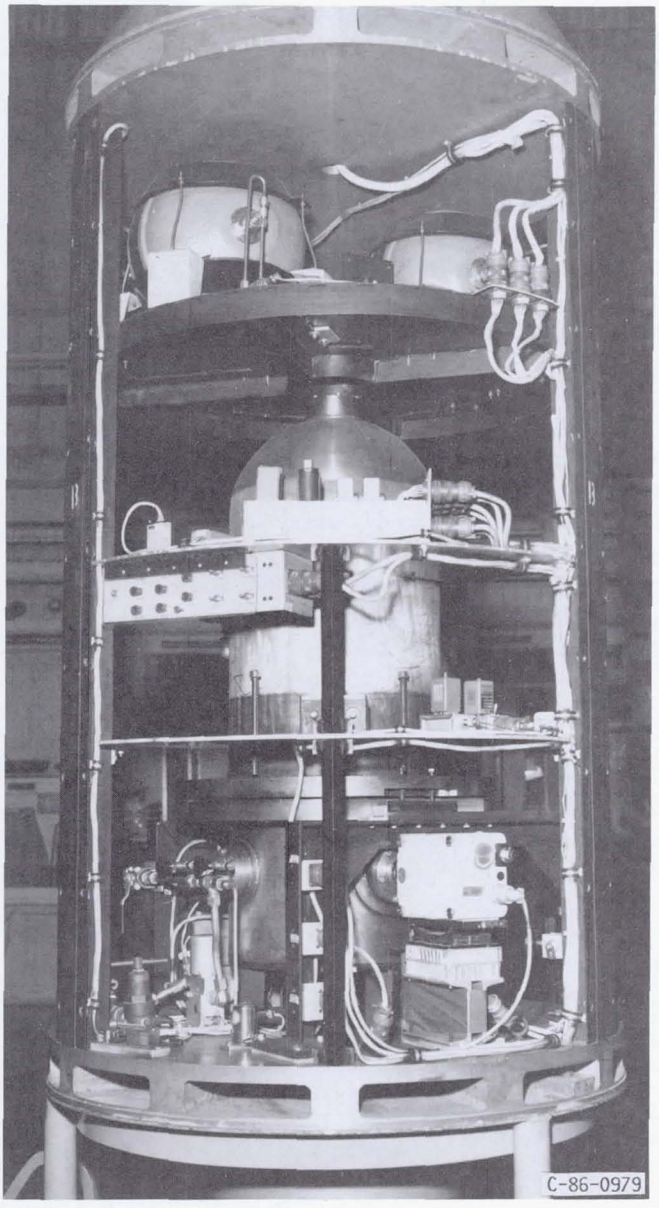

Figure 4.—Experiment bus for 5.18-sec Zero Gravity Facility.

Normal-gravity tests were allowed to burn the sample completely, so tests sometimes lasted as long as 1 min. The following table lists the sequence of events:

Time, sec	Event
−3	Camera is manually started Internal chamber light switches on Timing lights begin to mark film
0	Package released Internal chamber lights go out Igniter wire receives power
0.3	Igniter wire stops receiving power
End of test	Experiment shuts off

4.7 Data Requirements Technique

The only source of data from this work is the film record of the test. The films were analyzed with a film motion analyzer, which was connected to a personal computer. The film motion analyzer projected the image from the film onto a screen, which was also an electronic grid of digitized x and y coordinates. The film motion analyzer also counted the number of frames of film so that two-dimensional positions and their correlating time could be recorded. To record frame numbers and x and y coordinates, the film was advanced to the appropriate frame. The crosshairs of a hand-held cursor, or mouse, were lined up with the point to be measured, and the button on the mouse was depressed. The frame number and x and y coordinates corresponding to that point were transmitted to the attached computer as ASCII characters through an RS232 connection. The error involved in this positioning of the crosshairs correctly was operator dependent. The measurement error, determined by repeated measurements of a single point, was found to be ± 0.03 cm. Since this error was much smaller than other errors in the system, it will be neglected.

The software used in this work to measure and analyze the data from the films is listed in appendix D. The data listed in Appendix A were all determined by using this software. It should be noted that flame lengths, widths, and standoff distances, as shown in figure 1(a), are defined as L_f, W_f, and b, respectively.

4.8 Limitations of the Data

This section is a summary of the detailed error analysis found in appendix B.

The uncertainty in the sample length was found to be ± 0.3 cm, or 2 percent. Since this measurement was used to scale all length measurements, all measurements involving distance should be accurate to within two percent. In comparing the variation observed in the steady flame dimension data, this measure is of the correct order. Variations in the average flame dimensions were as much as 7.3 percent between tests at like conditions, but the author believes that this is due to the fluctuations in the dimensions and not due to measurement errors. It should be noted here that the error involved in making the measurement from the film is an order of magnitude less than, and thus insignificant compared to, the uncertainty in the sample length.

The timing was fairly accurate because of the use of timing lights to mark the film in 0.1-sec increments. This eliminated the error in unsteady camera speeds. The accuracy of times was thus calculated to be ± 0.083 sec on the basis of the slowest framing rate used.

The oxygen concentration within the chamber at the start of the experiment was known to within 1 percent. The ambient temperature at the start of the experiment was not controlled and thus varied between tests by as much as 15 °C (26 °F).

A large part of the data analysis involved a qualitative judgment on the part of the author to determine where to begin and end the curvefit analysis to determine spread rates, or, in terms of flame dimensions, what length to select as characteristic of the flame when the dimensions varied in time.

The data recorded just after ignition were frequently neglected in the calculation of the spread rates because the flame spread was transient, whereas steady-state flame spreads were desired. Steady-state linear flame spread rates were obtained in all normal-gravity experiments and in almost all of the microgravity experiments, despite the time limitations imposed by the microgravity facilities. Near the extinction limit, however, an oscillatory flame spread behavior was observed rather than a linear spread. In this case the first-order, least-squares fit was still used, but the data in appendix A are marked with a footnote to indicate that the oscillatory behavior was observed for that test.

The measured spread rates were found to vary for the single thickness of fuel by a maximum of 5.8 percent on the basis of repeated tests at the same conditions. For the double thickness of fuel, however, the spread rates were found to vary as much as 20 percent. This is believed to be due to the fact that no special technique was used to ensure bonding of the two fuel samples, so the air gap between the samples varied from test to test and increased the variation in spread rate.

In terms of the flame dimensions, the steady-state, or mean, value of a fluctuating dimension was recorded whenever possible. However, many of the flame dimensions were still transitioning to a steady-state value at the end of the microgravity test time. In these cases, the last value measured was recorded and that condition is marked in appendix A with a footnote to indicate that the dimension was still in transition.

Comparisons of repeated tests where steady-state dimensions were recorded indicate that lengths for the single thickness of fuel varied by a maximum of 3.9 percent. Widths for the single thickness of fuel varied by a maximum of 5.9 percent. Standoff distances, when they could be measured, varied by a maximum of 6.6 percent. Variations for the double thickness of fuel were typically of the same order.

5.0 Results and Discussion

5.1 Effect of Ambient Oxygen Concentration

In this section, the data from normal-gravity and microgravity tests for the single and double thicknesses of fuel are presented separately, and the effect of ambient oxygen concentration on each is discussed.

5.1.1 Discussion of microgravity results for a single thickness of fuel.—The effect of ambient oxidizer concentrations on a single thickness of fuel in microgravity was investigated for oxygen concentrations from 100 percent to the observed extinction limit of 21 percent oxygen at 1 atm pressure.

The steady-state spread rates of the flame are plotted as a function of oxygen concentration in figure 5. The relation of flame spread rate to oxygen concentration is slightly nonlinear over the entire range of oxygen concentrations. Near the extinction limit, the slope of the spread rate curve becomes steeper. This flame spread dependence on oxygen concentration is similar to that observed in previous normal-gravity experiments for similar fuels (refs. 13 and 17).

The flame shape varied substantially over the range of oxygen concentrations. Figure 6 shows three flames at 40, 30, and the limiting 21 percent oxygen. The visible flame length varied by a factor of 4.5, from 8.83 cm at high oxygen concentrations to 1.93 cm at the extinction limit. The width varied by a factor of two, from 3.03 cm at high oxygen concentrations to 1.57 cm at the extinction limit. The visible flame was very close to the fuel at higher oxygen concentrations, but as the level of oxygen was reduced, the flame moved farther away from the fuel. This was very pronounced at the limit, where the two halves of the flame were 0.49 cm apart. This distance, as indicated in figure 1(a), is the standoff distance b.

At oxygen concentrations higher than 60 percent, the tail region of the flame was closed, indicating complete fuel burnout. At lower oxygen concentrations, the flame tip was open, and the two halves of the flame were separate. The two halves of the tail independently varied slightly in length during tests at these lower oxygen concentrations. This is possibly due to aerodynamic effects in the post-pyrolysis, or wake, region of the flame.

It was impossible to determine from the films if all of the fuel had burned away at these lower oxygen concentrations or if there was a residual char remaining behind the flame. This was because during the test the level of light was insufficient to see the fuel surface, and any char that might

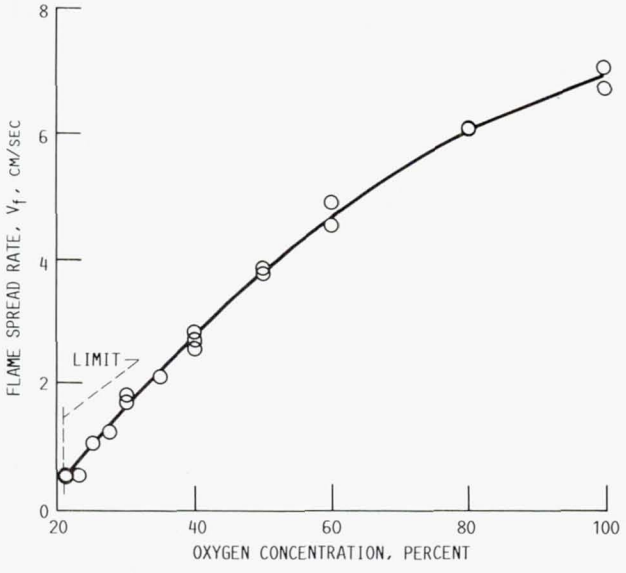

Figure 5.—Microgravity data for single thickness of fuel.

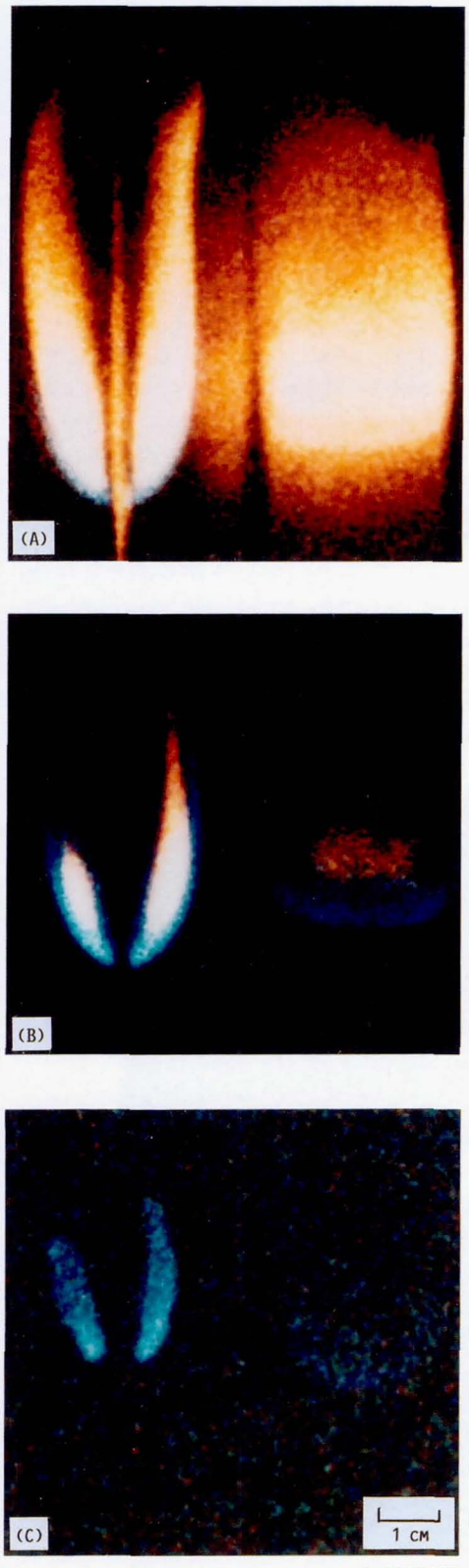

(a) 40 percent oxygen.
(b) 30 percent oxygen.
(c) 21 percent oxygen.

Figure 6.—Microgravity flames for single thickness of fuel.

have been left behind the flame disintegrated as the experiment package was decelerated at up to 50 g's at the end of the experiment time.

The flame color also varied considerably over the range of oxygen concentrations. At high oxygen concentrations the flame was almost white in intensity, with a blue halo at the leading edge. As the oxygen concentration decreased, the flame turned more yellow, and the blue leading-edge region became larger and brighter. The yellow soot region of the flame continued to shrink as more of the flame became blue. At oxygen concentrations less than 30 percent, no soot was observed to form in the entirely blue flames. Figure 6 shows this transition from a mostly sooty flame to an entirely blue flame.

Very near the extinction limit the flame spread rate became unstable and began to oscillate around a mean spread rate. Figure 7 shows this oscillatory behavior in a graph of the extinction-limit flame front position as a function of time. This flame spread behavior is in contrast to most of the steady-state linear flame spread rates measured away from the extinction limit in microgravity. The line drawn through the data is the least-squares fit of the data, and the slope of the line is the spread rate of the flame. The limiting spread flame of a single-thickness sample in microgravity is shown in figure 8, together with several other samples in microgravity and in normal gravity.

The extinguished flame at 20.5 percent oxygen was also analyzed for spread rate, and it was found that it too showed this oscillatory behavior in its spread. The flame was observed to stop propagating forward after 1.55 sec, which corresponded to an inflection point in this oscillatory behavior where the slope of the oscillation went to zero. After the flame could no longer propagate forward, it was observed to retreat slightly for 0.57 sec before the flame extinguished.

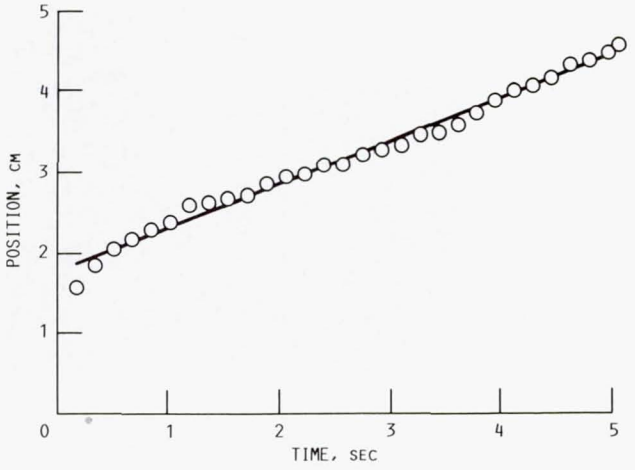

Figure 7.—Limit flame spread history for sample in microgravity, with single thickness of fuel.

It should be noted that after the gas-phase flames extinguished, there frequently appeared a red glow from the fuel surface which was interpreted to be smoldering. In most cases this smoldering lasted only a few tenths of a second after gas-phase extinction occurred, but in a few tests this smoldering continued unmoving for the remainder of the drop. It is very possible that the still hot igniter wire had an influence on the smoldering.

It is suggested here that the oscillatory behavior observed near extinction in microgravity is an indication of the slowing of the mechanism of flame spread near the extinction limit; that is, the coupling of the gas- and solid-phase heat and mass transfer. This can be explained as follows.

A flame propagates over a solid fuel by moving into new regions where oxidizer and pyrolized fuel vapor have mixed. As the ambient oxidizer concentration is reduced, the flame is forced to move farther from the fuel surface and become more diffusive to obtain sufficient oxidizer. This increases the distance over which the fuel must travel, so the fuel concentration in the region of the flame decreases. Thus the flame becomes weaker. The weaker flame produces less energy, and so less energy is fed back to the fuel surface and even less fuel vapor is produced. If the flame reaches a steady-state spread, the heat transferred back to the fuel is just sufficient to produce the proper amount of fuel vapor to sustain the flame spread.

The oscillatory behavior seen near the limit is an indication of the slowing of this time-dependent gas-solid coupling of heat and mass transfer. The flame spreads into a premixed region of fuel and oxidizer and produces energy during the part of the oscillation where the change in the slope is positive (i.e., the flame accelerating). Then, as it runs out of fuel, the flame slows (decelerates during the part of the oscillation where the change in the slope is negative), while the heat it has generated conducts to the fuel surface and pyrolyzes more fuel vapors. These fuel vapors then diffuse and/or convect ahead of the flame. These processes become slower as the temperature and species concentration gradients become less steep, so the feedback system takes more time. However, if the heat transferred to the solid is sufficient to produce enough fuel vapor ahead of the flame to allow the flame to propagate, then the flame is sustained. If not, and the flame spread rate becomes zero, then the flame extinguishes. Extinction is believed to be caused by quenching, as will be discussed in section 6.0.

The reason the flame appeared to retreat in the experiment is that extinction occurred at the leading edge of the flame, where the flame is stabilized over the fuel surface. As the

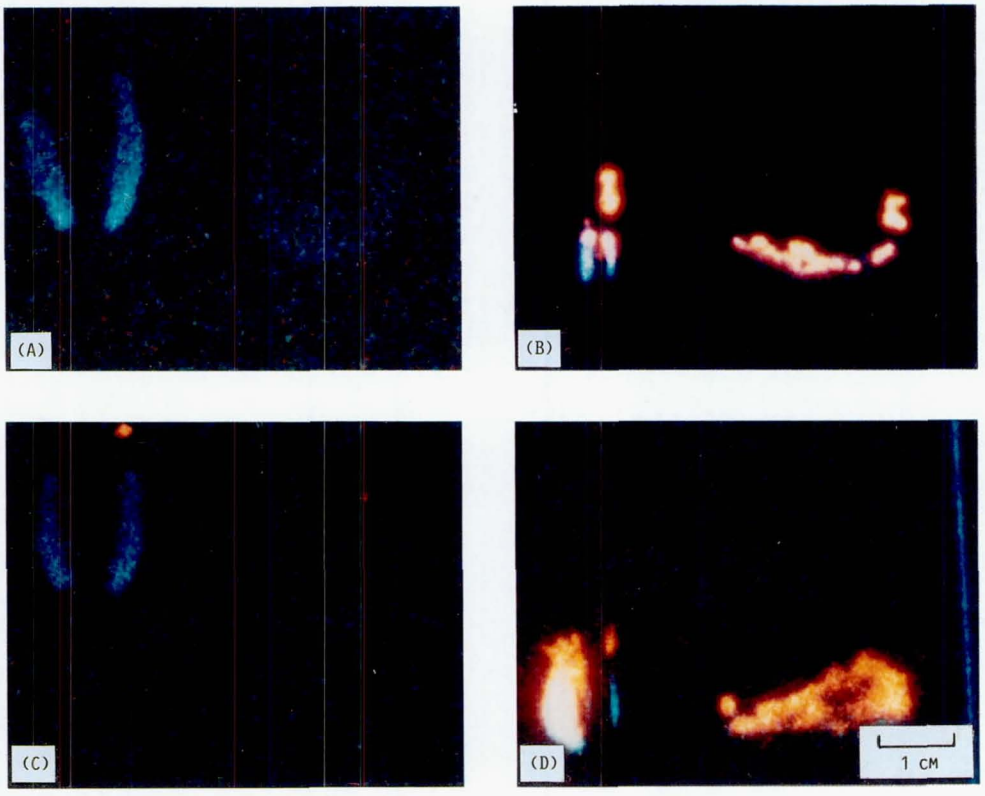

C-87-09957

(a) Microgravity, 0.0076-cm sample in 21 percent oxygen. (b) Normal-gravity, 0.0076-cm sample in 16.5 percent oxygen.
(c) Microgravity, 0.0152-cm sample in 26 percent oxygen. (d) Normal-gravity, 0.0152-cm sample in 16.9 percent oxygen.

Figure 8.—Four limit flames.

leading edge extinguished, the flame behind the leading edge became the new leading edge, which then also extinguished. The extinction propagated along the length of the flame until the entire flame was extinguished.

5.1.2 Discussion of normal-gravity results for a single thickness of fuel.—The effect of ambient oxidizer concentrations on a single thickness of fuel in normal gravity was investigated for oxygen concentrations from 100 percent to the observed extinction limit of 16.5 percent oxygen at 1 atm pressure.

The measured spread rates for these flames are plotted as a function of oxygen concentration in figure 9. As in the case of the microgravity flames, as well as in other normal-gravity experiments, the flame spread rate varies slightly nonlinearly with oxygen concentration and exhibits a non-zero spread rate at the extinction limit.

The visible flame shape varied considerably over the range of oxygen concentrations. The average flame length varied by a factor of eight, from 5.7 cm at 100 percent oxygen to 0.68 cm at the extinction limit. Additionally, there was a substantial change in the flame length during a test because of flickering. The flame width did not vary quite as much; it varied by a factor of almost four, from 1.82 cm at 100 percent oxygen to 0.47 cm at the limit. Only one standoff distance could be measured; at the limit the standoff was 0.17 cm. At higher oxygen concentrations, the flame standoff distance could not be measured because it was of the same order as the thickness of the sample holder.

All normal-gravity flames were observed to be closed-tipped, indicating complete fuel burnout. This is due to the buoyancy-induced flow of air around the flame. All of the fuel was burned over a very short distance under the flame, although glowing pieces of char were frequently observed to be torn away from the surface by the strong buoyant flows past the sample. In most cases these were small and did not influence the flame spread.

The flame color varied in intensity over the range of oxygen concentrations. At high oxygen concentrations most of the flame was white, with a blue halo around much of the flame. These flames also had exceptionally strong flickering actions. At lower oxygen concentrations the flame was dominated by yellow soot, and the flickering became less dramatic. Only very near the extinction limit did the blue leading edge enlarge substantially and the flame move away from the fuel surface. The soot region also became much smaller near the limit, and flicker was almost negligible. Figure 8(b) shows the limiting flame for the normal-gravity single thickness of fuel.

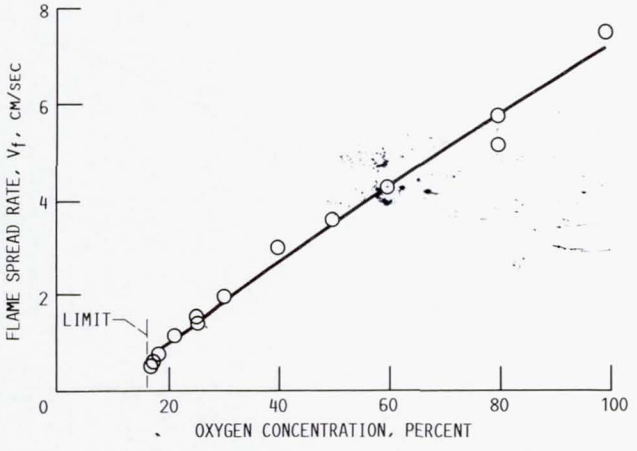

Figure 9.—Normal-gravity data for single thickness of fuel.

In examining the spread rates near extinction, there was no indication of any pronounced oscillatory behavior in the position of the flame front with time. At the limit the flame spread began linearly, but as the flame moved farther away from the igniter wire, the flame front position became stationary, and the gas-phase flame extinguished in 3.55 sec after ignition. No retreat of the flame front was observed because all of the fuel behind the flame was burned away. Extinction is believed to be caused by blowoff, as discussed in section 6.0.

5.1.3 Discussion of microgravity results for a double thickness of fuel.—The effect of ambient oxidizer concentrations on a double thickness of fuel in microgravity was investigated for oxygen concentrations from 100 percent to the observed extinction limit of 26 percent oxygen at 1 atm pressure.

Steady-state spread rates as a function of oxygen concentration are shown in figure 10. The slightly nonlinear relation is observed in this instance, as has been discussed in sections 5.1.1 and 5.1.2. Near the extinction limit, the spread rate curve becomes steeper than at higher oxygen concentrations and extinguishes at a non-zero spread rate.

The flame shape varied over the range of oxygen concentrations. The visible flame length varied by a factor of 5.6, from 9.32 cm at high oxygen concentrations to 1.67 cm at the limit. The flame width varied by a factor of 2.3, from 3.19 cm at high oxygen concentrations to 1.40 cm at the limit. The flame standoff distance was small at higher oxygen concentrations, but as the oxygen concentration was reduced it became larger as the flame moved away from the fuel surface. The standoff distance was 0.60 cm near the extinction limit.

At oxygen concentrations above 80 percent, the flame was observed to have a closed tail region. At oxygen concentrations less than 60 percent, the tail region was open and the two halves of the flame clearly separated. In the region from 60 to 80 percent, the tail region was still in transition during the test time, but it appeared that all of the solid fuel was vaporized for oxygen concentrations higher than 60 percent. Below that oxygen concentration, the light was insufficient to determine if all of the fuel had been vaporized.

The flame color again varied from white-blue to yellow and finally to a dim blue. The lowest oxygen concentration where soot was observed in the flame was 40 percent oxygen. Flames at lower oxygen concentrations were completely blue.

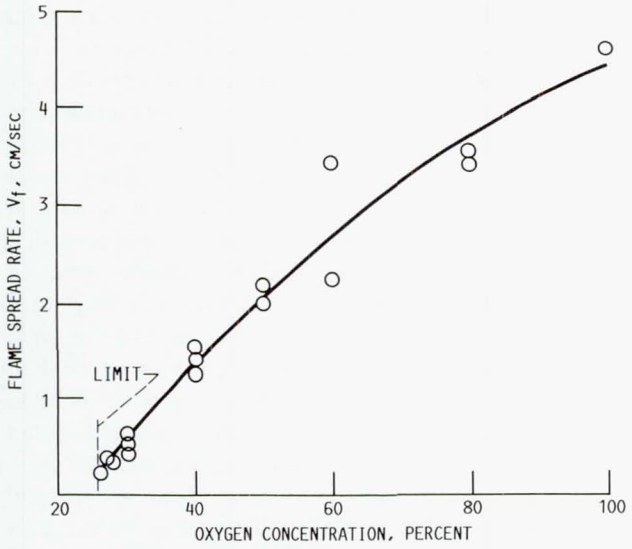

Figure 10.—Microgravity data for double thickness of fuel.

In the near-limit region, the flame propagation showed the same unstable, or oscillatory, spread behavior as was observed for the single thickness of fuel, but it was even more pronounced. Figure 11 shows this oscillation in a plot of flame front position as it varied with time during the limit burning test. Again the line drawn through the data is the least-squares fit to the data, and the slope of the line is the average spread rate of the flame. Figure 8(c) shows a picture of the limiting flame for the microgravity double thickness of fuel.

The quenched flame at 25 percent oxygen also oscillated prior to extinction. The flame propagated forward for 2.10 sec, at which time the slope of the oscillating spread went to zero and the flame began to retreat. The flame retreated slowly for another 2.33 sec before gas-phase extinction was observed. Since this was such a short time prior to the end of the drop, there was still some smoldering at the end of the microgravity time which began burning again upon impact. Extinction in microgravity was again caused by quenching.

5.1.4 Discussion of normal-gravity results for a double thickness of fuel.—The effect of ambient oxidizer concentration on a double thickness of fuel in normal gravity was investigated for oxygen concentrations from 100 percent to the observed extinction limit of 16.9 percent oxygen at 1 atm pressure.

The spread rates of the flame are plotted as a function of oxygen concentration in figure 12. The familiar nonlinear relationship is again indicated. The extinction limit is observed at a specific spread rate.

The flame shapes observed at the different oxygen concentrations varied considerably. The average visible flame length varied by a factor of 5.5, from 6.11 cm at high oxygen concentrations to 1.11 cm at the limit. The width varied by a factor of 2.0, from 2.11 cm at high oxygen concentrations to 1.03 cm at the limit. No standoff distances could be measured. All of the flames were observed to be closed-tipped because of the buoyant flows around the flame.

The flame color varied from almost whitish-blue at high oxygen concentrations to yellow and blue at lower oxygen concentrations. The flickering was very strong at high oxygen concentrations so that it was negligible near the extinction limit. Figure 8(d) shows the limiting flame for the normal-gravity double thickness of fuel.

In studying the spread rates at and near extinction, it was found that there was again no indication of oscillatory behavior for the normal-gravity flames. At extinction, the flame was observed to spread linearly for 2.66 sec, at which point the flame began to move away from the igniter wire and extinguished. Extinction was again caused by blowoff.

5.2 Effect of Gravity

In this section, the data from normal and low gravity for single and double thicknesses of fuel are compared to discuss the effect of gravity level on the flame spread process.

5.2.1 Comparison of normal-gravity and microgravity results for a single thickness of fuel.—The normal-gravity and microgravity flame spread rates as a function of oxygen concentration are plotted together in figure 13. At oxygen concentrations higher than roughly 40 percent oxygen, there is no appreciable difference in the flame spread rates in normal gravity and microgravity. However, at oxygen concentrations

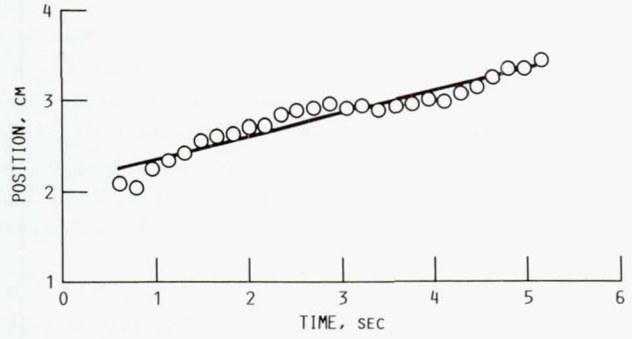

Figure 11.—Limit flame spread history for sample in microgravity, with double thickness of fuel.

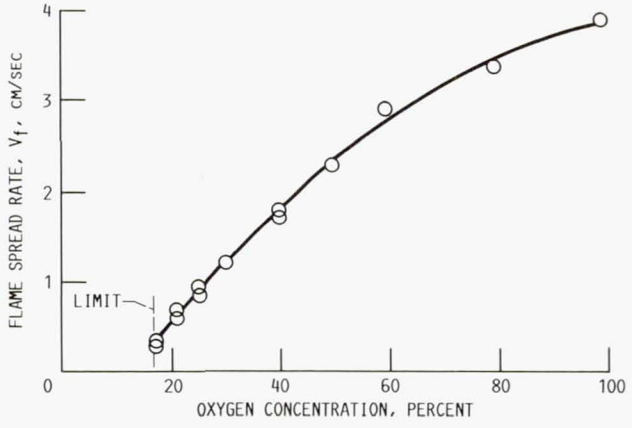

Figure 12.—Normal-gravity data for double thickness of fuel.

less than 40 percent oxygen, there is a definite difference in the flame spread rates. Thus it is concluded that, for this thin fuel and for oxygen concentrations higher than approximately 40 percent, gravity plays no significant role in the mechanism of flame spread.

Despite the fact that normal-gravity and microgravity flames spread at the same rate at the higher oxygen concentrations, there are some distinct differences in the flame shapes and colors in normal gravity and in microgravity. In microgravity the flames are roughly 1.5 times longer and wider than their normal-gravity counterparts. The microgravity flame does not flicker, and the reaction zone is more diffuse even at the higher oxygen concentrations. The flame tail becomes open at a high oxygen concentration, whereas the normal-gravity flames are always closed. If the leading edges of the flames are compared, however, it is observed that they are similar in overall shape and intensity in this region of the flame which controls the flame spread process.

For lower oxygen concentrations, however, there are distinct differences in the leading-edge regions of normal-gravity and microgravity flames. Figure 14 shows microgravity flames and their normal-gravity counterparts for 30 and 21 percent oxygen. The microgravity flame standoff distance is much larger than the corresponding normal-gravity flame standoff distance. The blue reaction zone of the microgravity flames

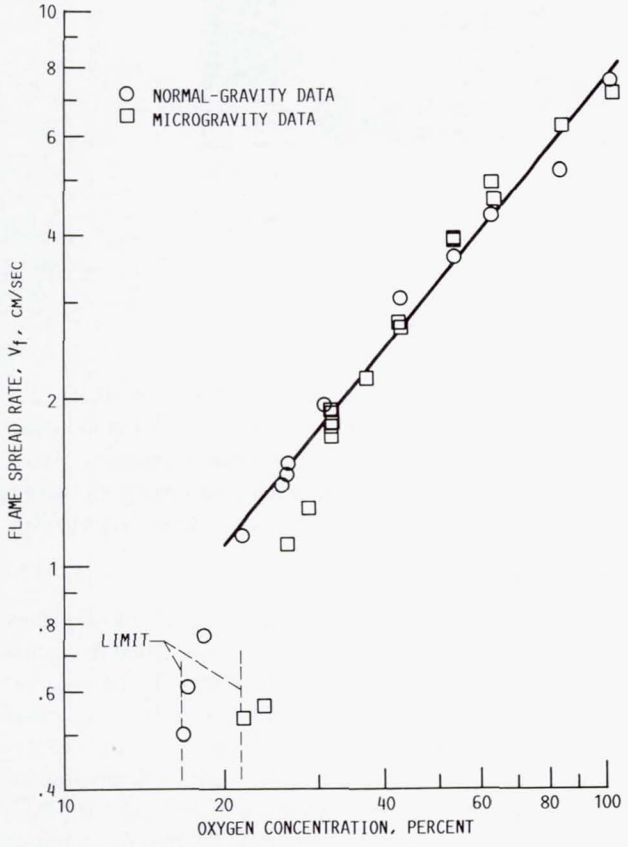

Figure 13.—Normal-gravity and microgravity data for single thickness of fuel.

is much thicker and yet is more diffuse than the blue reaction zone on the normal-gravity flames.

Because of these differences in the region of the flame which controls the spread process, it is not surprising that normal-gravity and microgravity flames spread at different rates at lower oxygen concentrations. Although the normal-gravity data show a shallow decrease in spread rate with decreasing oxygen concentration, the microgravity data show a sharper decrease in spread rate with decreasing oxygen concentration, and the flame extinguishes at a higher oxygen concentration than the normal-gravity flame. It is interesting to note that the flame spread rates at extinction for normal-gravity and microgravity flames are similar, although this could be coincidental.

The difference in the two flame spread rates at low oxygen concentrations indicates that there is clearly an important effect of gravity on the flame spread process at the lower oxygen concentrations. The primary role of gravity in flame spread is that caused by the buoyancy-induced flow on the flame.

In normal-gravity, opposed-flow flame spread, the relative motion of the flame with respect to the oxidizer is the gravity-induced velocity plus the flame spread rate, as shown in figure 1(b). In a low-oxygen environment, where the flame spread rate is small, the gravity-induced velocity dominates the flame spread. By comparison, the relative motion between the flame and the oxidizer environment in microgravity is the flame spread rate, which is an order of magnitude smaller than the normal-gravity relative motion.

The smaller relative velocity in microgravity affects the flame in two ways. First, in appearance, the flame standoff distance (quenching distance) from the paper fuel is much larger in microgravity than in normal gravity. Second, because of the larger flame standoff distance, the heat flux from the flame to the fuel is much smaller in microgravity than in normal gravity. Consequently, the heat release per unit area of fuel surface per time becomes small, which in turn makes heat losses such as radiation increasingly important.

When the relative velocity between the flame and the ambient oxidizer becomes small enough, the flame temperature drops because the reaction rate is decreased. A quenching extinction is caused when the temperature becomes too low, as suggested by previous theoretical analyses (refs. 5, 29 to 31). This explanation of the quenching extinction also offers an understanding of why the microgravity extinction limit is at a higher oxygen concentration than the normal-gravity extinction limit. The higher velocity buoyant flow acts to stabilize the flame in an oxygen environment where, in the absence of gravity, the flame extinguishes.

Because of these different extinction limits, the near-limit flame spread behavior in normal gravity and microgravity is also different (fig. 13). When the oxygen concentration is above 40 percent, the flame spread rate in microgravity becomes sufficiently fast that the heat loss effect becomes negligible, and the flame spread rates in normal gravity and microgravity become comparable.

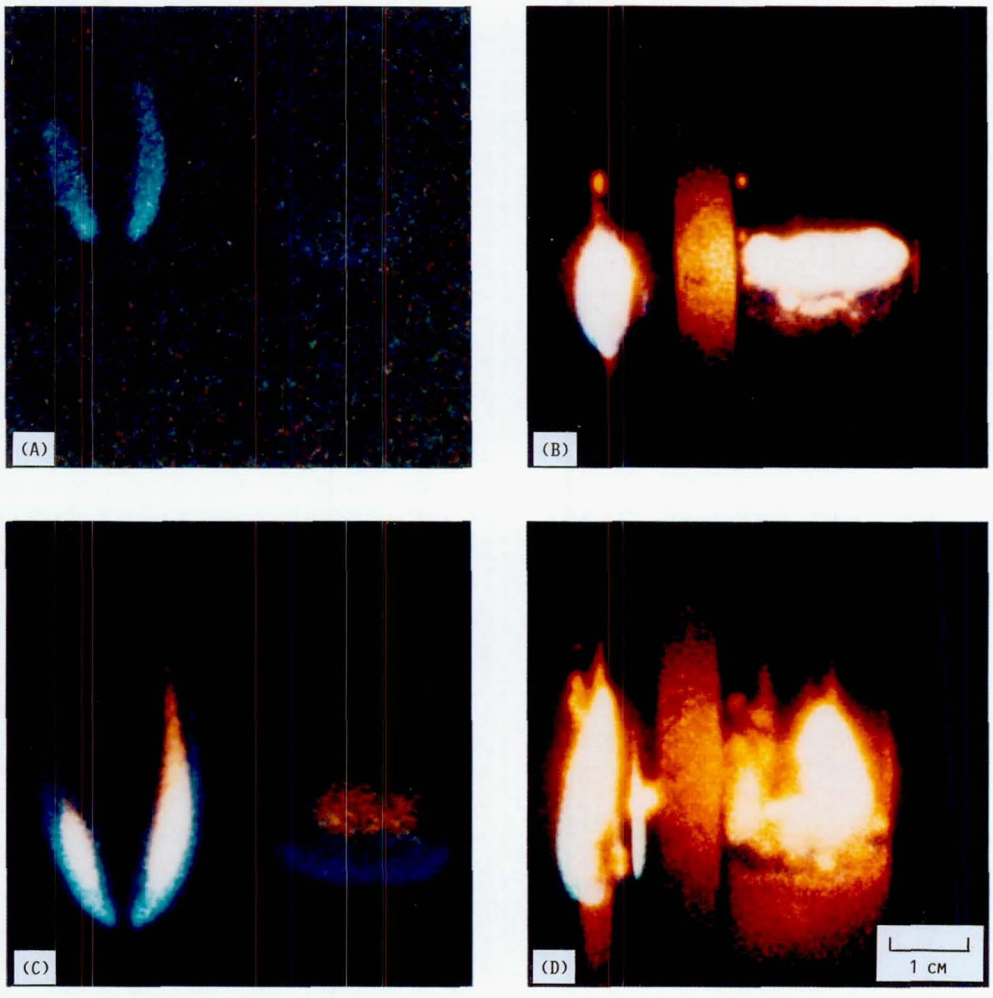

(a) Microgravity, 21 percent oxygen.
(b) Normal gravity, 21 percent oxygen.
(c) Microgravity, 30 percent oxygen.
(d) Normal gravity, 30 percent oxygen.

Figure 14.—Comparison of normal-gravity and microgravity flame shapes for single thickness of fuel.

5.2.2 Comparison of normal-gravity and microgravity results for a double thickness of fuel.—The normal-gravity and microgravity flame spread rates as a function of oxygen concentration are plotted together in figure 15. Again the two curves become one at oxygen concentrations higher than roughly 50 percent oxygen. Thus, for flames spreading in greater than 50 percent oxygen environments, there is no effect of gravity on the flame spread mechanism.

It is again observed that the leading-edge region of normal-gravity and microgravity flames is similar in overall shape and intensity at oxygen concentrations greater than 50 percent. For lower than 50 percent oxygen concentrations, however, some distinct differences in the two leading-edge regions become apparent. The blue reaction zone in microgravity becomes much thicker than the normal-gravity reaction zone, and it moves farther from the fuel surface. Thus, as for the single thickness of fuel, the characteristic length for gas-phase heat conduction is much greater in microgravity, which indicates that conductive heat transfer is reduced in microgravity. Again it is interesting to note that the flame spread rates at extinction for the normal-gravity and microgravity flames are similar.

5.3 Effect of Fuel-Bed Thickness

In this section, the data for the single and double thicknesses of fuel tests in normal and low gravity are compared to discuss the effect of fuel-bed thickness on the flame spread process.

5.3.1 Comparison of microgravity results for single and double thicknesses of fuel.—The microgravity spread rates for single and double thicknesses of fuel as a function of oxygen concentration are plotted together in figure 16. Both curves show the same general trend, but the double thickness curve drops more steeply and extinguishes at a higher oxygen

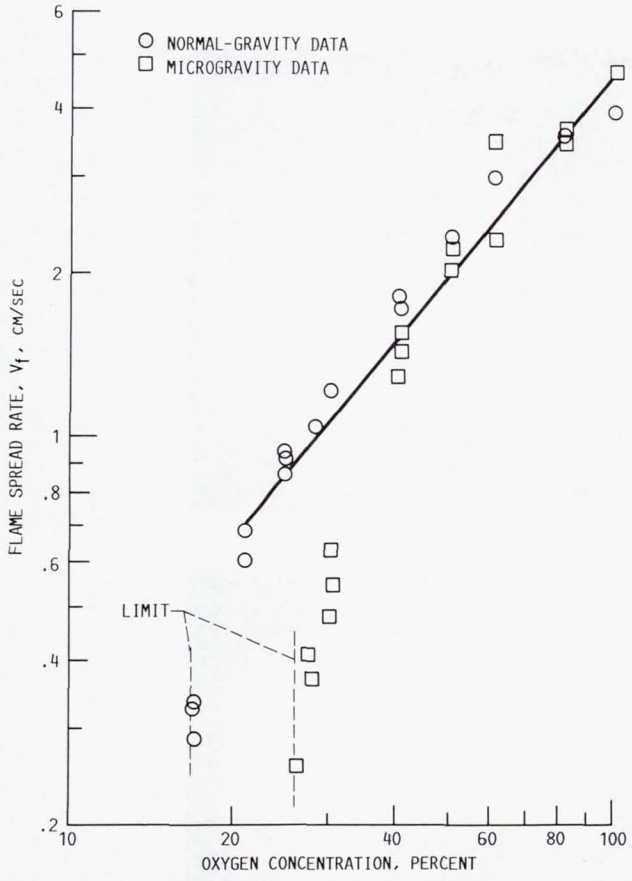

Figure 15.—Normal-gravity and microgravity data for double thickness of fuel.

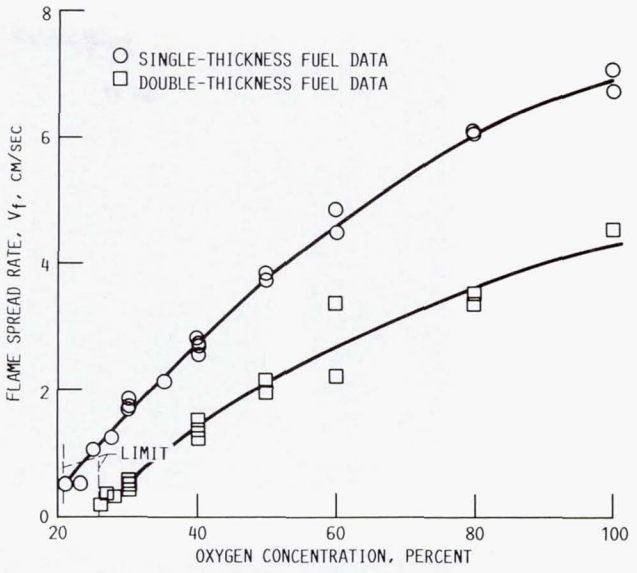

Figure 16.—Microgravity data for single and double thicknesses of fuel.

concentration than the single thickness curve. The spread rate for the single-thickness fuel was not quite twice that of the double-thickness fuel at the higher oxygen concentrations. However, as the oxygen concentration decreased below 40 percent, the flame spread rate of the double-thickness fuel dropped rapidly, so that at the limit of the double-thickness fuel the spread rate of the single-thickness fuel was more than four times that of the limiting spread rate for the double-thickness fuel. This is discussed further in section 6.0.

The extinction process appears to occur in the same manner for both thicknesses in microgravity. The closed-tail flame at high oxygen concentrations transitions to an open-tail flame as the oxygen concentration is reduced; for the double thickness this occurs at 80 percent oxygen, for the single thickness at 60 percent oxygen. As the oxygen concentration continues to decrease, the blue leading-edge region begins to enlarge as the soot region becomes smaller and less bright. Below a specific oxygen concentration, called the soot limit, the flames become completely blue; for the double thickness, this occurred at 40 percent, for the single thickness, at 30 percent.

Figure 17 shows flames at 30 and 40 percent oxygen for both single and double thicknesses of fuels. Comparing the single- and double-thickness flames at 30 percent, it can be seen that the single-thickness flame is a brighter blue and still sustains a soot region. This suggests that the single-thickness flame has a higher flame temperature than the double-thickness flame. One can conclude that the higher flame spread rate of the single-thickness fuel strengthens the flame just as the buoyant flow sustained the normal-gravity flame while the microgravity flame extinguished. Further decreases in the oxygen concentration caused the flame to move farther from the fuel surface until extinction was observed; for the double-thickness flame, this occurred at 26 percent, for the single thickness at 21 percent. In both cases the oscillatory flame spread was observed near extinction, and the flames were seen to retreat back toward the igniter wire just prior to extinction.

Flame lengths for the single thickness of fuel were slightly longer than flame lengths for the double thickness, and the difference became larger near the extinction limit for the double thickness of fuel. Flame widths were similar in the two cases, but flame standoff distances were roughly twice as large for the double thickness of fuel for the near-extinction flames where the standoff could be measured.

5.3.2 Comparison of normal-gravity results for single and double thicknesses of fuel.—The normal-gravity spread rate results for single and double thicknesses of fuel are plotted together as a function of oxygen concentration in figure 18. The single-thickness flame spread rate is not quite twice that of the double-thickness flame spread, which is the same ratio as that observed for the microgravity results at the higher oxygen concentrations. This is discussed further in section 6.0.

In normal gravity the extinction process occurs in the same manner for both the single and double thicknesses of fuel. The whitish-blue strongly flickering flame at the high oxygen concentrations turns more yellow, shrinks in size, and flickers less strongly as the oxygen concentration is reduced. As the extinction limits are approached, the flickering becomes very

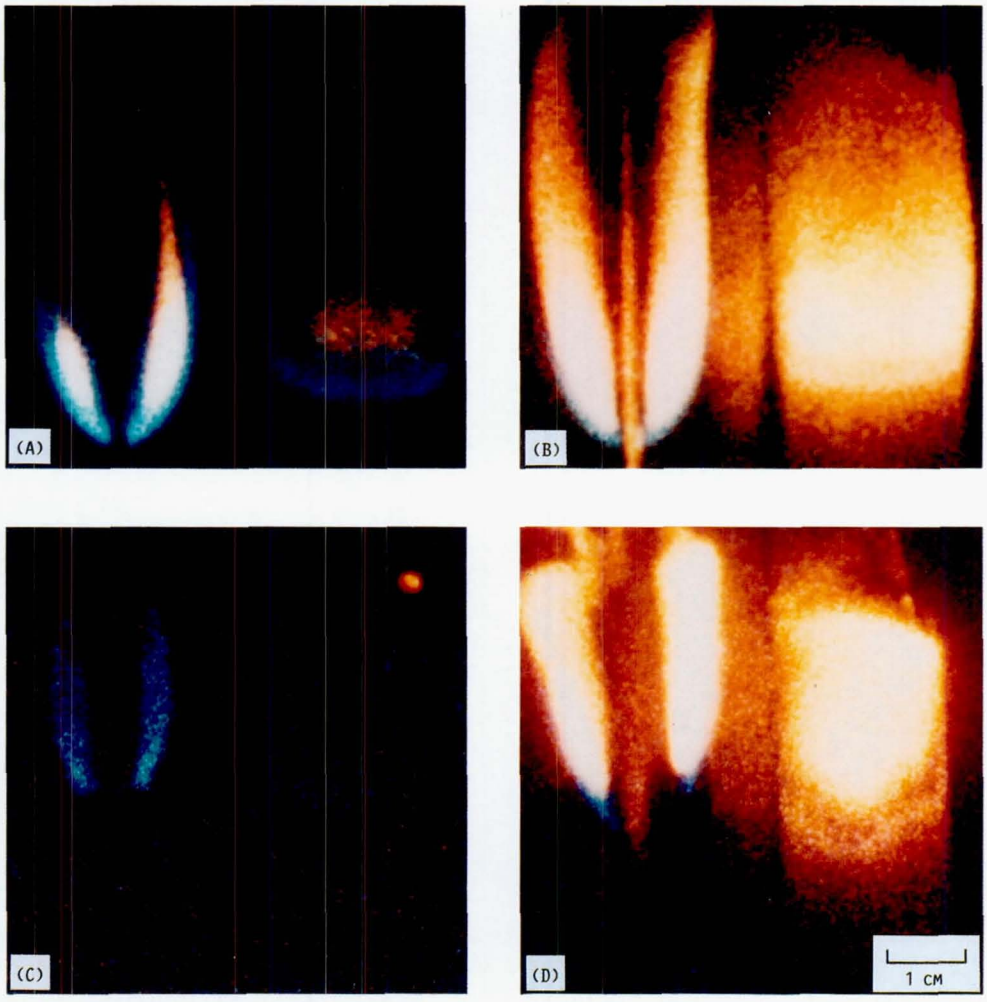

C-87-09959

(a) Single thickness of fuel, 30 percent oxygen.
(b) Single thickness of fuel, 40 percent oxygen.
(c) Double thickness of fuel, 30 percent oxygen.
(d) Double thickness of fuel, 40 percent oxygen.

Figure 17.—Microgravity flames at 30 and 40 percent oxygen for single and double thicknesses of fuel.

weak, and the blue region of the flame grows as the soot region becomes very small. At the extinction limit the flames spread only roughly 1 cm beyond the igniter wire before extinguishing. The flame spread rate decreases from a linear spread to zero spread very uniformly, with no indication of the oscillatory behavior observed in the microgravity extinction.

Flame lengths for the single thickness of fuel are slightly shorter than the flame lengths for the double thickness of fuel. The same is true for the flame widths. No comparison of standoff distances is possible.

5.4 Discussion of Extinction Mechanism

It is noted that there are large differences in the oxygen concentration at which extinction occurs for the single and double thicknessess of fuel in microgravity. In normal gravity, however, there is little difference in the oxygen concentration at which extinction occurs for the two thicknesses. The heat-

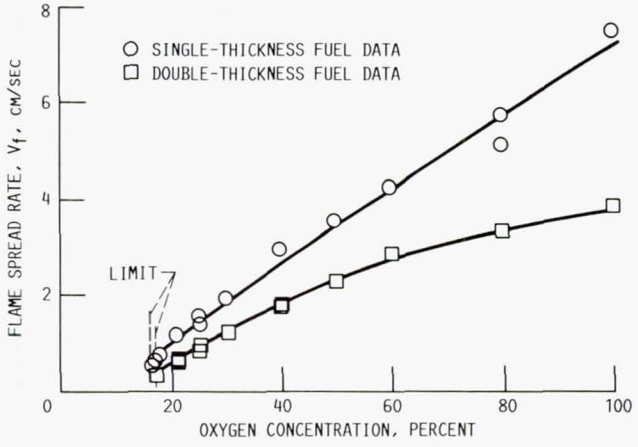

Figure 18.—Normal-gravity data for single and double thicknesses of fuel.

loss mechanism discussed in section 5.2.1 can be used to explain this difference in normal gravity and microgravity behavior.

In microgravity, the relative velocity between the flame and the oxygen environment is the flame spread rate. Since the spread rate is very small near the extinction limit, heat losses become important. The double-thickness flame spread rate is lower than the single-thickness flame spread rate at any given oxygen concentration. This means that heat losses are more important to the near-limit double-thickness flame, and its flame temperature is also lower than the single-thickness flame. This lower temperature results in a quenching extinction at a higher oxygen concentration.

On the other hand, in normal gravity, the buoyancy-induced velocity is much greater than the flame spread rate of either the single or the double thickness of fuel. The buoyant velocity is also nearly the same in the two cases, so blowoff extinction occurs at almost the same oxygen concentration for both thicknesses of fuel. This result supports previous experimental observations that blowoff is independent of fuel-bed thickness.

6.0 Comparison of Data With Other Data and Theories

6.1 Experimental Correlations

In this section, the data obtained from this work are compared with correlations used in previous experimental works. The appropriateness of the correlation and the fit of the data to that correlation are discussed.

6.1.1 Power-law relation between spread rate and percent oxygen.—McAlevy, Magee, and Lastrina (refs. 8 to 10) performed many normal-gravity experiments on downward flame spread over thermally thin fuels. They correlated the measured spread rates as a power law of the ambient oxidizer concentration and found that the flame spread rate varies nearly linearly with oxygen concentration.

To compare the data from this work with the previous data, the flame spread rates were plotted logarithmically against oxygen mole fraction. The resulting curve for normal-gravity and microgravity data for a single thickness of fuel is shown in figure 13. As can be seen from the curve, far from the extinction limits, a power law does seem to correlate the data in both normal and low gravity. The slope of the line for the normal-gravity data from 100 to 21 percent is 1.18, and the slope of the line for the microgravity data from 100 to 40 percent is 1.11. These slopes are the exponents in the power-law relation between flame spread rate and oxygen mass fraction, so this data also demonstrates a nearly linear relationship far from the extinction limits. Near the extinction limits, however, the functional relation changes, and the power-law correlation no longer fits the data.

The spread rate data for the double thickness of fuel in normal gravity and in microgravity is also correlated by using the power-law correlation in figure 15. As with the single-thickness data, the spread rates far from the extinction limit exhibit a nearly linear relationship with oxygen mole fraction. For the microgravity data from 100 to 50 percent, the power exponent is 1.11, as is the normal-gravity data exponent from 100 to 25 percent. Near the observed extinction limits the spread rate again departs from the power-law correlation.

The fact that the normal-gravity and microgravity power-law correlation exponents are very close for the normal- and low-gravity data for both thicknesses of fuel is further evidence that gravity is not playing a substantial role in the flame spread process away from the extinction limit. Near extinction, however, both sets of data demonstrate that gravity does begin to play a role.

It is interesting to note that the departure from the power-law correlation occurs not only in microgravity but in normal gravity as well. This deviation from linearity has also been observed near the extinction limit in normal gravity by Frey and T'ien (ref. 13), and is explained as being due to excessive heat losses to the sides of the holder (in that instance they were using a much narrower sample). In this work, however, the heat losses are believed to be from different sources. In microgravity, as explained in section 5.0, heat losses such as radiative loss from the fuel surface are believed to be the cause of the departure from the power-law correlation. In normal gravity, convective heat losses become important near the extinction limit and cause the nonlinearity. Thus the power-law correlation is applicable only far from the extinction limit, where the heat losses which inevitably cause extinction are not important.

The basic validity of the power-law correlation in improving the fundamental understanding of flame spread is questionable because it is based on stringent assumptions as to the form of the solid-phase pyrolysis rate. Nevertheless, it does give an explicit dependence of flame spread rate on ambient oxygen concentration for which none of the other theories to date can account. Because of this, its usefulness as a guideline to predicting spread rates is unchallenged.

6.1.2 Correlation of normal-gravity and microgravity data with elevated-gravity data.—Altenkirch (ref. 14) obtained flame spread data at elevated gravity levels by using a centrifuge. In order to compare the flame spread data obtained in this work with Altenkirch's data, which use a different thickness of fuel, the de Ris expression for the flame spread rate was used.

Altenkirch conducted tests at 21 percent oxygen and at 50 percent oxygen at 1 atm pressure for two cellulosic fuels of different thicknesses. The thinner fuel was paper tape with a half thickness of 0.0043 cm and an area density of 2.890×10^{-3} g/cm^2. The thicker fuel was an index card with a half thickness of 0.0098 cm and an area density of 7.381×10^{-3} g/cm^2. The relevant flame spread data are contained in table I. It should be pointed out here that a blowoff extinction limit was observed for the thicker fuel in air at elevated gravity levels above four times normal earth gravity.

The de Ris formula (eq. (2.2.1)) predicts that there is an inverse relation between flame spread rate and fuel-bed half-thickness or area density. Since the area density characterizes the fuel more accurately, it will be the quantity used to make the comparison between the measured spread rates from this work and those for elevated gravity levels. To "correct" the data from reference 14, the following equation was used, which is simply a ratio of the absolute spread rate to the corrected spread rate equated to the inverse ratio of the area densities from this work and from that of Altenkirch.

$$V_{f,\text{corrected}} = V_f \frac{(\rho\tau)_{\text{this work}}}{(\rho\tau)_{\text{Altenkirch}}} \tag{6.1.2a}$$

To test the ratio method of correcting spread rate data, the data for the thinner fuel used by Altenkirch were corrected to compare with the observed spread data for the thicker fuel. The corrected flame spread data is also contained in table I. The values corrected by using this ratio method compared very well with the measured spread rates for the thicker fuel, with a maximum error of 6 percent.

In addition, the normal-gravity data for all four conditions, as well as the microgravity data for 50 percent oxygen (recall that experimental results from this work indicated that there was no effect of gravity on the flame spread rate at this higher oxygen concentration), were compared with Altenkirch's data for both thicknesses and oxygen concentrations, also with good results. These data are contained in table II. The maximum error is 9 percent for the 50 percent oxygen, index card data, where all four spread rates are assumed to represent the same spread rate and their average is compared to the corrected spread rate for index cards at those conditions. The error is reasonable when the combined errors of the two measurements are considered.

The microgravity spread rate data for a single thickness of fuel in air is plotted with the corrected elevated-gravity data for both index cards and paper tape in figure 19. It can be seen that, except in microgravity, the flame spread rate drops with increasing gravity level, which also corresponds to an increasing buoyant velocity. The buoyant velocity used to calculate the characteristic velocity at elevated gravity levels was calculated by using a modified version of an equation derived by Altenkirch (ref. 14), which is

$$V_b = 7.4 \left[\frac{\nu g \, \Delta H_c m_{\text{ox},\infty}}{T_\infty i C_p} \right]^{1/3} \tag{6.1.2b}$$

The additional factor of 7.4 in the equation comes from a matching of the calculated buoyant velocity at blowoff as reported in reference 14 with the forced convection blowoff in air as reported in reference 18. Other property data are given in table III. The characteristic velocity in microgravity is the flame spread rate itself.

Figure 19 shows the entire range of flammability for a thin fuel; at high buoyant velocities a blowoff limit is reported by Altenkirch, and in microgravity, air is observed to be the limiting oxygen concentration for sustained spread. The maximum flame spread rate is observed to be at normal gravity; in microgravity the flame spread rate has dropped off. The question arises whether normal gravity is truly the optimum gravity level (i.e. buoyant flow environment) to maximize flame spread, or whether the flame spread rate continues to increase at lower characteristic velocities until it drops sharply at the extinction limit. The curve in figure 19 represents a second-order, least-squares fit to the data. The uncertainty in the shape of the curve can only be answered through further microgravity research on flame spread with opposed flow.

6.1.3 Comparison of extinction limits.—Three specific extinction limits are identified in this work: a normal-gravity, buoyancy-induced blowoff limit, which is essentially independent of fuel thickness, and two microgravity, fuel-thickness-dependent quenching limits. Figure 20 plots these limits as oxygen concentration as a function of characteristic velocity. In addition, normal-gravity, forced-convection blowoff data from reference 18 is plotted. The resulting curve represents an extinction boundary for flame spread over a thin fuel. The normal-gravity blowoff data, if it were extrapolated to low characteristic velocities, would not predict the presence of the observed quenching extinction branch. When the normal-gravity data is extrapolated to fit the microgravity data, however, a two-branch extinction boundary is defined. The meeting of the quenching and blowoff extinction branches occurs at a minimum oxygen concentration which represents a fundamental flammability limit for a thin fuel. This fundamental flammability limit corresponds to a characteristic velocity below that induced in normal gravity. This means that thin fuels are actually more flammable in low convective environments in microgravity than they are in normal gravity.

TABLE I.—COMPARISON OF ELEVATED-GRAVITY FLAME SPREAD DATA USING A RATIO OF AREA DENSITIES

Ratio of gravity levels, G/G_e	Flame spread rate, V_f, cm/sec		
	Paper tape[a]	Corrected paper tape for comparison with index card	Index cards[a]
1.0	0.396	0.155	0.154
1.5	.358	.140	.145
2.0	.363	.142	.134
2.5	.324	.127	----
3.0	.307	.120	----
3.5	.298	.117	.115
4.0	.285	.112	.112
4.25	----	----	Extinction

[a]Data from reference 14.

TABLE II.—COMPARISON OF CORRECTED NORMAL-GRAVITY AIR DATA AND NORMAL-GRAVITY AND MICROGRAVITY 50 PERCENT OXYGEN DATA

[Normal-gravity data from ref 14.]

Oxygen concentration, percent	Ratio of gravity levels, G/G_e	Fuel-bed half-thickness, τ, cm	Flame spread rate, V_f cm/sec	Corrected flame spread rate, $V_{f,corrected}$, cm/sec	Flame spread rate,[a] V_f, cm/sec	Ratio of gravity levels, G/G_e	Fuel-bed half-thickness, τ, cm
21	1	0.0038	1.12	0.39	0.396	1	0.0043
	1	.0038	1.12	.152	.154	1	.0098
50	0	0.0038	3.84	1.33	----	--	-----
	1	.0038	3.57	1.24	----	--	-----
	0	.0076	2.10	1.45	----	--	-----
	1	.0076	2.28	1.57	----	--	-----
Average	--	0.0043	----	1.40	1.498	1	0.0043
50	0	0.0038	3.84	0.52	----	--	-----
	1	.0038	3.57	.48	---	--	-----
	0	.0076	2.10	.57	----	--	-----
	1	.0076	2.28	.62	----	--	-----
Average	--	0.0098	----	0.55	0.602	1	0.0098

[a]Data from reference 14.

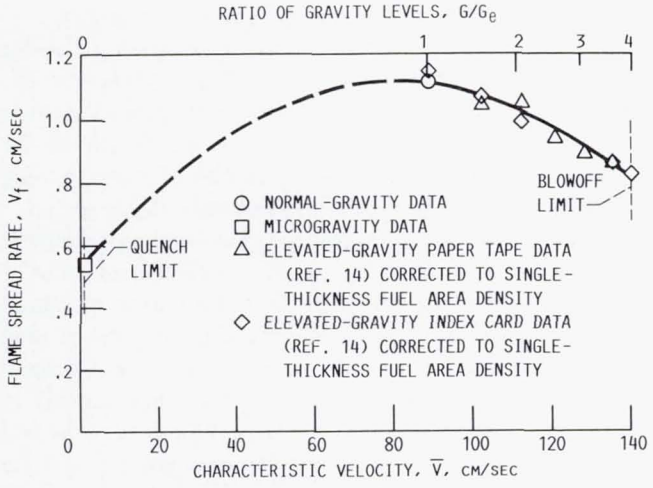

Figure 19.—Comparison of elevated-gravity and microgravity data in air.

6.2 Comparison With Theoretical Predictions

In this section, the data obtained from this work are compared with theoretical predictions of functional dependencies to determine, when possible, the accuracy and range of validity of the particular theory.

6.2.1 Comparison with de Ris theory.—As indicated in section 6.1.2, the thermal theory published by de Ris (ref. 2) predicts that the flame spread rate for a thermally thin fuel is inversely proportional to the fuel-bed half-thickness or its area density, if all other parameters in equation (2.2.1) remain constant. The spread rate data obtained in this work for single and double thicknesses of fuel are compared with this simple theory.

TABLE III.—PROPERTY DATA USED IN CALCULATIONS

Quantity	Value	Reference
Fuel-bed density, ρ_s, g/cm^3	0.263	This work
Gas-phase kinematic viscosity, ν, cm/sec	0.157	3
Heat of combustion, ΔH_c, cal/g	4×10^3	3
Ambient temperature, T_∞, K	300	This work
Oxygen-to-fuel mass ratio, i	1.185	15
Gas-phase heat capacity, C_p, cal/g K	0.240	3
Gas-phase thermal conductivity, λ, cal/sec cm K	6.16×10^{-5}	3
Flame temperature, T_f, K	f(percent 0_2)	15
Thermal diffusivity, α, cm^2/sec	f(percent 0_2, T_f)	32
Vaporization temperature, T_{vap}	618	13
Activation energy for pyrolysis rate law, E_s, cal/gmol	30×10^3	3
Preexponential factor for pyrolysis rate law, A_s, l/sec	1×10^{10}	3

A ratio of normal-gravity and microgravity flame spread rates for the single and double thicknesses of fuel is plotted as a function of oxygen concentration in figure 21. The dashed line indicates the predicted value of 2 for this ratio based on the thermal theory. As can be seen, in normal gravity for all oxygen concentrations and in microgravity for oxygen concentrations higher than 40 percent, the ratio is slightly lower than theory would predict by a maximum of 15 percent. This is of the same magnitude as the error in the spread rates

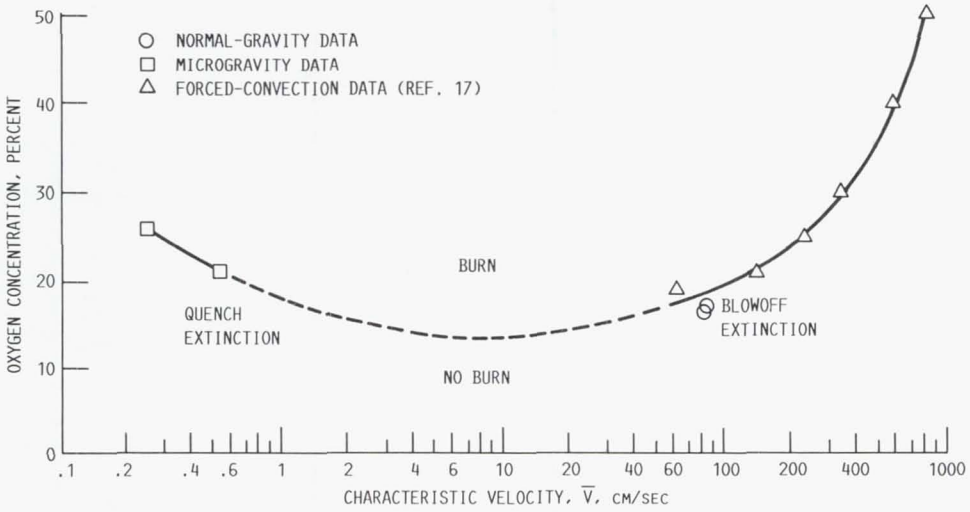

Figure 20.—Extinction boundary for flame spread over a thin fuel.

themselves, and thus the theory appears to be valid for these conditions. The reason that all of the data fall lower than the predicted value of two is because the double thickness of fuel is actually two single thicknesses of fuel imperfectly joined together. The resulting spread rate for the double thickness of fuel is thus slightly higher than it would be were a single piece of thicker fuel used, and so the overall ratio is lower.

In microgravity, for oxygen concentrations less than 40 percent, however, there is a clear divergence from theory indicated. As the extinction limit is approached in microgravity, the ratio of flame spread rates increases and actually goes to infinity at oxygen concentrations less than 26 percent oxygen (the extinction limit for the double thickness of fuel).

The explanation of why the thermal theory does not predict flame spread behavior near the extinction limit is clear when the mechanism of flame spread near extinction is understood. The thermal theory neglects finite-rate chemistry. When finite-rate chemistry becomes important, the flame temperature decreases. The thermal theory assumes a constant flame temperature and thus does not describe the heat balance in the near-limit microgravity flame properly.

6.2.2 Appropriateness of characteristic length.—In nondimensionalizing the governing equations for flame spread, a characteristic length is frequently used as defined by $l^* = \alpha/\overline{V}$, where $\overline{V}$ is the flame spread rate in microgravity plus the buoyant velocity V_b as defined in equation (6.1.2b). To test if this is of the correct scale, a comparison is made here of the value of l with the half-standoff distance as measured from the flames in normal gravity and in microgravity.

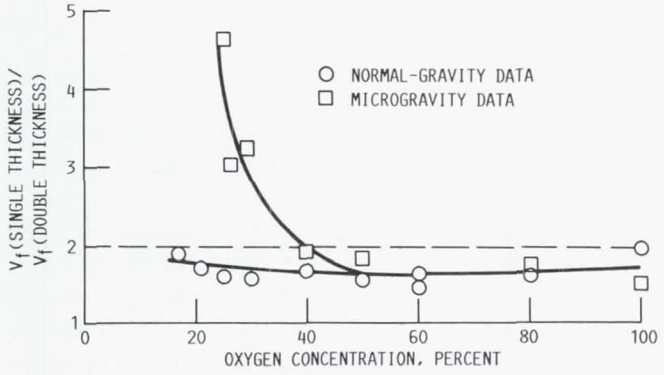

Figure 21.—Effect of thickness on flame spread rate V_f.

For those oxygen concentrations where the standoff distance b could be measured, values of l^* and $b/2$ are listed in table IV. The normal-gravity, half-standoff distance is of the same order of magnitude as the calculated characteristic length, so the scaling used in the nondimensionalization of the governing equations is appropriate for normal-gravity flame spread.

It is observed, however, that the calculated characteristic lengths for the microgravity data are more than an order of magnitude greater than the half-standoff distances measured in this work. This is a clear indication that the scaling frequently used in the nondimensionalization of the governing equations is not appropriate to model flame spread in microgravity. In microgravity the large difference in the fuel and oxidizer diffusivities becomes more important, and the approximation of unity Lewis number is no longer good. A different scale must be used, but an appropriate characteristic length for microgravity flame spread needs to be determined.

Comparing 30 percent oxygen data from table IV for single- and double-thickness fuel samples, it is noted that the standoff distance b for the double-thickness fuel is roughly twice that of the single-thickness fuel. This indicates that the standoff distance is a good experimental measure of the characteristic length of the experiment. This also shows that the inverse relation of characteristic length with characteristic velocity is reasonable. It is suggested here that a diffusion coefficient might be more appropriate than the thermal diffusivity in the equation for l^* because, for this nonunity Lewis number gas-solid system, the diffusion length is more representative of the scale of the experiment than is the thermal length.

TABLE IV.—COMPARISON OF CALCULATED CHARACTERISTIC LENGTH WITH MEASURED HALF-STANDOFF DISTANCES

Fuel-bed half-thickness, τ, cm	Oxygen concentration, percent	Characteristic length, l^*, cm	Half-standoff distance, $b/2$, cm	$l^*/(b/2)$
0.0076	[a]16.5	0.032	0.085	0.376
0.0076	21	6.76	0.245	27.6
	23	6.51	.23	28.3
	25	3.66	.19	19.3
	27.5	3.52	.13	27.1
	30	2.69	.105	25.7
	40	2.48	.075	33.1
0.0152	26	18.68	0.275	67.9
	27	10.86	.30	36.2
	28	12.56	.285	44.1
	30	8.87	.25	35.5

[a]Indicates normal-gravity data.

6.2.3 Effect of Damkohler number on flame spread rate.—Based on the original theory of Frey and T'ien (ref. 3), the flame spread rate, nondimensionalized by using the limit spread rate as expressed by de Ris (eq. (2.2.1)), is plotted as a function of the Damkohler number as defined by

$$Da = \frac{\text{flow time}}{\text{chemical time}} = \frac{\dfrac{l^*}{\overline{V}}}{\dfrac{\rho_s}{\dot{w}_p}} \tag{6.2.3}$$

where $\dot{w}_p = \rho_s A_s \exp(-E_s/RT_{vap})$ is the pyrolysis rate.

In the expression for the Damkohler number Da, $\overline{V}$ is the characteristic velocity, and l^* is the characteristic length. The effect of the change in flame temperature on the chemical reaction time is not contained in the definition of the Damkohler number. The characteristic length is taken to be one half of the flame standoff distance in microgravity, but in normal gravity $l^* = \alpha/\overline{V}$ is used. The characteristic velocity is taken to be the buoyant velocity plus the flame spread rate in normal gravity or just the flame spread rate in microgravity. The other property data used are found in table III.

Figure 22 plots nondimensional spread rate as a function of the Damkohler number. The normal-gravity data show the previously observed trend of increasing nondimensional spread rate with increasing Damkohler number. The values of nondimensional spread rate approach the expected maximum of unity as would be expected.

The microgravity data, however, show the opposite trend. As the Damkohler number increases, the nondimensional spread rate decreases from near unity. A similar nonmonotonic behavior with the Damkohler number has been predicted in previous theories with nonpropagating flames (refs. 5 and 29) and is believed to be the result of thermal loss. As the quenching limit is approached, the results for the single and double thicknesses of fuel diverge, and quenching extinction occurs at two different Damkohler numbers for the two thicknesses of fuel. Figure 22 thus clearly demonstrates that the Damkohler number cannot be the only nondimensional parameter used to characterize flame spread and extinction. An additional nondimensional parameter (such as a radiative loss parameter) would be needed in the low-velocity (high Da) regime.

This trend in the microgravity data indicates that there is an upper quenching limit to values of the Damkohler number for which steady flame propagation is observed for a given thickness of fuel, as well as a lower limit at high opposed-flow velocities where extinction occurs because of blowoff. The blowoff limit is independent of fuel thickness. The upper quenching limit has never been observed experimentally before for solid-fuel flame spread, because in normal gravity the maximum Damkohler number is fixed by the minimum buoyant flow velocity.

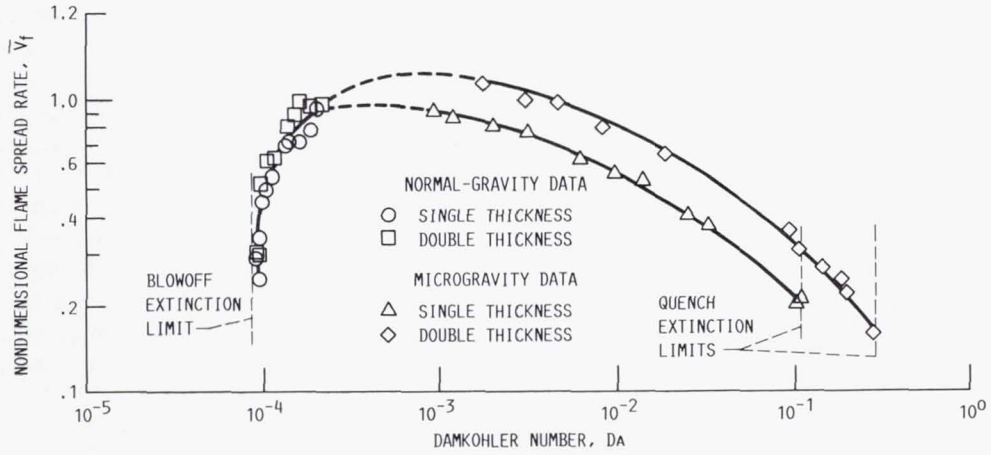

Figure 22.—Nondimensional spread rate as function of Damkohler number.

7.0 Conclusions and Recommendations for Further Research

7.1 Conclusions

A flame spreading over a thin solid fuel in normal gravity and in microgravity was studied over a wide range of oxygen concentrations and for two different fuel thicknesses. The experiments were conducted at the NASA Lewis Research Center 2.2-sec Drop Tower and 5.18-sec Zero Gravity Facility.

Flame spread rates vary nonlinearly with oxygen concentration for both thicknesses of fuel in normal gravity and in microgravity. Gravity was found to influence the flame spread for oxygen concentrations of less than 50 percent. The normal-gravity flames were spread more rapidly than the microgravity flames at these lower oxygen concentrations because gravity sets up buoyant flows opposing the flame spread and feeds fresh oxidizer to the flame. This fresh oxidizer allows the normal-gravity flame to be stabilized closer to the fuel surface than the microgravity flame, which increases the heat transfer to the fuel. In microgravity the velocities are much slower, and thus for low oxygen concentrations finite-rate chemistry and heat losses to the environment become important. For oxygen concentrations greater than 50 percent oxygen, the spread rate is independent of gravity.

The extinction limits for both thicknesses of fuel were determined in both normal gravity and in microgravity. The normal-gravity extinction limits are close for both thicknesses of fuel at 16.5 and 16.9 percent oxygen. Blowoff extinction occurs at approximately the same oxygen concentration because the buoyant flow for the two flames is similar; therefore, blowoff extinction is independent of fuel-bed thickness.

In microgravity the extinction limits occur at much higher oxygen concentrations, and there is a significant difference in the limits for the two thicknesses. The single thickness of fuel quenches at 26 percent oxygen. The fact that flames extinguish at higher oxygen concentrations in microgravity than in normal gravity indicates that the buoyant flow in normal gravity, which provides fresh oxidizer to the flame, stabilizes the flame at oxygen concentrations where microgravity flames in a quiescent environment cannot exist. The double thickness of fuel quenches at a higher oxygen concentration than the single thickness of fuel because the flame spreads more slowly at a given oxygen concentration and generates less heat per unit time. It is thus more sensitive to heat losses such as radiation. Therefore quenching extinction is a function of the fuel-bed thickness, even for thermally thin fuel.

The thickness of the fuel sample influences the flame spread rate in both normal gravity and in microgravity. In normal gravity the flame spread rate varies inversely with thickness, as predicted by the thermal theory of de Ris. This inverse relation is also observed in microgravity for oxygen concentrations greater than 50 percent oxygen, where gravity is found to be unimportant. For lower oxygen concentrations, however, a significant departure from this inverse relation is observed. The ratio of single- to double-thickness spread rates increases and goes to infinity near the extinction limits for the microgravity flames. Since finite-rate chemical kinetics are believed to be an important part of the flame spread near extinction, the thermal theory, which assumes infinite-rate kinetics, cannot describe the near-extinction flame spread process.

Comparisons were made of normal-gravity and microgravity flame spread data with the elevated-gravity flame spread data obtained by Altenkirch. The normal-gravity data obtained in this work shows good agreement with the normal-gravity data reported by Altenkirch when it was corrected to account for the difference in the fuel thicknesses. The microgravity data, when plotted with Altenkirch's corrected elevated-gravity data as a function of the gravity level or characteristic velocity, show that a maximum flame spread rate should exist between microgravity and normal gravity. This maximum indicates where the characteristic velocity of the system, which is a combination of the flame spread velocity and the buoyant velocity, optimizes the balance between heat losses and supply and removal of fresh oxidizer and combustion products.

Plotting extinction limit data from this work with forced convective blowoff data from reference 18 yields an extinction boundary for flame spread over a thin fuel. This extinction curve consists of a blowoff branch at high characteristic velocities, and a quenching branch at very low characteristic velocities. The two branches, which show opposite variations with velocity, should merge at a minimum oxygen concentration which corresponds to a fundamental flammability limit and which occurs at a characteristic velocity well below that induced by gravity.

The flame spread rates in normal gravity and in microgravity, nondimensionalized with the limiting flame spread rate from the thermal theory, are plotted as a function of the Damkohler number. The normal-gravity data show the appropriate trend of nondimensional flame spread approaching unity at increasing Damkohler numbers. The microgravity data, however, show the opposite trend. As the Damkohler number increases, the nondimensional spread rate decreases from near unity until extinction occurs.

This upper extinction branch at a large Damkohler number has not been observed previously because buoyant flows fixed the maximum Damkohler number obtainable in normal gravity. Additionally, the data for single and double thicknesses of fuel fall along separate curves, and the quenching limit at high Damkohler number is found to occur at different Damkohler numbers for the two thicknesses of fuel. These findings support the theoretical suggestion that Damkohler number alone is insufficient to describe the flame spread dependence on opposed-flow velocity when the relative velocity between the oxidizer and the flame becomes so small that thermal losses become important.

7.2 Recommendations for Further Research

This work provides some baseline data for the study of flame spread in microgravity. Many questions as to the controlling mechanisms of flame spread remain unanswered, and many new questions are surfacing as a result of this research.

Of particular interest and concern to NASA Lewis is the question of spacecraft fire safety. In the environment of spacecraft, ventilation systems provide a flow of fresh air to the astronauts, but undesirably would also provide fresh oxidizer flow to a flame. The results of this work clearly indicate that flow of oxidizer to the flame is critical to the stability of the flame in oxygen concentrations currently used and being considered for use in spacecraft. These same results suggest that there is a maximum flame spread hazard somewhere between normal-gravity buoyant flow and quiescent microgravity flow. Research into the effects of low-velocity forced convection on flame spread in microgravity is thus very important.

In order to better understand the mechanism of extinction in microgravity, the heat transfer processes of conduction, convection, and radiation need to be measured so that their relative importance in the extinction process can be quantified. Temperature measurements in the solid and gas phases are needed. Additionally, species concentration profiles around the leading edge of the flame will reveal much useful information concerning the gas- and solid-phase kinetics.

Acknowledgments

The author wishes to thank her thesis advisor James S. T'ien from Case Western Reserve University for his interpretation of data and questions concerning the flame spread process in microgravity. The author would also like to express her thanks to Jim Tressler and Ray Sotos for their development of the sample holder apparatus and modification of that apparatus to meet both the hardware and science requirements constraints.

Appendix A
Data Sheets

Tables A–I to A–IV contain the flame spread rate, length, width, and standoff distances as measured from the film of the experiments. Table A–I contains the data for the microgravity, single-thickness flame tests, and table A–II contains the normal-gravity data for this thickness. Double-thickness data for microgravity and normal gravity are contained in tables A–III and A–IV, respectively.

In some tests, because of insufficient light, overexposure of the film, or insufficient resolution, certain measurements could not be made. Microgravity flame spread rates which exhibited the oscillatory behavior discussed in section 4.8 are marked with a footnote. Flame dimensions in microgravity which were still clearly in transition at the end of the test time are also marked with a footnote.

Normal-gravity dimensions fluctuated a great deal because of flame flicker, but every attempt was made to measure a consistent time during the flicker process so that the flame lengths could be compared. The shape of the flame in normal gravity which most resembled the microgravity flame occurred during the low point in the flicker, and so the shortest length of the flame during the flicker was measured for comparison.

TABLE A–I.—FLAME SPREAD RATE AND DIMENSION DATA FOR SINGLE THICKNESS OF FUEL IN MICROGRAVITY

[0.0076-cm-thick sample.]

Oxygen concentration, percent	Flame spread rate, V_f, cm/sec	Average V_f, cm/sec	Flame length, L_f, cm	Flame width, W_f, cm	Standoff distance, b, cm
21	[a]0.53	0.54	[b]1.93	[b]1.57	0.49
	[a].55	----	----	----	----
	[a].54	----	----	----	----
23	[a]0.56	----	[b]1.92	[b]1.60	0.46
25	[a]1.09	----	[b]2.86	[b]1.91	0.38
27.5	1.26	----	[b]3.40	1.99	0.26
30	1.74	1.81	3.51	1.94	----
	1.81	----	3.43	1.97	----
	1.86	----	3.65	2.03	----
	1.72	----	3.35	1.87	----
	1.88	----	----	----	----
	1.84	----	4.50	2.21	0.21
35	2.17	----	----	3.95	----
40	2.63	2.73	----	----	----
	2.67	----	4.71	2.15	----
	2.85	----	4.51	2.13	----
	2.63	----	[b]5.64	[b]2.51	----
	2.86	----	[b]6.19	[b]2.30	----
	2.72	----	4.78	2.11	----
50	3.78	3.84	5.42	1.95	----
	3.89	----	5.93	[b]2.79	----
60	4.94	4.75	----	----	----
	4.55	----	6.44	2.71	----
80	6.11	6.12	----	----	----
	6.13	----	[b]8.83	3.03	----
100	7.09	6.92	[b]8.20	2.95	----
	6.74	----	6.66	2.82	----

[a]Oscillatory behavior observed.
[b]Dimension in transition at end of test time.

TABLE A–II.—FLAME SPREAD RATE AND DIMENSION DATA FOR SINGLE THICKNESS OF FUEL IN NORMAL GRAVITY

[0.0076-cm-thick sample.]

Oxygen concentration, percent	Flame spread rate, V_f, cm/sec	Average V_f, cm/sec	Flame length, L_f, cm	Flame width, W_f, cm	Standoff distance, b, cm
16.5	0.50	----	0.68	0.47	0.17
17	0.61	----	0.89	0.83	----
18	0.75	----	1.40	0.79	----
21	1.12	----	1.70	0.94	----
25	1.55	1.47	2.62	1.08	----
	1.39	----	----	----	----
	1.54	----	2.46	1.02	----
	1.38	----	----	----	----
30	1.92	----	2.29	1.02	----
40	2.97	----	2.77	1.20	----
50	3.57	----	2.90	1.36	----
60	4.28	----	4.50	1.46	----
80	5.18	5.46	5.60	1.87	----
	5.75	----	4.82	1.87	----
100	7.51	----	5.70	1.82	----

TABLE A-III.—FLAME SPREAD RATE AND DIMENSION DATA FOR DOUBLE THICKNESS OF FUEL IN MICROGRAVITY

[0.0152-cm-thick sample.]

Oxygen concentration, percent	Flame spread rate, V_f, cm/sec	Average V_f, cm/sec	Flame length, L_f, cm	Flame width, W_f, cm	Standoff distance, b, cm
26	[a]0.25	----	1.67	1.40	0.55
27	[a]0.40	----	1.83	1.36	0.60
28	[a]0.36	----	1.95	1.56	0.57
30	0.47 .63 .54	0.55 ---- ----	[b]3.42 2.43 2.10	1.66 1.60 1.68	0.55 0.49 0.47
40	1.42 1.29 1.55	1.42 ---- ----	3.69 3.01 ----	2.72 2.74 ----	---- ---- ----
50	2.00 2.19	2.10 ----	4.32 4.98	2.95 2.88	---- ----
60	2.26 3.42	2.84 ----	4.75 [b]5.86	2.84 [b]3.19	---- ----
80	3.44 3.55	3.50 ----	6.40 [b]7.65	2.74 2.95	---- ----
100	4.59 2.72	---- ----	[b]9.32 4.78	[b]3.06 2.11	---- ----

[a]Oscillatory behavior observed.
[b]Dimension in transition at end of test time.

TABLE A-IV.—FLAME SPREAD RATE AND DIMENSION DATA FOR DOUBLE THICKNESS OF FUEL IN NORMAL GRAVITY

[0.0152-cm-thick sample.]

Oxygen concentration, percent	Flame spread rate, V_f, cm/sec	Average V_f, cm/sec	Flame length, L_f, cm	Flame width, W_f, cm	Standoff distance, b, cm
16.9	0.28 .33	0.31 ----	1.11 1.25	---- 1.03	---- ----
17	0.32	----	1.31	1.06	----
18	0.75	----	1.40	1.79	----
21	0.59 .67 .68 .67	0.65 ---- ---- ----	2.06 2.20 2.23 ----	1.06 1.17 1.05 ----	---- ---- ---- ----
25	0.85 .94 .91	0.90 ---- ----	2.66 2.47 2.56	1.24 1.13 1.26	---- ---- ----
30	1.21	----	2.88	1.37	----
40	1.80 1.72	1.76 ----	2.66 3.41	1.52 1.52	---- ----
50	2.28	----	3.80	1.62	----
60	2.90	----	3.84	1.62	----
80	3.34	----	4.83	1.75	----
100	3.86	----	6.11	2.11	----

Appendix B
Error Analysis

B.1 Experimental Errors

In this section the errors involved in the experiment are estimated, and some suggestions are made for minimizing these errors in future work.

B.1.1 Error in measurement of sample length.—Samples were cut by hand from 14.5- by 17-cm sheets of material. Because the material tended to stretch as it was cut, the samples varied slightly in length. This variation was measured by measuring a random selection of 20 cut samples. The length of the samples was found to be 15 ± 0.2 cm. However, when the samples were mounted in the experiment holder, it was noted that again the material had a tendency to stretch slightly. All samples were measured for length prior to burning, and analysis revealed that samples as mounted in the holder had a length of 15 ± 0.3 cm. This measurement is important in determining the accuracy of the measured flame spread rate.

A modification to the holder design would eliminate this error due to material stretch. Rather than leaving the bottom of the sample free, it is possible to clamp it between the two metal plates. In this way, by mounting the top of the sample at a predetermined location, the sample would always be 15 cm long. This would also eliminate the problem of double-thickness materials bowing away from each other, which was observed in some of the double-thickness tests.

B.1.2 Error in sample width.—Because both sides of the sample were clamped between the metal plates of the holder, the cutting of the sample and the stretch of the material during mounting did not affect the width. The width did vary, however, because of a slightly uneven cut of the metal plates. The cutout width of the metal plates was measured at various locations down the length of the sample, and the width was found to be 3 ± 0.2 cm. Since the width of the sample does not come into the calculations other than to ensure a two-dimensional flame, this error is not significant.

B.1.3 Error in measurement of sample area density.—The area density of the sample material was measured so that comparisons with other data could be made. Five 36.8- by 43.2-cm sheets of the sample material were carefully measured on all four sides to determine the exact area of each sheet. These 5 sheets could be cut to make more than 150 samples. The sheets were then placed in a dry box maintained at a very low humidity level with anhydrous calcium sulfate ($CaSO_4$) as a dessicant and dry nitrogen flow. The samples were left in the dry box for 3 days. The final humidity reading at weighing was less than 0.5 percent relative humidity at 66 °F.

The samples were weighed by using a Sartorius model electronic scale with a built-in calibration. In addition, a calibration was performed by using calibration weights in the same range of weights as the sample sheets, and the scale was found to be accurate to within ± 0.2 percent. The scale was placed in the dry box at the same time the samples were so that the samples would not be exposed to humidity during weighing. The average area density for the sheets was 1.998×10^{-3} g/cm^2 ± 5.5 percent based on the total thickness of the material.

The error in the area density is believed to be caused by variations within the material and thus would be difficult to reduce short of selecting a more uniform material.

B.1.4 Error in oxygen concentration of chamber environment.—Since two different gas mixing systems were used, two different error estimates were made. The larger of the two errors was then generalized to all of the data.

In the 2.2-sec Drop Tower mixing system, the resolution of the pressure measurement was 0.001 atm. Filling of the experiment chamber was done by method of partial pressures. This method assumes the ideal gas law and isothermal filling. Every attempt was made to ensure that filling took place slowly enough that the assumption of isothermal filling was reasonable. Filling of the chamber (48.4 l) typically took 10 to 12 min. Thus the error of the oxygen concentration due to filling would not be much greater than 0.001 atm.

There is a much more significant error, however, to be accounted for. The vacuum pump attached to the mixing system was only able to evacuate the chamber to approximately 0.092 atm. Thus the uncertainty of the mixture was 0.92 percent.

In the 5.18-sec Zero Gravity Facility, a much better vacuum pump was used which reduced the pressure to less than 0.001 atm. In addition, the resolution of the pressure measurement was also 0.001 atm, so the error in these tests was of that order, which is much less than the 2.2-second Drop Tower error.

Therefore, the error in the oxygen concentration was 0.92 percent. The obvious way to reduce this error is to get a better vacuum pump.

B.1.5 Error in initial temperature of the experiment.—The temperature of the ambient environment at the start of each test was not controlled. Since temperature is known to play a role on the combustion process, however, it was recorded. Temperatures recorded prior to each test varied from 290 to 305 K. Thus the error involved in the initial temperature was 298 K ± 2.7 percent.

There was a relatively large fluctuation in the ambient environment temperature, primarily because the 2.2-sec Drop Tower has a very poor heating system and no cooling system. Thus an experiment conducted early in the morning is at a cool temperature, whereas in the afternoon it is at an uncomfortably warm temperature. The only way to minimize this error would be to better control the facility environment.

B.1.6 Error in determination of extinction limits.—The extinction limits for both normal gravity and microgravity, single- and double-thickness flame spread are reported here. The normal-gravity extinction limits are accurate to within

0.1 percent oxygen. The single thickness of fuel extinguished at 16.4 percent oxygen but burned at 16.5 percent. The double thickness of fuel extinguished at 16.8 percent but burned at 16.9 percent.

Because of the limited number of microgravity tests, the microgravity limits were not determined as accurately. The single-thickness-fuel extinction limit is accurate to within 0.5 percent oxygen; the fuel burned at 21 percent oxygen but extinguished at 20.5 percent. The double-thickness-fuel extinction limit is only good to 1 percent oxygen; the fuel burned at 26 percent oxygen but extinguished at 25 percent.

B.2 Calculation Errors

In this section the errors involved in the analysis of the data are estimated. Some of the previous experimental errors are used in the estimations.

B.2.1 Repeatability of point measurement.—Most of the films were analyzed with a Photo Digitizing Systems model 76–1 film motion analyzer. The unit consisted of a projection head, a projection grid, a digitizer, and a controller. The system was tied to a leading-edge computer which ran the software that stored and analyzed the digitized data from the films. Copies of the software used in the analysis of data are found in appendix D.

In order to determine the accuracy of measurement of a specific point, the same point from a film was measured more than 50 times. A very dim blue leading edge was selected as the true test of accuracy of measurement because of the difficulty in making measurements from these very diffusive flames. It was found that the same point could be measured to within ± 0.03 cm by the author. This error was operator dependent. The resolution of the screen was ± 0.007 cm. The only way to reduce this error is to measure brighter, more distinct objects or get better a operator.

B.2.2 Error in determination of time.—The timing during each test was recorded on the film with timing marks made by a timing light generator operating at 10 Hz. As a check of the timing light system, the number of frames recorded after the drop began was divided by the drop time. In most cases the two framing rates were the same; the exceptions were those instances where the timing lights failed to work during part or all of the test. In these cases the second method of determining timing was assumed to be valid.

To estimate the error involved in the determination of time, the slowest framing rate of 12 frames/sec was used. The uncertainty of the exact timing of an event was then ± 0.083 sec, or 1.6 percent of the 5.18-sec drop time. This error is unavoidable until a more sensitive film is developed so that the framing rate can be increased to a reasonable value.

B.2.3 Error in estimate of flame spread rate.—The flame spread rates were determined by using a least-squares fit to flame front position as a function of time data from each test. The correlation of the data to this line varied depending on the oxygen concentration of the test as well as the gravity level. Additionally, error in length and time measurements become important.

A correlation coefficient was used as a guide to the fit of the data to the line. This was done more as a validation of the analysis technique than as an estimate of the error of the flame spread rate. For normal-gravity data, the lowest correlation coefficient was 0.9948, which indicates a good fit. In microgravity, however, as the oxygen concentration is reduced, the flames spread rate begins to oscillate around a mean spread rate so that correlations are not as good. At the limit the correlation coefficient is as low as 0.9723. Thus the question arises: what good is a linear fit to obviously nonlinear data? The approach used here at these low oxygen concentrations was to take the least-squares-fit estimate of the flame spread rate as an overall flame spread rate while recognizing that variations occur in the spread rate within the test. Those tests near the limit where the spread process was observed to be oscillatory are marked in appendix A with a footnote. The most straightforward method of determining the error in a given spread rate measurement is to redo the same experiment a number of times and determine the error in the repeated measurement. This was done in two cases, where the same test was repeated six and seven times. Many tests were redone two or three times. The maximum variation in the average spread rate from these repeated tests for the single thickness was 5.8 percent. Considering the other errors in this experiment which are coupled in the spread rate measurement, this error is quite reasonable.

For the double-thickness fuels, however, the errors were considerably larger. This is believed to be due to the variation in the closeness of the two halves of the sample thickness. The largest error for the double-thick spread rates was 15 percent. It is clear from these errors that a better technique of bonding the multiple thickness samples is needed to minimize these errors.

One possible method would be to soak the samples in distilled water and then dry the multiple sheets under weight. In this way the fibers from the sheets would entangle and the material would act as a solid sample rather than two samples side by side.

B.2.4 Error in estimate of flame dimensions.—The flame dimensions were determined by plotting the dimension of interest as it varied during the test. Some dimensions transitioned to a steady value in time. However, many were observed to still be in transition at the end of the test time, or oscillating around an average value. Whenever possible, the steady or average value was chosen as the most representative dimension. If the dimension was still in obvious transition at the end of the test time, the last value measured was selected as the most representative dimension. These values are marked with an footnote in appendix A.

Because of the transient nature of much of the data, it is difficult to assess an accuracy of the measure. Comparing repeated experiments in microgravity where a steady dimension was recorded in more than one instance, the

maximum variation in the length data was 3.9 percent for the single thickness and 7.3 percent for the double thickness of fuel. Width data seemed much more steady, in general, and the variation was somewhat less, as well; for the single thickness of fuel, the maximum variation in the steady data was 2.8 percent and for the double thickness of fuel, it was 2.5 percent.

Normal-gravity lengths were very difficult to measure because of the flicker of the flames, especially at higher oxygen concentrations, but every attempt was made to take average values. The maximum variation for the single-thickness length was 3.1 percent and for the double-thickness length was 12.4 percent. Widths were again more stable. The maximum variation for the single-thickness width was 5.9 percent and for the double-thickness width was 7.0 percent.

Standoff distances could only be measured in a handful of cases because they became so small at higher oxygen concentrations that they could not be distinguished from the holder thickness. Only one had repeated measurements. The variation of the data in that case was 6.6 percent.

Appendix C
Experimental Facilities

C.1 Rationale for Use of Two Facilities

It was decided after some preliminary microgravity tests in the 2.2-sec Drop Tower that it would be necessary to conduct the tests with oxygen concentrations less than 40 percent in the 5.18-sec Zero Gravity Facility to allow the flame to develop and spread away from the igniter wire. For oxygen concentrations higher than 40 percent, the flame spreads fast enough that 2.2 sec is sufficient to determine the spread rate and, in most cases, the appropriate flame dimensions. Additionally, all of the normal gravity tests were conducted in the 2.2-sec Drop Tower experiment package.

C.2 Experiment Package for 2.2-sec Drop Tower

The test package used in the 2.2-sec Drop Tower for the microgravity tests from 40 to 100 percent oxygen and all of the normal-gravity tests is shown in figure 3. The package consists of a cylindrical combustion chamber, a high-speed camera, an electrical control system, and a power supply.

The combustion chamber is 30.5 cm in diameter and 61 cm in height for an internal volume of 48.4 l. This volume contains more than 900 times the oxygen required to burn a single thickness of the sample. There are four 13-cm-diameter ports around the base of the chamber; one of these is used as a viewing port with a quartz window, the second is used as an access port to install the holder within the chamber, the third provides electrical access to the interior of the chamber, and the fourth was not used in this experiment. There are three valves located near the top of the chamber. One is used as a relief valve, the second is used to evacuate and fill the chamber, and the third is used as a bleed valve.

A 16-mm high-speed Milliken camera is mounted in front of the window to film the experiments. An electrical box with time delay relays control the sequence of events during a test. The power supply for the experiments package is mounted under the camera and supplies 28 V dc.

Also shown in figure 3 is the gas-mixing system used to fill the chamber with the appropriate oxygen concentration. As many as three different gases can be used with this system at any one time. Each gas is controlled with an on/off valve and a flow control valve. A Datel Systems, Inc. digital pressure meter indicates absolute pressure in torr to within ± 0.001 atm over a range of 0 to 2 atm. The mixing system is also attached to a vacuum pump capable of evacuating the experiment chamber to less than 0.001 atm.

In preparation for a test, the sample holder was mounted within the chamber, and the chamber was sealed. The chamber with the sample holder was actively evacuated for a minimum of 4 hr and filled with the appropriate gas mixture. The mixing system was then disconnected from the package so the package could be loaded for a test.

C.3 Operations of 2.2-sec Drop Tower

A schematic diagram of the 2.2-sec Drop Tower is shown in figure 23. The facility consists of an eight-floor building 6.4 m square by 30.5 m tall. Contained within this building is the drop area, which is 27 m tall with a cross section of 1.5 by 2.75 m.

The experiment package is encased within a drag shield with three deceleration spikes attached to the bottom. The drag shield is hoisted to the eighth floor where the final preparations for a test are made. Electrical connections are made and the drag shield is suspended by a single wire. The drop is initialized by notching the wire, causing it to fail within milliseconds.

Microgravity is obtained in this facility by allowing the experiment package to freefall within the drag field. The experiment package and the drag shield fall independently of each other so that, although the drag shield is sustaining substantial drag, the experiment package experiences very little in its 20-cm fall with respect to the drag shield.

The drag shield is decelerated in a 2.2-m-deep sand pit by the deceleration spikes. The entire assembly is then hoisted back to the preparation area and the experiment package removed from the drag shield for post-test operations.

C.4 Experiment in 5.18-sec Zero Gravity Facility

The experiment bus used in the 5.18-sec Zero Gravity Facility for tests with oxygen concentrations less than 40 percent is shown in figure 4. It contains a bell-shaped experiment chamber, a camera, an electrical control system, and a power supply. Except for the experiment chamber, the equipment used on this bus is functionally the same as that on the 2.2-sec Drop Tower package.

The chamber is 39.6 cm in diameter and has an internal volume of 113 l, over twice the volume of the chamber in the 2.2-sec Drop Tower. There are 5-cm-diameter ports in the chamber; four located around the base of the chamber and one at the top of the dome. One of the base ports is used with a quartz window to view the experiment.

The gas-mixing system used in this facility is similar in function to that described for the 2.2-sec Drop Tower experiment, but the accuracy of the mixing by partial pressures is much better overall at 0.001 atm for this facility.

C.5 Operations of 5.18-sec Zero Gravity Facility

A schematic of the larger 5.18-sec Zero Gravity Facility is shown in figure 24. The facility houses a 6.1-m-diameter, 145-m-deep vacuum chamber which provides the 132-m drop distance required for 5.18 sec of free-fall.

The experiment bus, which contains the experiment chamber, is enclosed in a protective cover and suspended over the chamber by a single, specially designed bolt. A cover is placed over the chamber and the entire chamber is evacuated to 1.3×10^{-5} atm to reduce the air drag experienced by the experiment. This takes a few hours so that only one experiment can be done in this facility per day.

Microgravity is initiated by shearing the bolt to release the experiment. The bus falls free of drag in the near vacuum. At the end of its 5.18-sec descent, the bus is decelerated in a container of polystyrene pellets. It is interesting to note that the deceleration is caused not by the crushing of the pellets but by the drag induced by the flow of the pellets past the bus. The experiment bus is retrieved from the container of pellets and hoisted back up the work area to complete the experiment cycle.

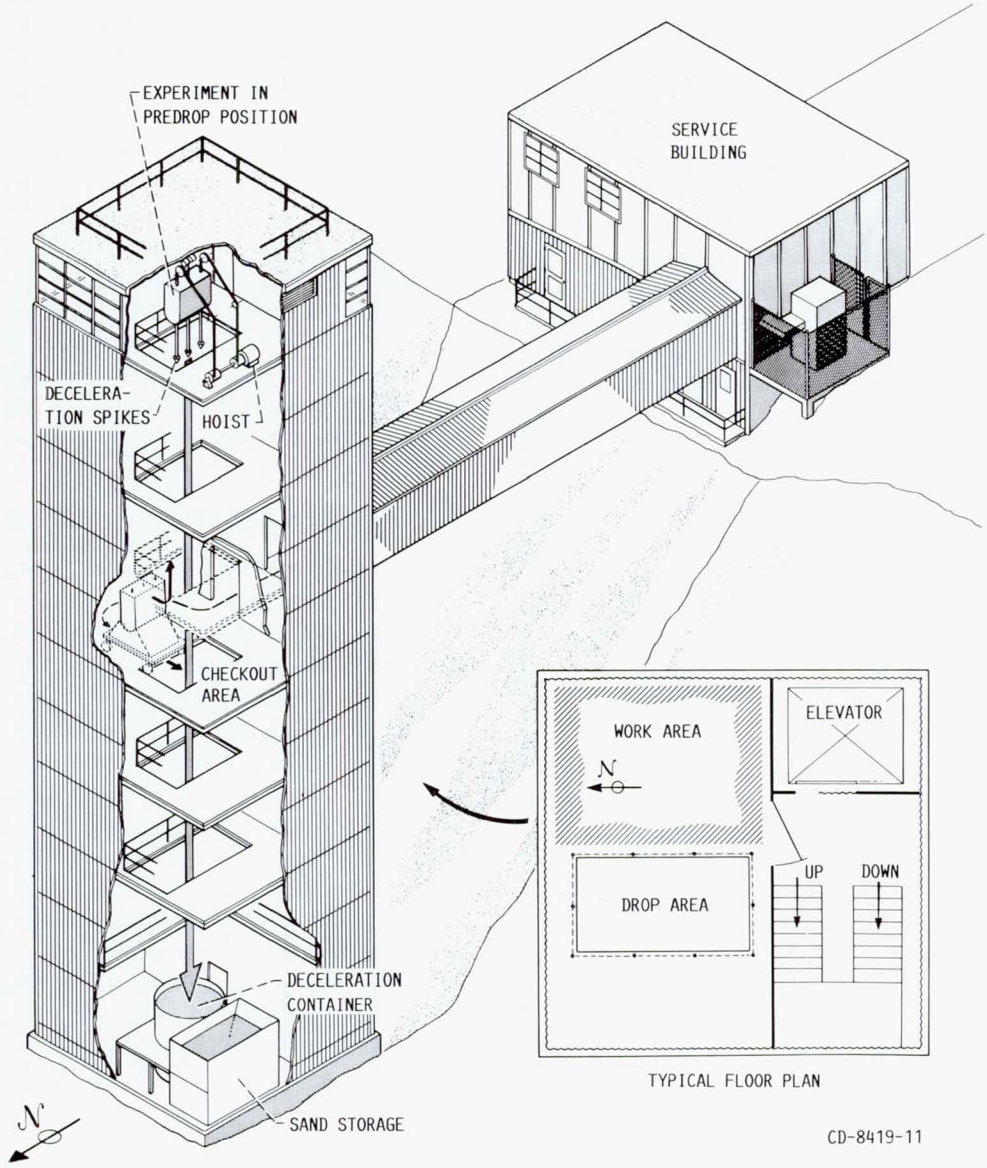

Figure 23.—Schematic of 2.2-sec Drop Tower.

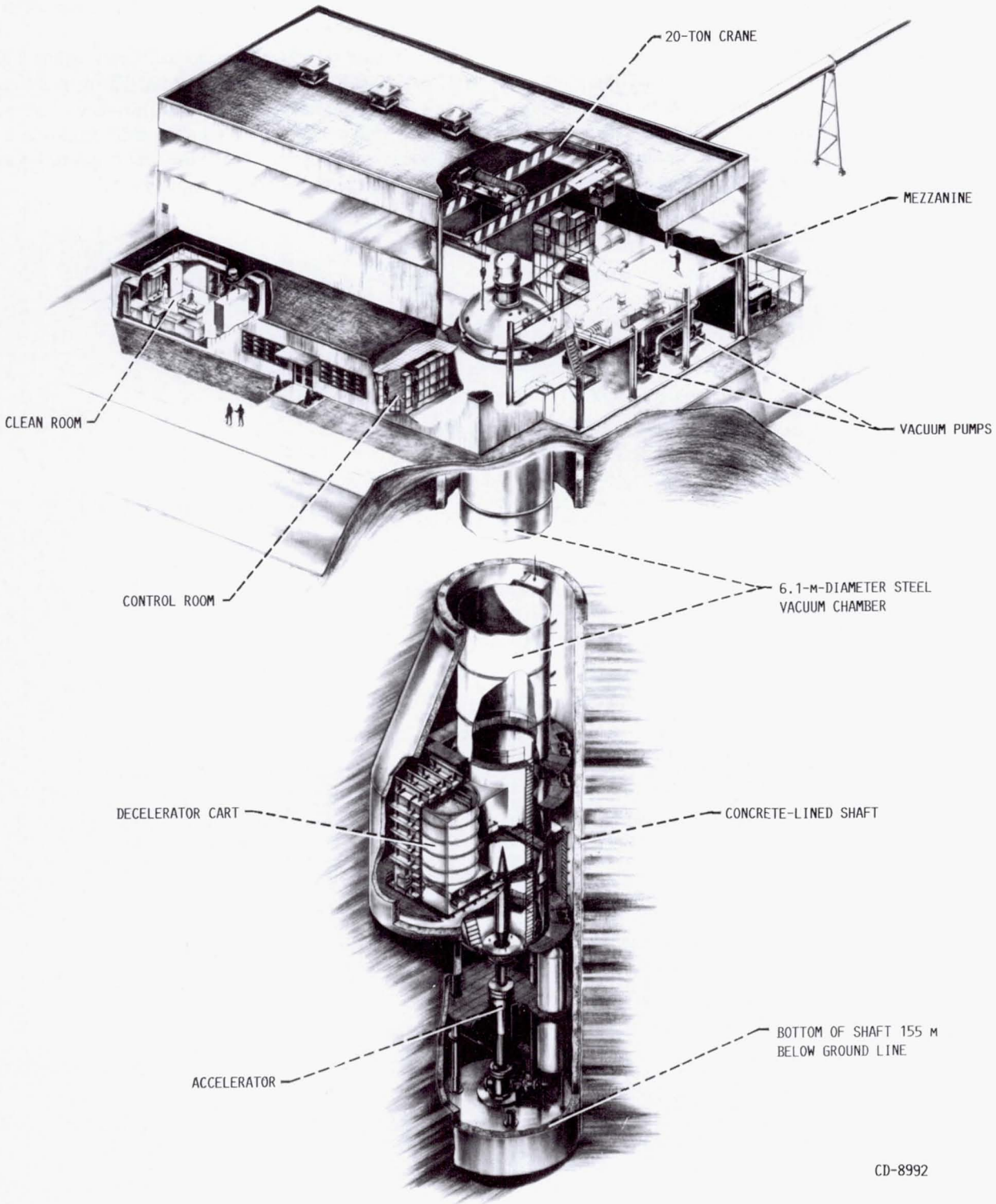

Figure 24.—Schematic of Zero Gravity Facility.

Appendix D
Supporting Computer Software

D.1 Film Analysis Program

The following program was used to analyze the film in conjunction with the film motion analyzer. The film motion analyzer sends ASCII signals containing frame number and x and y coordinates to the computer. The program receives this information and stores it in a data file. Additionally, after the data have been stored, the program uses the data to calculate flame length, width, and standoff distances as well as flame spread rates.

The software is written in basic and is compatible with the IBM BASICA.EXE language program. The original version of this program was written by Paul Ronney, currently at Princeton University, but substantial modifications to it have been made by the author so that the data could be taken and analyzed for the flame spread experiments.

```
list
1000 'fosswof;data entry/analysis program ♣
1010 ' ♣
1020 CLS ♣
1030 ON ERROR GOTO 2680 ♣
1040 DIM RAWDATA$(999):DRIVE$="A:" ♣
1050 ' ♣
1060 'BEGIN ♣
1070   KEY 1, "NEW RECORD"+CHR$(13): KEY 2, "MODIFY OLD"+CHR$(13):
       KEY 3, "CALCULATE"+CHR$(13):  KEY 4, "NO BURN"+CHR$(13):
           KEY 5, "CHANGE"+CHR$(13):     KEY 7, "ADD"+CHR$(13) ♣
1080   KEY 8, "NO"+CHR$(13):KEY 9,"YES"+CHR$(13):KEY 6,"BURN"+CHR$(13) ♣
1090 ' ♣
1100 WHILE INKEY$<>"":WEND ♣
1110   INPUT "NEW RECORD, MODIFY OLD RECORD, OR CALCULATE VANGUARD DATA";MODE$ ♣
1120   IF MODE$ = "NEW RECORD" THEN 1190 ELSE IF MODE$ = "MODIFY OLD"
          THEN 1910 ELSE IF MODE$ = "CALCULATE" THEN 2190 ♣
1130 ' ♣
1140 CLOSE ♣
1150   KEY 1,"load "+CHR$(34):KEY 2,"save "+CHR$(34):KEY 3,"files ":
       KEY 4,"list ":KEY 5,"run"+CHR$(13): ♣
1160   KEY 6,"print ":KEY 7,"goto ":KEY 8,"gosub ":KEY 9,"edit."+CHR$(13):
       KEY 10, "cont"+CHR$(13) ♣
1170 END ♣
1180 ' ♣
1190 'NEWRECORD ♣
1200   DATA "GRAVITY","ONE-G OR ZERO-G" ♣
1210   DATA "KEYS","PAPER","KIMWIPE","NYLON VELCRO","NOMEX VELCRO","ENDKEYS",
          "FUEL","FUEL NAME" ♣
1220   DATA "SIZE","FUEL SIZE","WEIGHT","FUEL WEIGHT","%O2","OXYGEN CONCENTRATIO
N","%N2","NITROGEN CONCENTRATION","PRESSURE","INITIAL PRESSURE (TORR)" ♣
1230   DATA "TEMPERATURE","INITIAL TEMPERATURE (degrees C)" ♣
1240   DATA "EQUILIB. PRESSURE","PRESSURE AFTER COMBUSTION (TORR)" ♣
1250   DATA "IGNITER TDR","TIME IGNITER RECEIVED POWER(SEC)","IGNITER RESIST.",
         "IGNITER RESISTANCE(OHMS)","PAPER THICKNESS","SAMPLE THICKNESS(CM)" ♣
1260   DATA "REFERENCE POINTS","MARK REFERENCE POINT","MARK XY-ZERO","MARK XY-15
" ♣
1270   DATA "TIMING","FRAME ON WHICH DROP STARTS","FRAME ON WHICH DROP ENDS","EL
APSED TIME" ♣
1280   DATA"KEYS","FRONT","STANDOFF","LENGTH","WIDTH","SPREADRATE ","SOOTLENGTH"
,              "QUIT VANGUARD","ENDKEYS","VANGUARD DATA" ♣
1290   DATA "KEYS","BURN","NON-IGNITION","EXTINGUISHED","NOT STEADY","NOT SYMMET
RIC","ENDKEYS","COMMENTS" ♣
1300   DATA "NOMORE" ♣
1310 ' ♣
1320 'STARTRUNIN ♣
1330   OPEN "com1:9600,n,8,2,rs,cs,ds,cd" AS #1 ♣
1340   GOSUB 4010 ♣
1350   ON COM(1) GOSUB 2810 ♣
1360   INPUT "RUNNUMBER";RUNNUMBER$:IF VAL(RUNNUMBER$)=0 THEN CLOSE:GOTO 1060 ♣
1370   RESTORE:ERASE RAWDATA$:DIM RAWDATA$(9999): I=-1 ♣
1380 ' ♣
1390 'DATAIN ♣
1400   READ TEXT$:INDEX=1 ♣
1410   IF TEXT$="KEYS" THEN INDEX=2 ♣
1420   IF TEXT$="VANGUARD DATA" THEN INDEX=3 ♣
1430   IF TEXT$="COMMENTS" THEN INDEX=4 ♣
1440   IF TEXT$="NOMORE" THEN INDEX=5 ♣
1450   IF TEXT$="REFERENCE POINTS" THEN INDEX=6 ♣
1460   IF TEXT$="TIMING" THEN INDEX=7 ♣
```

```
1470   ON INDEX GOSUB 1560,1590,1700,1630,1500,3040,3150 ♣
1480   GOTO 1390 ♣
1490 ' ♣
1500 'FINISHED ♣
1510   GOSUB 2760:OPEN FILENAME$ FOR OUTPUT AS #2 ♣
1520   FOR K=0 TO I:WRITE #2,RAWDATA$(K):NEXT K:CLOSE ♣
1530   GOTO 1320 ♣
1540 ' ♣
1550 'NORMAL DATA ♣
1560   GOSUB 1680:READ TEXT$:PRINT TEXT$;:INPUT TEXT$:GOSUB 1680:RETURN ♣
1570 ' ♣
1580 'FILL KEYS ♣
1590   FOR J=1 TO 10:READ TEXT$ ♣
1600   IF TEXT$="ENDKEYS" THEN RETURN ELSE KEY J,TEXT$+CHR$(13):NEXT J ♣
1610 ' ♣
1620 'COMMENTS ♣
1630   PRINT TEXT$;:GOSUB 1680 ♣
1640   INPUT TEXT$:IF LEN(TEXT$)=0 THEN 1650 ELSE GOSUB 1680:GOTO 1640 ♣
1650   TEXT$="END COM":GOSUB 1680:RETURN ♣
1660 ' ♣
1670 'ADDIT ♣
1680   I=I+1:RAWDATA$(I)=TEXT$:RETURN ♣
1690 ' ♣
1700 'VANGUARD ♣
1710   GOSUB 4010 ♣
1720   COM(1) ON ♣
1730   PRINT TEXT$:GOSUB 1680 ♣
1740   INPUT"FRONT,STANDOFF, LENGTH, WIDTH, SPREADRATE, SOOTLENGTH, OR QUIT VANG
UARD",        WAY$ ♣
1750   IF WAY$="QUIT VANGUARD" OR WAY$="" THEN 1870 ELSE TEXT$=WAY$:GOSUB 1680:
       GOTO 1855 ♣
1760   PRINT "FRAME NUMBER, REFERENCE POSITION? "; ♣
1770   WHILE BUTTON.FLAG=0:WEND:BUTTON.FLAG=0:REFX = X: REFY = Y: F# = FRAMES ♣
1780   IF X>80 OR Y>80 THEN PRINT:GOTO 1860 ♣
1785  TEXT$ = "REF DATA": GOSUB 1680 ♣
1790   TEXT$=STR$(F#):PRINT " FRAME = ";TEXT$;:GOSUB 1680 ♣
1795   TEXT$=STR$(REFX):PRINT" , REFX = ";TEXT$;:GOSUB 1680: TEXT$=STR$(REFY):
        PRINT" , REFY =";TEXT$;:GOSUB 1680 ♣
1797   IF WAY$="LENGTH" OR WAY$="WIDTH" THEN J=0 ♣
1798   IF WAY$="STANDOFF" OR WAY$="SOOTLENGTH" THEN J=0 ♣
1800   PRINT "POINT TO BE MEASURED?"; ♣
1805   WHILE BUTTON.FLAG=0:WEND: BUTTON.FLAG=0 ♣
1807   IF X>80 OR Y>80 THEN GOTO 1760 ♣
1808   TEXT$ = "DATA": GOSUB 1680 ♣
1810   TEXT$=STR$(FRAMES): PRINT" FRAME , POSITION X,Y = ";TEXT$;:GOSUB 1680 ♣
1850  TEXT$=STR$(X): PRINT" , ";TEXT$:GOSUB 1680:TEXT$=STR$(Y):PRINT ", ";TEXT$:
      GOSUB 1680 ♣
1852   IF WAY$="STANDOFF" OR WAY$="SOOTLENGTH" THEN J=J+1 ♣
1853  IF WAY$="LENGTH" OR WAY$="WIDTH" THEN J=J+1 ♣
1855  IF WAY$="SPREADRATE" OR WAY$="FRONT" THEN GOTO 1760:GOTO 1800 ♣
1856  IF J=1 THEN GOTO 1800 ♣
1857  IF WAY$="LENGTH" OR WAY$="WIDTH" THEN GOTO 1760:GOTO 1800 ♣
1858   IF WAY$="STANDOFF" OR WAY$="SOOTLENGTH" THEN GOTO 1760: GOTO 1800 ♣
1860   TEXT$="END "+WAY$:GOSUB 1680:GOTO 1740 ♣
1870   TEXT$="END VANGUARD DATA":GOSUB 1680 ♣
1880   COM(1) OFF ♣
1890 RETURN ♣
1900 ' ♣
1910 'MODIFY ♣
1920   INPUT"RUN NUMBER TO BE MODIFIED";RUNNUMBER$:IF VAL(RUNNUMBER$)=0
         THEN 1060 ♣
1930   ERASE RAWDATA$:DIM RAWDATA$(9999) ♣
1940   DRIVE=2:GOSUB 2760:OPEN FILENAME$ FOR INPUT AS #1 ♣
1950   FOR I=0 TO 9999:IF EOF(1) THEN CLOSE #1 ELSE INPUT #1,RAWDATA$(I):NEXT I
1960   PRINT "HERE ARE THE FILE ENTRIES":PRINT:PRINT:ENTRY=0:PRINT ENTRY; ♣
1970   FOR J=0 TO INT((I-1)/4)+1 ♣
1980   FOR K=0 TO 3:ENTRY=4*J+K:PRINT TAB(8+18*K);RAWDATA$(ENTRY);:NEXT K:
         PRINT:PRINT ENTRY+1;:NEXT J ♣
1990   PRINT ♣
2000   INPUT "ADD ENTRY OR CHANGE";TEXT$:IF TEXT$="ADD" THEN GOSUB 2060
         ELSE GOSUB 2140 ♣
2010   OPEN FILENAME$ FOR OUTPUT AS #1 ♣
2020   FOR K=0 TO I:WRITE #1,RAWDATA$(K):NEXT K:CLOSE #1 ♣
2030   GOTO 1060 ♣
2040 ' ♣
2050 'ADD ♣
2060   INPUT "AFTER WHAT ENTRY#";ENTRY ♣
2070   INPUT "WHAT DATA WOULD YOU LIKE TO ADD";TEXT$ ♣
2080   FOR J=I TO ENTRY+1 STEP -1:RAWDATA$(J+1)=RAWDATA$(J):NEXT J ♣
```

```
2090    RAWDATA$(ENTRY+1)=TEXT$:I=I+1 ♣
2100    INPUT "ANY MORE ADDITIONS";TEXT$ ♣
2110    IF TEXT$="YES" THEN 2060 ELSE RETURN ♣
2120 ' ♣
2130 'CHANGE ♣
2140    INPUT "WHAT ENTRY #";ENTRY ♣
2150    INPUT "WHAT WOULD YOU LIKE THIS ENTRY CHANGED TO";TEXT$ ♣
2160    RAWDATA$(ENTRY)=TEXT$ ♣
2170    INPUT "ANY MORE CHANGES";TEXT$:IF TEXT$="YES" THEN 2140 ELSE RETURN ♣
2180 ' ♣
2190 'CALCULATE ♣
2210    INPUT "START AT WHAT RUN NUMBER";STARTNUM ♣
2220    INPUT "STOP AT WHAT RUN NUMBER";STOPNUM ♣
2230    FOR RUNNUMBER=STARTNUM TO STOPNUM:PRINT RUNNUMBER ♣
2240      ERASE RAWDATA$:DIM RAWDATA$(9999) ♣
2250      RUNNUMBER$=RIGHT$(STR$(RUNNUMBER),LEN(STR$(RUNNUMBER))-1) ♣
2260      GOSUB 2760 ♣
2270      OPEN FILENAME$ FOR INPUT AS #1 ♣
2280      FOR I=0 TO 9999 ♣
2290        IF EOF(1) THEN CLOSE #1 ELSE INPUT #1,RAWDATA$(I):
              IF RAWDATA$(I)<>"PROCESSED VANGUARD DATA" THEN NEXT I
              ELSE CLOSE #1:GOTO 2410 ♣
2300      LENFILE=I ♣
2310      FOR J=0 TO LENFILE ♣
2320        IF RAWDATA$(J)="DROP START " THEN DROPSTART=VAL(RAWDATA$(J+1)) ♣
2330        IF RAWDATA$(J)="DROP ENDS " THEN DROPENDS=VAL(RAWDATA$(J+1)) ♣
2340        IF RAWDATA$(J)="ELAPSED TIME" THEN DROPTIME=VAL(RAWDATA$(J+1)) ♣
2350        IF RAWDATA$(J)="RX0" THEN RX0=VAL(RAWDATA$(J+1)) ♣
2353        IF RAWDATA$(J)="RY0" THEN RY0=VAL(RAWDATA$(J+1)) ♣
2354        IF RAWDATA$(J)="X0" THEN X0=VAL(RAWDATA$(J+1)) ♣
2355        IF RAWDATA$(J)="Y0" THEN Y0=VAL(RAWDATA$(J+1)) ♣
2357        IF RAWDATA$(J)="X15" THEN X15 = VAL(RAWDATA$(J+1)) ♣
2360        IF RAWDATA$(J)="Y15" THEN Y15=VAL(RAWDATA$(J+1)) ♣
2370        IF RAWDATA$(J)="VANGUARD DATA" THEN J=J+1: WAY$=RAWDATA$(J): PRINT WA
Y$:          TEXT$="PROCESSED VANGUARD DATA":GOSUB 1680:PRINT "PROCESSING":GOSUB
2440 ♣
2380        NEXT J ♣
2390      OPEN FILENAME$ FOR OUTPUT AS #1 ♣
2400      FOR K=0 TO I:WRITE #1,RAWDATA$(K):NEXT K:CLOSE #1 ♣
2410    NEXT RUNNUMBER ♣
2420    GOTO 1060 ♣
2430 ' ♣
2440 'STARTCRUNCH ♣
2445   SCALEFACTOR= 15/(Y0 - Y15) ♣
2450    FRAMESPEED = (DROPENDS - DROPSTART)/DROPTIME ♣
2460    IF (RAWDATA$(J)="FRONT") OR (RAWDATA$(J)="SPREADRATE") THEN  GOSUB 2520:
         GOSUB 2570 ♣
2465    IF (RAWDATA$(J)="STANDOFF") OR (RAWDATA$(J)="SOOTLENGTH")THEN GOSUB 2520:
        GOSUB 2570 ♣
2470    IF (RAWDATA$(J)="LENGTH") OR (RAWDATA$(J)="WIDTH") THEN GOSUB 2520:
  GOSUB 2570 ♣
2480    IF RAWDATA$(J)<> "END VANGUARD DATA" THEN 2440 ♣
2490    TEXT$="END PROCESSED VANGUARD DATA":GOSUB 1680 ♣
2500 RETURN ♣
2510 ' ♣
2520 'WAYLABEL ♣
2540    GOSUB 1680:J=J+1 ♣
2550 RETURN ♣
2560 ' ♣
2570 'WAYCALC ♣
2580    IF RAWDATA$(J)="END "+WAY$ THEN 2650 ♣
2583    IF WAY$="FRONT" THEN GOTO 2590 ♣
2584    IF WAY$="LENGTH" THEN GOTO 2622 ♣
2585    IF WAY$="SPREADRATE" THEN GOTO 2590 ♣
2586    IF WAY$="WIDTH" THEN GOTO 2630 ♣
2587    IF WAY$="STANDOFF" THEN GOTO 2630 ♣
2588    IF WAY$="SOOTLENGTH" THEN GOTO 2622 ♣
2590   IF RAWDATA$(J)="REF DATA" THEN TEXT$ = "REF DATA":GOSUB 1680:
        T=(VAL(RAWDATA$(J+1))-DROPSTART)/FRAMESPEED: TEXT$= STR$(T):GOSUB 1680:
        REF=VAL(RAWDATA$(J+3)):TEXT$=STR$(REF):GOSUB 1680:J=J+4:GOTO 2570 ♣
2600    IF RAWDATA$(J)= "DATA" THEN TEXT$="DATA": GOSUB 1680: TEXT$=STR$((VAL(RAW
DATA$(J+1)) - DROPSTART)/FRAMESPEED):GOSUB 1680:  TEXT$=STR$(SCALEFACTOR*(Y0-RY0
-VAL(RAWDATA$(J+3))+REF)) ♣
2610    GOSUB 1680:J=J+4 ♣
2620    GOTO 2570 ♣
2622    IF RAWDATA$(J)="REF DATA" THEN TEXT$="DATA":GOSUB 1680 ♣
2624    TEXT$=STR$((VAL(RAWDATA$(J+1))-DROPSTART)/FRAMESPEED):GOSUB 1680 ♣
2626    TEXT$=STR$(ABS(SCALEFACTOR*(VAL(RAWDATA$(J+11))-VAL(RAWDATA$(J+7))))):
        GOSUB 1680 ♣
```

```
2628   J=J+12:GOTO 2570 ♣
2630   IF RAWDATA$(J)="REF DATA" THEN TEXT$="DATA":GOSUB 1680 ♣
2635   TEXT$=STR$((VAL(RAWDATA$(J+1))-DROPSTART)/FRAMESPEED):GOSUB 1680 ♣
2640   TEXT$=STR$(ABS(SCALEFACTOR*(VAL(RAWDATA$(J+10))-VAL(RAWDATA$(J+6))))):
         GOSUB 1680 ♣
2645   J=J+12: GOTO 2570 ♣
2650   TEXT$="END PROCESSED "+WAY$:GOSUB 1680:J=J+1 ♣
2660 RETURN ♣
2670 ' ♣
2680 'ERROR CHECK ♣
2690   IF ERR=57 THEN BEEP:RESUME 2810 ♣
2700   IF ERR=69 THEN BEEP:GOSUB 4010:RESUME ♣
2710   IF NOT(ERR=53) THEN ON ERROR GOTO 0:END ♣
2720   IF (DRIVE$="B:" OR CHECK.BOTH=0) AND MODE$="CALCULATE"
         THEN STARTNUM=RUNNUMBER+1:RESUME 2230 ♣
2730   IF (DRIVE$="B:" OR CHECK.BOTH=0) AND MODE$<>"CALCULATE"
         THEN PRINT "FILE NOT FOUND":GOTO 1060 ♣
2740   DRIVE="B:":GOSUB 1030:RESUME ♣
2750 ' ♣
2760 'NAME FILE ♣
2765   INPUT "Vf, Lf, Bf, Wf, Ls:"; FILE$ ♣
2770   FILENAME$=DRIVE$+FILE$+RUNNUMBER$+".RAW":PRINT FILENAME$ ♣
2780  RETURN ♣
2790 ' assumes data disk in B: drive (default) ♣
2800 ' ♣
2810 WHILE NOT EOF(1) ♣
2820   READING$="":BUTTON.FLAG=0 ♣
2830   GOSUB 3000 ♣
2840   WHILE NOT (A$=CHR$(13)) ♣
2850     READING$=READING$+A$ ♣
2860     GOSUB 3000 ♣
2870   WEND ♣
2880   GOSUB 3000 ♣
2890   WHILE NOT (A$=CHR$(10)) ♣
2900     GOSUB 3000 ♣
2910   WEND ♣
2920   HEADER$=LEFT$(READING$,2) ♣
2930   IF HEADER$="Fr" THEN FRAMES=VAL(MID$(READING$,4,6)):GOTO 2960 ♣
2940   IF HEADER$="F " THEN X=VAL(MID$(READING$,3,5))/1000:
         Y=VAL(MID$(READING$,9,5))/1000:BUTTON.FLAG=1:GOTO 2960 ♣
2950   BEEP ♣
2960 WEND ♣
2970 RETURN ♣
2990 'GET CHARACTER FROM RS-232 PORT ♣
3000   WHILE EOF(1):WEND ♣
3010   A$=CHR$(ASC(INPUT$(1,#1)) AND 127) ♣
3020 RETURN ♣
3030 ' ♣
3040 'REFERENCE POINTS ♣
3050   GOSUB 4010 ♣
3060   COM(1) ON ♣
3070   READ TEXT$:PRINT TEXT$; ♣
3085   WHILE BUTTON.FLAG=0:WEND:BUTTON.FLAG=0:RX0 = X:RY0 = Y: PRINT STR$(RX0):
         PRINT STR$(RY0) ♣
3090   IF RX0=0 OR RY0=0 THEN BEEP: GOTO 3085 ♣
3095   TEXT$="RX0":GOSUB 1680:TEXT$=STR$(RX0):GOSUB 1680:TEXT$="RY0":GOSUB 1680:
         TEXT$=STR$(RY0):GOSUB 1680: READ TEXT$:PRINT TEXT$; ♣
3100   WHILE BUTTON.FLAG=0:WEND:BUTTON.FLAG=0:X0=X: Y0 = Y: PRINT STR$(X0):
         PRINT STR$(Y0) ♣
3105   IF X0 = 0 OR Y0=0 THEN BEEP: GOTO 3100 ♣
3107   TEXT$="X0":GOSUB 1680:TEXT$=STR$(X0):GOSUB 1680:TEXT$="Y0":GOSUB 1680:
       TEXT$=STR$(Y0):GOSUB 1680:READ TEXT$:PRINT TEXT$; ♣
3110   WHILE BUTTON.FLAG=0:WEND: BUTTON.FLAG=0: X15=X:Y15 = Y:PRINT STR$(X15):
         PRINT STR$(Y15) ♣
3113   IF X15=0 OR Y15=0 THEN BEEP: GOTO 3110 ♣
3115   TEXT$="X15":GOSUB 1680:TEXT$=STR$(X15):GOSUB 1680:TEXT$="Y15":GOSUB 1680:
         TEXT$=STR$(Y15):GOSUB 1680 ♣
3120   COM(1) OFF ♣
3130 RETURN ♣
3140 ' ♣
3150 'TIMING ♣
3160   GOSUB 4010 ♣
3170   COM(1) ON ♣
3180   READ TEXT$:PRINT TEXT$;: ♣
3190   TEXT$="DROP START ": GOSUB 1680 ♣
3200   WHILE BUTTON.FLAG=0: WEND: BUTTON.FLAG=0: F#=FRAMES ♣
3203   IF F# = 0 THEN BEEP: GOTO 3200 ♣
3205   DROPSTART=F#:TEXT$=STR$(F#): GOSUB 1680 ♣
3215   PRINT TEXT$ ♣
```

```
3220    READ TEXT$:PRINT TEXT$;: ♣
3230    TEXT$= "DROP ENDS ": GOSUB 1680 ♣
3240    WHILE BUTTON.FLAG=0:WEND: BUTTON.FLAG=0: F# = FRAMES ♣
3250    IF F# = 0 THEN BEEP: GOTO 3240 ♣
3253    DROPENDS=F#:TEXT$=STR$(F#):GOSUB 1680 ♣
3255    PRINT TEXT$ ♣
3260    READ TEXT$: PRINT TEXT$;:GOSUB 1680 ♣
3290    LINE INPUT TEXT$ ♣
3300    GOSUB 1680 ♣
3310    COM(1) OFF ♣
3320 RETURN ♣
3330 ' ♣
3520 ' ♣
4000 'FLUSH RS-232 AND KEY BUFFERS ♣
4010 WHILE NOT EOF(1):DUMMY$=INPUT$(1,#1):WEND:WHILE INKEY$<>"":WEND:RETURN ♣
4020 ' ♣
Ok
```

D.2 Plotting and Least-Squares-Fit Program

The following program was used to analyze the data generated by the previous program. It reads directly the data file created by that program and graphically plots the data using the coordinates of choice. Additionally, it can calculate a first- or second-order curvefit to the data or a portion of the data and will plot that curvefit alone or with the data. Finally, it will accept keyboard inputs to create a new data file to be curvefitted, as was done for many of the figures in this work.

This program is written in basic and is compatible with the IBM BASICA.EXE language program. This program was written in 1986 by the author's summer student Matthew Hart, who is a 1987 graduate from Purdue University in aerospace and mechanical engineering.

```
10  REM plotter.basBAS ♣
20  DIM ATAPTS$ (999,2), ATAPTS (999,2), LABELOR (20), LABELAB (20) ♣
30  DIM F(100,6), FT(6,100), A(6,6), B(6), C(6), CURVFIT(51) ♣
40  DIM XFIT(99), YFIT(999) ♣
50  CHECK2=0 ♣
60  CLS ♣
70  GOTO 680 ♣
80  CLS ♣
90  K=0:N=0:CHECK=0:CHECK2=1:CHECK5=1 ♣
100  REM input name of datafile, abscissia, ordinate, and title of plot------ ♣
110  WHILE NUMBER=7 ♣
120  INPUT "DATASET NAME? ",DATASET$ ♣
130  GOTO 150 ♣
140  WEND ♣
150  INPUT "NAME OF ABSCISSIA? ",ORD$ ♣
160  INPUT "NAME OF ORDINATE? ",ABC$ ♣
170  INPUT "TITLE OF THIS PLOT? ",TITLE$ ♣
180  REM input data from datafile---------------------------------------------- ♣
190  WHILE NUMBER=7 ♣
200  OPEN DATASET$ FOR INPUT AS #1 ♣
210  FOR I=1 TO 999 ♣
220  ON ERROR GOTO 260 ♣
230  INPUT #1,  ATA$ ♣
240  IF ATA$="HDATA" OR ATA$="WDATA" OR ATA$="DATA" THEN K=K+1:FOR J=1 TO 2: INP
UT #1, ATAPTS$(K,J):NEXT J ♣
250  NEXT I ♣
260  RESUME 270 ♣
270  CLOSE ♣
280  ON ERROR GOTO 0 ♣
290  REM change data from strings to numbers------------------------------------
300  FOR I=1 TO K ♣
300  FOR I=1 TO K ♣
310    N=N+1 ♣
320    FOR J=1 TO 2 ♣
330      ATAPTS(N,J)=CSNG(VAL(ATAPTS$(I,J))) ♣
340    NEXT J ♣
350  NEXT I ♣
360  NUMBER=0 ♣
370  WEND ♣
380  REM input data from keyboard and store it in a file------------------------
 ♣
390  WHILE NUMBER=8 ♣
400   INPUT "WHAT WOULD YOU LIKE TO NAME THIS DATASET?", DATASET$ ♣
410  OPEN DATASET$ FOR OUTPUT AS #1 ♣
420  INPUT "HOW MANY DATA POINTS? ", N ♣
430  PRINT "INPUT DATA POINTS ("ORD$", "ABC$")" ♣
440  FOR I=1 TO N ♣
```

```
450    INPUT "> ", ATAPTS(I,1), ATAPTS(I,2) ♣
460   WRITE #1, "HDATA" ♣
470   WRITE #1, STR$(ATAPTS(I,1)) ♣
480   WRITE #1, STR$(ATAPTS(I,2)) ♣
490  NEXT I ♣
500  CLOSE ♣
510  NUMBER=0 ♣
520  WEND ♣
530  REM bubble sort data on the abscissia-------------------------------------
 ♣
540  WHILE CHECK5=1 ♣
550    CHECK5=0 ♣
560    FOR I=1 TO N-1 ♣
570      IF ATAPTS(I+1,1)<ATAPTS(I,1) THEN CHECK5=1:FOR J=1 TO 2:HOLD=ATAPTS(I,J
):ATAPTS(I,J)=ATAPTS(I+1,J):ATAPTS(I+1,J)=HOLD:NEXT J ♣
580    NEXT I ♣
590  WEND ♣
600  REM determine maximum values of ordinate and abscissia--------------------
 ♣
610  MAXORD=ATAPTS(N,1) ♣
620  MAXABS=ATAPTS(1,2) ♣
630  FOR I=2 TO N ♣
640    IF ATAPTS(I,2)>MAXABS THEN  MAXABS=ATAPTS(I,2) ♣
650  NEXT I ♣
660  REM select option and branch to area of program--------------------------
630  CLS ♣
670  CLS ♣
680  PRINT "OPTION:  (1) LIST DATA" ♣
690  PRINT "         (2) PLOT DATA" ♣
700  PRINT "         (3) CURVE FIT DATA (FIRST ORDER FIT)" ♣
710  PRINT "         (4) CURVE FIT DATA (SECOND ORDER FIT)" ♣
720  PRINT "         (5) PLOT CURVE FIT" ♣
730  PRINT "         (6) PLOT COMPOSIT OF DATA AND CURVE FIT" ♣
740  PRINT "         (7) NEW DATA" ♣
750  PRINT "         (8) CREATE YOUR OWN DATASET" ♣
760  PRINT "         (9) LINK DATASETS TOGETHER" ♣
770  PRINT"         (10) END" ♣
780  INPUT "SELECT DESIRED OPTION (1-10)", NUMBER ♣
790  IF NUMBER<7 AND CHECK2=0 THEN GOTO 1340 ♣
800  IF NUMBER=1 THEN GOTO 1360 ♣
810  IF NUMBER=2 OR NUMBER=5 OR NUMBER=6 THEN GOTO 870 ♣
820  IF NUMBER=3 OR NUMBER=4 THEN GOTO 1530 ♣
830  IF NUMBER=7 OR NUMBER=8 THEN GOTO 80 ♣
840  IF NUMBER=9 THEN GOTO 3750 ♣
850  IF NUMBER=10 THEN END ♣
860  GOTO 680 ♣
870  REM plotting routine ------------------------------------------------------
880  IF CHECK=0 AND NUMBER<>2 THEN GOTO 1320 ♣
890  CLS ♣
900  SCREEN 2 ♣
910  VIEW (16,10)-(636,196) ♣
920  LINE (38,165)-(620,165) ♣
930  LINE (38,8)-(38,165) ♣
940  TAB=40-CINT((LEN(TITLE$))/2) ♣
950  LOCATE 2, TAB, 1 ♣
960  PRINT TITLE$ ♣
970  REM begin to determine increment size on axis-----------------------------
 ♣
980  DUMMY2=MAXORD:GOSUB 3630 ♣
990  SIZABS=DUMMY1:SIZEX=SIZABS:GOSUB 3070 ♣
1000   IF CHECK7<>0 THEN CHECK7=0:ORD$=ORD$+"x10^"+STR$(E1) ♣
1010  DUMMY2=MAXABS:GOSUB 3630 ♣
1020  SIZORD=DUMMY1:SIZEY=SIZORD:GOSUB 3290 ♣
1030   IF CHECK7<>0 THEN CHECK7=0:ABC$=ABC$+"x10^"+STR$(E1) ♣
1040  PSET(24,166) ♣
1050  DRAW"R5F1D4G1L5H1U4R1D4R1U1R1U1R1U1R1U1R1D4" ♣
1060  REM print lables on axis ♣
1070  COL=LEN(ABC$) ♣
1080  ROW=LEN(ORD$) ♣
1090  LOCATE 24, 80-ROW, 1 ♣
1100  PRINT ORD$ ♣
1110  FOR I=1 TO COL ♣
1120    FLAG$=RIGHT$(LEFT$(ABC$,I),1) ♣
1130    LOCATE I+1, 1, 1 ♣
1140    PRINT FLAG$ ♣
1150  NEXT I ♣
1160  IF CHECK=0 THEN RADIUS=5 ♣
1170  IF NUMBER=5 OR NUMBER=6 THEN GOTO 1780 ♣
1180  REM calculate pixel location of datapoints, draw lines and circles--------
```

```
 ♣
1190  FOR I=1 TO N-1 ♣
1200    ORDPT1=CINT(ATAPTS(I,1)*562/MAXORD)+40 ♣
1210    ORDPT2=CINT(ATAPTS(I+1,1)*562/MAXORD)+40 ♣
1220    ABSPT1=CINT(ATAPTS(I,2)*151/MAXABS) ♣
1230    ABSPT2=CINT(ATAPTS(I+1,2)*151/MAXABS) ♣
1240    IF NUMBER=2 THEN LINE (ORDPT1,165-ABSPT1)-(ORDPT2,165-ABSPT2) ♣
1250    CIRCLE (ORDPT1, 165-ABSPT1), RADIUS ♣
1260  NEXT I ♣
1270    IF NUMBER=2 OR NUMBER=6 THEN CIRCLE (ORDPT2, 165-ABSPT2), RADIUS ♣
1280  LOCATE 24,1,1 ♣
1290  INPUT "STRIKE 'RETURN' TO CONTINUE", RET$ ♣
1300  SCREEN 3 ♣
1310  GOTO 680 ♣
1320  PRINT "DATA HAS NOT YET BEEN CURVE FITTED. SELECT (3) OR (4)." ♣
1330  GOTO 680 ♣
1340  PRINT "DATA HAS NOT BEEN INPUT YET, SELECT (7) OR (8)." ♣
1350  GOTO 680 ♣
1360  REM print data points ----------------------------------------------------
 ♣
1370  CLS ♣
1380  PRINT ORD$, ABC$ ♣
1390  PRINT "        " ♣
1400  COUNT=0 ♣
1410  FOR I=1 TO N ♣
1420    COUNT=COUNT+1 ♣
1430    PRINT ATAPTS(I,1), ATAPTS(I,2) ♣
1440    IF COUNT=18 THEN COUNT=0:PRINT" ":PRINT" ":INPUT"MORE DATA; STRIKE 'RETU
RN' TO CONTINUE", RET$:CLS ♣
1450  NEXT I ♣
1460  PRINT "        " ♣
1470  PRINT "MAXIMUM " ORD$ " IS " MAXORD ♣
1480  PRINT "MAXIMUM " ABC$ " IS " MAXABS ♣
1490  PRINT "      " ♣
1500  INPUT "STRIKE 'RETURN' TO CONTINUE", RET$ ♣
1510  GOTO 670 ♣
1520  REM print output from curvefit ------------------------------------------
 ♣
1530  GOSUB 1870 ♣
1540  CLS ♣
1550  PRINT "      " ♣
1560  IF NUMBER=3 THEN GOTO 1580 ♣
1570  IF NUMBER=4 THEN GOTO 1620 ♣
1580  PRINT "FIRST ORDER FIT FOR "TITLE$" :" ♣
1590  PRINT "      " ♣
1600  PRINT ABC$" = C1 + C2 * "ORD$ ♣
1610  GOTO 1650 ♣
1620  PRINT "SECOND ORDER FIT FOR "TITLE$" :" ♣
1630  PRINT "      " ♣
1640   PRINT ABC$" = C1 + C2 * "ORD$" + C3 * "ORD$" **2" ♣
1650  PRINT "WHERE:" ♣
1660  FOR I=1 TO NUMC ♣
1670    PRINT "C"I" = "C(I) ♣
1680  NEXT I ♣
1690  PRINT "      " ♣
1700  PRINT "STANDARD DEVIATION ON "ABC$" =",SIGMAE ♣
1710  PRINT "      " ♣
1720  PRINT "CURVE FIT STARTS AT "ORD$" =",XORD ♣
1730  PRINT "CURVE FIT ENDS AT "ORD$" =",XORD2 ♣
1740  PRINT "      " ♣
1750   IF NUMBER=3 THEN PRINT "CORRELATION COEFFICIENT=", R ♣
1760  GOTO 1500 ♣
1770  REM determine pixel location for curvefit curve and draw curve
1700  FOR I=1 TO N1 ♣
1780  FOR I=1 TO N1 ♣
1790  CURVPT1=CINT(CURVFIT(I)*151/MAXABS) ♣
1800  CURVPT2=CINT(CURVFIT(I+1)*151/MAXABS) ♣
1810  XPT1=CINT(XFIT(I)*562/MAXORD)+40 ♣
1820  XPT2=CINT(XFIT(I+1)*562/MAXORD)+40 ♣
1830  LINE (XPT1, 165-CURVPT1)-(XPT2, 165-CURVPT2) ♣
1840  NEXT I ♣
1850  IF NUMBER=5 THEN GOTO 1280 ♣
1860  IF NUMBER=6 THEN GOTO 1190 ♣
1870  REM curvefit ------------------------------------------------------------ ♣
1880    CHECK=1 ♣
1890    NUMC=CINT(NUMBER-1) ♣
1900    REM determine where to begin and end curvefitting-------------------- ♣
1910    PRINT "AT WHAT "ORD$" WOULD YOU LIKE TO START CURVE FITTING?" ♣
1920    INPUT " ", START ♣
1930    PRINT "AT WHAT "ORD$" WOULD YOU LIKE TO STOP CURVE FITTING?" ♣
```

```
1940   INPUT " ",STP ♣
1950   FOR I=1 TO N ♣
1960     IF ATAPTS(I,1)>=START THEN LB=I:XORD=ATAPTS(I,1):GOTO 1980 ♣
1970   NEXT I ♣
1980   FOR I=LB TO N ♣
1990     IF ATAPTS(I,1)>STP THEN UB=I-1:XORD2=ATAPTS(I-1,1):GOTO 2010 ♣
2000   NEXT I ♣
2010   REM GENERATE F MATRIX ♣
2020   IF STP=0 OR STP>=MAXORD THEN UB=N:XORD2=MAXORD:STP=MAXORD ♣
2030   IF START<ATAPTS(1,1) THEN START=ATAPTS(1,1) ♣
2040   N1=UB-LB ♣
2050   FOR I=LB TO UB ♣
2060    F(I,1)=1:F(I,2)=ATAPTS(I,1):F(I,3)=ATAPTS(I,1)*ATAPTS(I,1) ♣
2070   NEXT I ♣
2080   REM generate f transpose matrix----------------------------------------
2090   FOR I=LB TO UB ♣
2100   FOR J=1 TO NUMC ♣
2110    FT(J,I)=F(I,J) ♣
2120   NEXT J:NEXT I ♣
2130   REM determine coefficient matrix A for simultaenous system------------ ♣
2140   FOR I=1 TO NUMC ♣
2150   FOR J=1 TO NUMC ♣
2160    A(I,J)=0 ♣
2170   FOR K=LB TO UB ♣
2180    A(I,J)=A(I,J)+FT(I,K)*F(K,J) ♣
2190   NEXT K ♣
2200  NEXT J:NEXT I ♣
2210  REM determine the column of constants for simultaenous systems----------
2220  FOR I=1 TO NUMC ♣
2230   B(I)=0 ♣
2240   FOR K=LB TO UB ♣
2250    B(I)=B(I)+FT(I,K)*ATAPTS(K,2) ♣
2260  NEXT K:NEXT I ♣
2270  FOR I=1 TO NUMC ♣
2280   A(I,NUMC+1)=B(I) ♣
2290  NEXT I ♣
2300  REM determine coefficient values ♣
2310  MP1=NUMC+1 ♣
2320  REM calculate first row fo upper triangular matrix ♣
2330  FOR J=2 TO MP1 ♣
2340   A(1,J)=A(1,J)/A(1,1) ♣
2350  NEXT J ♣
2360  REM calculate other elements of U and L matricies-----------------------
♣
2370  FOR I=2 TO NUMC ♣
2380   J=I ♣
2390   FOR II=J TO NUMC ♣
2400    SUM=0:JM1=J-1 ♣
2410    FOR K=1 TO JM1 ♣
2420     SUM=SUM+A(II,K)*A(K,J) ♣
2430    NEXT K ♣
2440    A(II,J)=A(II,J)-SUM ♣
2450   NEXT II ♣
2460   IP1=I+1 ♣
2470   FOR JJ=IP1 TO MP1 ♣
2480    SUM=0:IM1=I-1 ♣
2490    FOR K=1 TO IM1 ♣
2500     SUM=SUM+A(I,K)*A(K,JJ) ♣
2510    NEXT K ♣
2520    A(I,JJ)=(A(I,JJ)-SUM)/A(I,I) ♣
2530  NEXT JJ:NEXT I ♣
2540  REM solve for the C(I)'s by back substitution----------------------------
2460  C(NUMC)=A(NUMC,NUMC+1) ♣
2550  C(NUMC)=A(NUMC,NUMC+1) ♣
2560  L=NUMC-1 ♣
2570  FOR NN=1 TO L ♣
2580   SUM=0:I=NUMC-NN:IP1=I+1 ♣
2590   FOR J=IP1 TO NUMC ♣
2600    SUM=SUM+A(I,J)*C(J) ♣
2610   NEXT J ♣
2620   C(I)=A(I,MP1)-SUM ♣
2630  NEXT NN ♣
2640  SUM=0 ♣
2650  SQUAREX=0 ♣
2660  SQUAREY=0 ♣
2670  SUMX=0 ♣
2680  SUMY=0 ♣
2690  IF NUMBER=3 THEN GOTO 2720 ♣
2700  IF NUMBER=4 THEN GOTO 2900 ♣
2710  REM calcualte standard deviation and correlation coefficient------------
```

```
 ♣
2720   FOR I=LB TO UB ♣
2730   YFIT(I)=C(1)+C(2)*ATAPTS(I,1) ♣
2740   SUMX=SUMX+ATAPTS(I,1) ♣
2750   SUMY=SUMY+ATAPTS(I,2) ♣
2760   NEXT I ♣
2770   XBAR=SUMX/N1 ♣
2780   YBAR=SUMY/N1 ♣
2790   FOR I=LB TO UB ♣
2800     SQUAREX=SQUAREX+(ATAPTS(I,1)-XBAR)*(ATAPTS(I,1)-XBAR) ♣
2810     SQUAREY=SQUAREY+(ATAPTS(I,2)-YBAR)*(ATAPTS(I,2)-YBAR) ♣
2820     SUM=SUM+(ATAPTS(I,1)-XBAR)*(ATAPTS(I,2)-YBAR) ♣
2830   NEXT I ♣
2840   SIGMAX=SQR(SQUAREX/(N1-1)) ♣
2850   SIGMAY=SQR(SQUAREY/(N1-1)) ♣
2860   R=(SUM/(N1-1))/(SIGMAX*SIGMAY) ♣
2870   C(3)=0 ♣
2880   GOTO 2930 ♣
2890   REM calculate curvefit points to plot-----------------------------------
 ♣
2900   FOR I=LB TO UB ♣
2910     YFIT(I)=C(1)+C(2)*ATAPTS(I,1)+C(3)*ATAPTS(I,1)*ATAPTS(I,1) ♣
2920   NEXT I ♣
2930   E=0 ♣
2940   FOR I=LB TO UB ♣
2950     E=E+(ATAPTS(I,2)-YFIT(I))*(ATAPTS(I,2)-YFIT(I)) ♣
2960   NEXT I ♣
2970   SIGMAE=SQR(E/(N1-1)) ♣
2980   RADIUS=CINT(SIGMAE*156/MAXABS) ♣
2990   IF RADIUS<5 THEN RADIUS=5 ♣
3000   SIZE=(STP-START)/N1 ♣
3010   FOR I=1 TO N1+1 ♣
3020    XFIT(I)=START+SIZE*(I-1) ♣
3030    CURVFIT(I)=C(1)+C(2)*XFIT(I)+C(3)*XFIT(I)*XFIT(I) ♣
3040   NEXT I ♣
3050   RETURN ♣
3060   REM make nice numbers on abscissia -------------------------------------
3070   WHILE SIZEX<=DUMMY2+.000001 ♣
3080    CHECK3=0:CHECK4=0:CHECK6=0 ♣
3090    XPT=CINT(SIZEX*562/DUMMY2)+40 ♣
3100    LINE (XPT,160)-(XPT,165) ♣
3110    SIZEX$=STR$(SIZEX) ♣
3120    IF SIZEX<1 THEN SIZEX$="0"+SIZEX$:CHECK6=1 ♣
3130    IF SIZEX=CINT(SIZEX)  AND SIZEX<10 THEN SIZEX$=SIZEX$+".0" ♣
3140    LSD=LEN(SIZEX$) ♣
3150    FOR I=1 TO LSD ♣
3160      FRAG$=RIGHT$(LEFT$(SIZEX$,I),1) ♣
3170      PSET(XPT-18+8*(I-1),166) ♣
3180      IF FRAG$="2" THEN PSET(XPT-18+8*(I-1),167) ♣
3190      IF FRAG$="." THEN PSET(XPT-18+8*(I-1),171):CHECK3=1 ♣
3200      IF FRAG$="0" AND CHECK6=1 THEN PSET(XPT-12+8*(I-1),166) ♣
3210      GOSUB 3510 ♣
3220      IF CHECK3=1 THEN CHECK4=CHECK4+1 ♣
3230      IF CHECK4=2 THEN GOTO 3250 ♣
3240    NEXT I ♣
3250    SIZEX=(CINT((SIZEX+SIZABS)*10))/10 ♣
3260   WEND ♣
3270   RETURN ♣
3280   REM make nice numbers on the ordinate-----------------------------------
 ♣
3290   WHILE SIZEY<=DUMMY2+.000001 ♣
3300     CHECK3=0:CHECK4=0:CHECK6=0 ♣
3310     YPT=CINT(SIZEY*151/DUMMY2) ♣
3320     LINE (38,165-YPT)-(43,165-YPT) ♣
3330     SIZEY$=STR$(SIZEY) ♣
3340     IF SIZEY<1 THEN SIZEY$="0"+SIZEY$:CHECK6=1 ♣
3350     IF SIZEY=CINT(SIZEY) AND SIZEY<10 THEN SIZEY$=SIZEY$+".0" ♣
3360     LSD=LEN(SIZEY$) ♣
3370     FOR I=1 TO LSD ♣
3380       FRAG$=RIGHT$(LEFT$(SIZEY$,I),1) ♣
3390       PSET(1+8*(I-1),161-YPT) ♣
3400       IF FRAG$="2" THEN PSET(1+8*(I-1),162-YPT) ♣
3410       IF FRAG$="." THEN PSET(1+8*(I-1),166-YPT):CHECK3=1 ♣
3420       IF FRAG$="0" AND CHECK6=1 THEN PSET(7+8*(I-1),161-YPT) ♣
3430       GOSUB 3510 ♣
3440       IF CHECK3=1 THEN CHECK4=CHECK4+1 ♣
3450       IF CHECK4=2 THEN GOTO 3470 ♣
3460     NEXT I ♣
3470     SIZEY=(CINT((SIZEY+SIZORD)*10))/10 ♣
```

```
3480  WEND ♣
3490  RETURN ♣
3500  REM draw numbers----------------------------------------------------------
 ♣
3510  IF FRAG$="1" THEN DRAW"R1D6R2L5R2U5L1G1":GOTO 3620 ♣
3520  IF FRAG$="2" THEN DRAW"R1U1R3D1R1D1L1D1L1D1L1D1L1D1L1R5":GOTO 3620 ♣
3530  IF FRAG$="3" THEN DRAW"R5G1L1D1L1R1F1R1D1L1D1R1G1L3U1L1":GOTO 3620 ♣
3540  IF FRAG$="4" THEN DRAW"R2D6L1U5L2D1L1D1L1D1R6":GOTO 3620 ♣
3550  IF FRAG$="5" THEN DRAW"R5L5D1R1D1L1R4D1R1D1L1D1R1G1L4U1R1":GOTO 3620 ♣
3560  IF FRAG$="6" THEN DRAW"R3L3D6R3U1R1U1L1U1L4D2U4":GOTO 3620 ♣
3570  IF FRAG$="7" THEN DRAW"R5D1L1D1L1D1L1D3L1U2":GOTO 3620 ♣
3580  IF FRAG$="8" THEN DRAW"R3D1R1D1L1D2R1D1L1D1L3U1L1U1R1U1R2L2U1L1U1R1":GOTO
 3620 ♣
3590  IF FRAG$="9" THEN DRAW"R3F1D4G1L3R3U5D2L3U1L1U1R1":GOTO 3620 ♣
3600  IF FRAG$="0" THEN DRAW"R5F1D4G1L5H1U4R1D4R1U1R1U1R1U1R1U1R1D4":GOTO 3620 ♣
3610  IF FRAG$="." THEN DRAW"R1D1L1" ♣
3620  RETURN ♣
3630  REM choose increments-----------------------------------------------------
3500  CHECK7=0:E1=0 ♣
3640  CHECK7=0:E1=0 ♣
3650  E=(LOG(DUMMY2))/(LOG(10)) ♣
3660  IF E<((LOG(.6))/(LOG(10))) OR DUMMY2<.6 THEN DUMMY2=DUMMY2*10:E1=E1+1:CHEC
K7=1:GOTO 3650 ♣
3670  IF E>((LOG(900))/(LOG(10))) OR DUMMY2>900 THEN DUMMY2=DUMMY2/10:E1=E1-1:CH
ECK7=1:GOTO 3650 ♣
3680  IF E>CINT(E) THEN E=CINT(E)+1 ELSE E=CINT(E) ♣
3690  IF 0<DUMMY2 AND DUMMY2<=1*10^(E-1) THEN DUMMY1=1*10^(E-2): GOTO 3730 ♣
3700  IF 1*10^(E-1)<DUMMY2 AND DUMMY2 <=2.5*10^(E-1)  THEN DUMMY1=2*10^(E-2)  :G
OTO 3730 ♣
3710  IF 2.5*10^(E-1)<DUMMY2 AND DUMMY2 <=5*10^(E-1)  THEN DUMMY1=5*10^(E-2)  :G
OTO 3730 ♣
3720  IF 5*10^(E-1)<DUMMY2 THEN DUMMY1=10*10^(E-2) ♣
3730  IF DUMMY1<1 THEN DUMMY1=(CINT(DUMMY1*1*10^(E+2)))/(1*10^(E+2)) ♣
3740  RETURN ♣
3750   REM link files---------------------------------------------------------- ♣
3760   CLS ♣
3770   INPUT "NAME MASTER FILE? ", DATASET$ ♣
3780   INPUT "HOW MANY FILES DO YOU WANT TO LINK? ", N ♣
3790   FOR I=1 TO N ♣
3800     PRINT "NAME OF FILE NUMBER ",I ♣
3810     INPUT "> ", FILE$(I) ♣
3820   NEXT I ♣
3830   PRINT " ":PRINT " ":PRINT " ":PRINT " " ♣
3840   PRINT "LINKING....." ♣
3850   OPEN DATASET$ FOR OUTPUT AS #1 ♣
3860   FOR I=1 TO N ♣
3870    OPEN FILE$(I) FOR INPUT AS #2 ♣
3880    ON ERROR GOTO 3930 ♣
3890    FOR J=1 TO 999 ♣
3900     INPUT #2, HOLD$ ♣
3910     WRITE #1, HOLD$ ♣
3920     NEXT J ♣
3930    RESUME 3940 ♣
3940    CLOSE #2 ♣
3950   NEXT I ♣
3960   CLOSE ♣
3970   GOTO 670 ♣
Ok
```

References

1. Hirano, T.; Noreikis, S.E.; and Waterman, T.E.: Measured Velocity and Temperature Profiles Near Flames Spreading Over a Thin Combustible Solid. Combust. Flame, vol. 23, 1974, pp. 83–96.
2. de Ris, J.N.: Spread of a Laminar Diffusion Flame. Twelfth Symposium (International) on Combustion, The Combustion Institute, 1969, pp. 241–252.
3. Frey, A.E., Jr.; and T'ien, J.S.: A Theory of Flame Spread Over a Solid Fuel Including Finite-Rate Chemical Kinetics. Combust. Flame, vol. 36, no. 3, Nov. 1979, pp. 263–289.
4. Vedha-Nayagam, M.; and Altenkirch, R.A.: Backward Boundary Layers in Downward Flame Spread. Twentieth Symposium (International) on Combustion, The Combustion Institute, 1984, pp. 1583–1590.
5. Chen, C.H.: Diffusion Flame Extinction in Slow Convective Flow Under Microgravity Environment. NASA TM–88799, 1986.
6. Friedman, R.: A Survey of Knowledge About Idealized Fire Spread Over Surfaces. Fire Research Abstracts and Reviews, vol. 10, 1968, pp. 1–8.
7. McAlevy, R.F., III; and Magee, R.S.: The Mechanism of Flame Spreading Over the Surface of Igniting Condensed-Phase Materials. Twelfth Symposium (International) on Combustion, The Combustion Institute, 1969, pp. 215–227.
8. Magee, R.S.; and McAlevy, R.F., III: The Mechanism of Flame Spread. J. Fire Flammability, vol. 2, Oct. 1971, pp. 271–296.
9. Lastrina, F.A.; Magee, R.S.; and McAlevy, R.F., III: Flame Spread Over Fuel Beds: Solid-Phase Energy Considerations. Thirteenth Symposium (International) on Combustion, The Combustion Institute, 1971, pp. 935–948.
10. Campbell, A.S.: Some Burning Characteristics of Filter Paper. Combust. Sci. Technol., vol. 3, no. 3, May 1971, pp. 103–120.
11. Campbell, A.S.: Fire Spread Over Paper. J. Fire Flammability, vol. 5, 1974, pp. 167–178.
12. Parker, W.J.: Flame Spread Model for Cellulosic Materials. J. Fire Flammability, vol. 3, 1972, pp. 254–268.
13. Frey, A.E., Jr.; and T'ien, J.S.: Near-Limit Flame Spread Over Paper Samples. Combust. Flame, vol. 26, no. 2, Apr. 1976, pp. 257–267.
14. Altenkirch, R.A.; Eichorn, R.; and Shang, P.C.: Buoyancy Effects on Flames Spreading Down Thermally Thin Fuels. Combust. Flame, vol. 37, no. 1, Jan. 1980, pp. 71–83.
15. Hirano, T.; and Sato, K.: Effects of Radiation and Convection on Gas Velocity and Temperature Profiles of Flames Spreading Over Paper. Fifteenth Symposium (International) on Combustion, The Combustion Institute, 1975, pp. 233–241.
16. Sibulkin, M.; Ketelhut, W.; and Feldman, S.: Effect of Orientation and External Flow Velocity on Flame Spreading Over Thermally Thin Paper Strips. Combust. Sci. Technol., vol. 9, nos. 1–2, 1974, pp. 75–77.
17. Fernandez-Pello, A.C.; Ray, S.R.; and Glassman, I.: Flame Spread in Opposed Forced Flow: The Effect of Ambient Oxygen Concentration. Eighteenth Symposium (International) on Combustion, The Combustion Institute, 1981, pp. 579–589.
18. Ray, S.R.: Flame Spread Over Solid Fuels. PhD. Thesis, Princeton University, 1982.
19. Kimzey, J.H., et al.: Flammability in Zero-Gravity Environment. NASA TR R–246, 1966.
20. Neustein, R.A., et al.: The Effect of Atmosphere Selection and Gravity on Burning Rate and Ignition Temperature. (DAC–62431, McDonnell-Douglas Astronautics Co.; NASA Contract NASW–1539) NASA CR–106652, 1969.
21. Kimzey, J.H.: Skylab Experiment M–479, Zero Gravity Flammability. NASA JSC–22293, 1986.
22. Andracchio, C.R.; and Aydelott, J.C.: Comparison of Flame Spreading Over Thin Flat Surfaces in Normal Gravity and Weightlessness in an Oxygen Environment. NASA TM X–1992, 1970.
23. Andracchio, C.R.; and Cochran, T.H.: Burning of Solids in Oxygen-Rich Environments in Normal and Reduced Gravity. NASA TM X–3055, 1974.
24. Andracchio, C.R.; and Cochran, T.H.: Gravity Effects on Flame Spreading Over Solid Surfaces. NASA TN D–8228, 1976.
25. Altenkirch, R.A.: Science Requirements Document for the Solid Surface Combustion Experiment. NASA Contract NAS3–23901 Report, Revision A, Sept. 12, 1985.
26. Liñan, A.: The Asymptotic Structure of Counterflow Diffusion Flames for Large Activation Energies. Acta Astronautica, vol. 4, nos. 7–8, July-Aug. 1974, pp. 1007–1039.
27. Wichman, I.S.; and Williams, F.A.: Comments on Rates of Creeping Spread of Flames Over Thermally Thin Fuels. Combust. Sci. Technol., vol. 33, nos. 1–4, 1983, pp. 207–214.
28. Altenkirch, R.A.; Vedha-Nayagam, M.; and Srikantaiah, N.: Scientific Support for an Orbiter Middeck Experiment on Solid Surface Combustion. NASA Contract NAS3–23901, Contractor Monthly Progress Report Feb. 1986, Mar. 18, 1986.
29. T'ien, J.S.: Diffusion Flame Extinction at Small Stretch Rates: The Mechanism of Radiative Loss. Combust. Flame, vol. 65, no. 1, July 1986, pp. 31–34.
30. Foutch, D.W.; and T'ien, J.S.: Extinction of a Stagnation-Point Diffusion Flame at Reduced Gravity. AIAA J., vol. 25, no. 7, July 1987, pp. 972–976.
31. Olson, S.L.; and T'ien, J.S.: A Theoretical Analysis of the Extinction Limits of a Methane-Air-Opposed-Jet Diffusion Flame. Combust. Flame, vol. 70, no. 2, Nov. 1987, pp. 161–170.
32. Welty, J.R.; Wicks, C.E.; and Wilson, R.E.: Fundamentals of Momentum, Heat, and Mass Transfer. Second Edition, John Wiley & Sons, New York, 1976.

NASA
National Aeronautics and Space Administration

Report Documentation Page

1. Report No.	2. Government Accession No.	3. Recipient's Catalog No.
NASA TM-100195		

4. Title and Subtitle	5. Report Date
The Effect of Microgravity on Flame Spread Over a Thin Fuel	December 1987
	6. Performing Organization Code

7. Author(s)	8. Performing Organization Report No.
Sandra L. Olson	E-3785
	10. Work Unit No. 674-22-05

9. Performing Organization Name and Address	11. Contract or Grant No.
National Aeronautics and Space Administration Lewis Research Center Cleveland, Ohio 44135-3191	
	13. Type of Report and Period Covered Technical Memorandum
12. Sponsoring Agency Name and Address	14. Sponsoring Agency Code
National Aeronautics and Space Administration Washington, D.C. 20546-0001	

15. *Supplementary Notes*

This report was a thesis submitted in partial fulfillment of the requirements for the Degree of Master of Science to Case Western Reserve University, Cleveland, Ohio in August 1987.

16. Abstract

A flame spreading over a thermally thin cellulose fuel was studied in a quiescent microgravity environment obtained through the use of the NASA Lewis Research Center microgravity facilities. Flame spread over two different fuel thicknesses was studied in ambient oxygen-nitrogen environments from the limiting oxygen concentration to 100 percent oxygen at 1 atm pressure. Comparative normal-gravity tests were also conducted. Gravity was found to play an important role in the mechanism of flame spread. In lower oxygen environments, the buoyant flow induced in normal gravity was found to accelerate the flame spread rate as compared to the microgravity flame spread rates. It was also found to stabilize the flame in oxidizer environments, where microgravity flames in a quiescent environment extinguish. In oxygen-rich environments, however, it was determined that gravity does not play an important role in the flame spread mechanism. Fuel thickness influences the flame spread rate in both normal gravity and in microgravity. The flame spread rate varies inversely with fuel thickness in both normal gravity and in an oxygen-rich microgravity environment. In lower oxygen microgravity environments, however, the inverse relation breaks down because finite-rate kinetics and heat losses become important. Two different extinction limits were found in microgravity for the two thicknesses of fuel. This is in contrast to the normal-gravity extinction limit, which was found to be independent of fuel thickness. The extinction mechanism in microgravity was determined to be different from that in normal gravity. In microgravity the flame is quenched because of excessive thermal losses, whereas in normal gravity the flame is extinguished by blowoff. An extinction boundary for flame spread over a thin fuel is presented and suggests that there is a fundamental low oxygen flammability limit at a forced-flow velocity lower than the normal-gravity buoyant velocity at extinction.

17. Key Words (Suggested by Author(s))	18. Distribution Statement
Combustion Microgravity Solids Flame spread	Unclassified – Unlimited Subject Category 25

19. Security Classif. (of this report)	20. Security Classif. (of this page)	21. No of pages	22. Price*
Unclassified	Unclassified	49	A03

*For sale by the National Technical Information Service, Springfield, Virginia 22161